THE MESSENGER

EL MENSAJERO

No. 52 – June 1988

KEY PROGRAMMES ON LA SILLA: First Round

H. VAN DER LAAN, Director General, ESO

RESPONSE TO THE PRELIMINARY ENQUIRY

My request in the *Messenger* No. 51 for reactions has met an ample response. Numerous letters, phone calls and visiting astronomers dropping by in my office supplemented some sixty preliminary proposals on the forms designed for that purpose. In this article I wish to report briefly about the composition and extent of this response.

Apprehensions and Possible Misunderstandings

As announced earlier, the deadline for the first round of ESO's Key Programmes is 15 October 1988. Because the timespan between the moment ESO's users first saw my March article and 30 April 1988 was rather short, some people could not respond to the preliminary enquiry at all or not as well as they would have preferred. Let me emphasize that this in no way prejudices their opportunity for participation. The chief goal of the preliminary enquiry was to establish whether there is a deep and broad interest in the concept I have proposed, and if so, what the main themes and trends of that interest are.

The sixty or so principal investigators and some two hundred and fifty co-investigators who did respond and submitted a preliminary proposal achieved more than helping me reach the goal just stated. Their work goes a long way towards preparing the actual proposal for the deadline appropriate for them. (As will become clear below, that could be one or two years later than the next deadline.) Moreover, we can now identify affinity and/or overlap between many separate initiatives; by informing PI's of such common elements, new combinations may result.

That brings me to another worry expressed by some: "Will we be forced to work in large consortia with merged programmes?" The answer is no. All ESO will do is inform investigators of mutual interests and overlapping proposals, evident from the response to the preliminary enquiry. Whether they wish to collaborate is entirely the proposers' decision. Obviously, telescope time will be granted in a manner that is effective and economical, serving the stated purposes of the Key Programmes concept. In cases of clear overlap, the best pro-

In mid-May 1988, the unusual shape of the NTT building stands out against the observatory skyline. (Good news about the NTT on page 10 and 51.)

gramme will get all, the others nothing. It is that risk which forms, among others, an incentive for collaborations.

Finally the fear, heard here and there, that Key Programmes will lead to monopolies on some subjects or areas. This is an understandable concern which I share. ESO's archiving policy, described elsewhere in this issue, will go some way to reduce this risk. The OPC will undoubtedly help to minimize detrimental effects on this score.

Key Programme Initiatives

Approximately sixty tentative proposals reached us in response to the preliminary enquiry. In Table 1 an overview is provided of the distribution of the 3,400 nights required over the six telescopes involved. Also shown is the variation in team sizes and the internationality of these plans (Fig. 1).

I find the response very satisfactory. Evidently, there exists a good deal of collaboration already among astronomers in member states. Within each category there may be overlap and strong affinity among proposals. In the next month or so these will be analysed and PI's will be informed of such circumstances. The involvement of ESO staff at Headquarters and on La Silla is widespread, a desideratum I expressed in the March article.

A few words about the different proposal groups, without, at this stage, specifying their contents (see OPC Classification; "K" signifies Key Programme):

- K1 has 14 proposals, seven of which involve deep redshift surveys of galaxies, all using the 3.6-m and the NTT. Some reconfiguration of teams seems logical and discussions among PI's will be suggested from ESO.
- K2 concerns both quasar surveys and gravitational lense studies as major activities, sketched in 15 proposals.
- K3 is concerned with the Magellanic Clouds, including SN 1987A, and the half dozen proposals aim at a significant use of the smaller telescopes as well.
- K4, interstellar matter, is heterogeneous, but the six proposals thus far request primarily big telescope time.
- K5, on star clusters and galactic structure, has two proposals and
- K6 for X-ray sources has two initiatives for satellite programme follow-up: ROSAT and SIGMA.
- K7 is for stars and contains twelve proposals for this major area, with small telescopes heavily contributing.
- K8 is a sole comet programme involving five telescopes.

TABLE 1: *Distribution of number of proposals (figures given within brackets) and of required nights – distinguished by 3.6 m plus NTT on the one hand, and the smaller instruments on the other – over the nine categories distinguished by the OPC. An overview of the distribution of the nights over the six telescopes is also provided. Not included in this table are the 130 nights requested at the 1-m telescope which was not involved in the inquiry.*

Telescope / Category	3.6 m	3.5 m NTT	2.2 m	1.5 m	1.5 m D	1.4 m CAT
K 1	(10) 590	← (4) →		110		
K 2	(5) 465	← (8) →		(2) 460		
K 3	(1) 170	← (4) →		110		
K 4	(4) 200	← (1) →		40		
K 5	(2) 120					
K 6	(1) 120	← (1) →		50		
K 7	(3) 180	← (3) →		(3) 475		
K 8	15	← (1) →		240		
K 9				(1) 45		
TOTAL	1075	785	480	660	315	75

Note: Only the 54 proposals in which both the telescopes and the number of nights required were indicated have been taken into consideration for constructing this table.

- K9 concerns HST follow-up and a major speckle programme.

Call for Proposals

The harvest of sixty initiatives, numerous individual reactions as well as the endorsement by the Users Committee and the Scientific Technical Committee of ESO together form a very encouraging base for a good start. However, given the rather modest availability of the NTT in Period 43 and the continued commissioning of instrumentation in Period 44, the time available for Key Programmes in the first round is correspondingly limited. The allocation space that has been set for these two semesters is given in Table 2.

This total of 125 nights on the two big telescopes is a rather modest start, leaving room for new proposals next year. For the second round, deadline October 15, 1989, Periods 45 and 46

TABLE 2: *Number of nights to be allocated to Key Programmes*

Telescope	3.6 m	3.5 m NTT	2.2 m	1.5 m ESO	1.5 m Dan.	1.4 m CAT CES
Period						
43	40	15	20	25	15	30
44	40	30	20	25	15	30

(April 1, 1990–March 31, 1991), we expect the number of nights devoted to Key Programmes on the 3.6 m and the NTT to increase to a level of about 200 nights. The amount of time on the smaller telescopes will be more elastic, depending on proposal pressure. With EFOSC II on the 2.2-m a shift of some 3.6-m work to this intermediate size telescope may be expected.

ESO community astronomers, whether they responded to the preliminary enquiry or not, are invited to submit proposals to the Visiting Astronomers Section at ESO Headquarters before October 15, 1988. Copies of a form designed for this purpose will soon be available from this Section on request.

With the great reservoir of plans and the modest beginning just outlined, many potential proposers may wish to postpone their initiative by one or two years: Key Programmes are long term . . . Proposals not successful in any round may be resubmitted in identical or modified form for later rounds. Proposals for the first round will be sent to referees outside ESO's OPC. Their reports, gradings plus explicit commentaries supporting the grade, will be submitted to the OPC for preparing its recommendations to me.

After the first round the whole process will be evaluated and, if necessary, adapted. Through the *Messenger* the community will be informed of progress. Successful programme proposals will be summarized by the PI's in future issues of the *Messenger*.

OPC Classification

1 – GALAXIES
2 – QUASARS, SEYFERTS, RADIO GALAXIES
3 – MAGELLANIC CLOUDS
4 – INTERSTELLAR MATTER
5 – CLUSTERS AND GALACTIC STRUCTURE
6 – X-RAY SOURCES
7 – STARS
8 – SOLAR SYSTEM
9 – MISCELLANEOUS

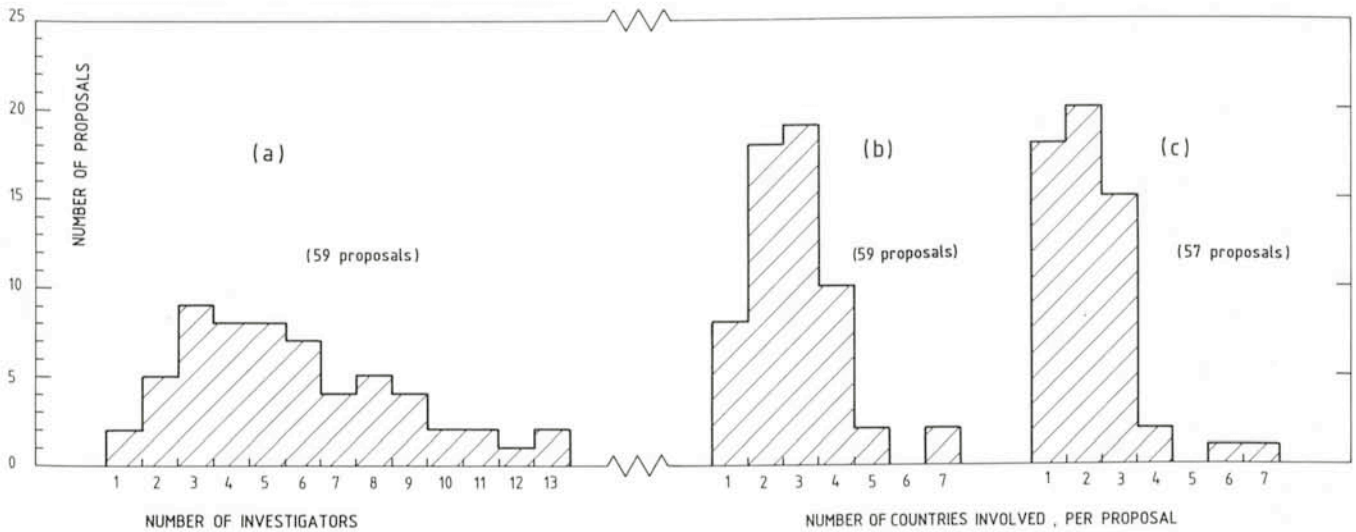

Figure 1: *Histograms showing the distribution of the proposals, (a) as a function of the number of investigators involved; (b) as a function of the number of institutional nationalities per proposal when ESO and ESA institutes are included, (c) when ESO and ESA institutes are excluded. The programme related to HST follow-up, which involves 32 investigators from 19 institutes, is not included.*

ESO Archiving Policy

The following statement is a set of premisses and principles for a data-archiving policy which ESO will implement gradually in the next several years. It has been discussed in the Users Committee, in the Scientific-Technical Committee and in the Observing Programmes Committee. All three committees approve of this policy intent.

Introduction

It is important to archive data obtained at ESO's La Silla Observatory. The three main reasons for maintaining an archive are:

(a) to keep a historical record of objects. This enables the investigation of long-term changes in objects which otherwise could not be performed;
(b) to re-use the data for other programmes or purposes. By avoiding duplication of observations the effective use of telescope time can be increased;
(c) to enable archival research such as surveys of different types of objects. A homogeneous archive with well defined calibrations will open the possibility to study large numbers of objects for statistical purposes.

An indispensable requirement for the archive is very high quality of the data both in terms of good documentation of the individual observations and reliable calibration data. Only when this is achieved will the archive serve its purpose to fully utilize data acquired at ESO.

The archive consists of two main parts, namely

– the *data archive* which contains the actual data

and

– the *catalogue of observations* holding sufficient information to allow astronomers to locate data and judge their usefulness for a given programme.

Data Archived

Spectroscopic and imaging data obtained during ESO observing time are archived. All scientific data are saved in

raw form. Observational logs, technical data, and calibrations are also archived to give a full description of scientific data. Archiving of data from a given instrument is started when procedures have been implemented to record all relevant observational parameters and provide reliable calibration data. Priority for establishment of such procedures is given to the major ESO telescopes and instruments.

Proprietary Period

The proprietary period for scientific data is one year after termination of the observations. The prime investigator of an observing programme can apply to the OPC for an extension of this period. This is granted in special cases only. All other data (i.e. observing logs, technical and calibration data) are public immediately after the observations. Astronomers may request to have the list of targets concealed during the proprietary period in their application for observing time. The OPC can grant such requests in exceptional cases.

Location and Access to Archive

The ESO archive, both data archive and catalogue, is located and managed at the ESO Headquarters in Garching. A copy of all digital data obtained at the ESO Observatory is kept in Chile to allow recoveries of errors. This security copy is erased after a period of six months. The catalogue is accessible for queries at the ESO computer facilities in Garching and over computer networks. Access to the non-proprietary part of the data archive can be made at ESO Garching. Limitations to the volume of accessed data can be imposed for technical reasons. The requests for retrieval and shipment of data from the ESO archive are subject to a scientific evaluation. A modest charge may be applied for large volumes of data.

H. VAN DER LAAN, ESO

Diskettes for "Astronomy and Astrophysics" (First Announcement)

Main Journal

In the future, contributors to *Astronomy and Astrophysics* using TEX will get the opportunity to submit their manuscripts on diskettes. In agreement with the Board of Directors and the Editors of *Astronomy and Astrophysics*, Springer-Verlag will offer a macro-package on a diskette together with a set of instructions. Texts formatted with Springer's macros will be produced on your printer in essentially the same way as they will appear later in the journal, and, furthermore, they allow typesetting directly from the author's input. In 1988 the product will be tested by Springer in co-operation with astronomical institutes and the typesetter. It is hoped that by 1989 this new system will allow a more speedy and more efficient processing of the articles. Similar macros are offered to the authors of Springer-Verlag's new journal *The Astronomy and Astrophysics Review,* which will be launched in 1989. More details will be given in the next issue of the *ESO Messenger.* For information please contact the Editors of *Astronomy and Astrophysics.*

H.-U. DANIEL, Springer-Verlag

Supplement Series

Les Editions de Physique can now accept manuscripts for *Astronomy and Astrophysics* in the form of diskettes containing text generated by TEX or by MATHOR. MATHOR allows interactive, wysiwyg editing of text and formulae with the possibility of automatic conversion to TEX format.

Chr. ARDEN, Les Editions de Physique

STAFF MOVEMENTS

Arrivals

Europe:

LINSSEN, Marion (NL), Secretary
HOOK, Richard (GB), Fellow
HUIZINGA, Jan (NL), Student

Chile:

GOJAK, Domingo (YU), Electronic Engineer
PERSSON, Glenn (S), Telescope Software Scientist

Departures

Europe:

DEMIERRE, Ulla (CH/D), Secretary to the Director General
GUZZO, Luigi (I), Associate
RICHMOND, Alan (GB), Associate

Chile:

MURPHY, David (USA), Telescope Software Scientist

Transfers

MAGAIN, Pierre (B), Fellow (from Chile to Europe)

2nd NOAO/ESO Conference on "High Angular Resolution by Interferometry"

In 1985 the Director of the National Optical Astronomy Observatories (NOAO), J. Jefferies, and the Director General of ESO, L. Woltjer, stimulated the idea of having regular workshops jointly organized by the two institutions.

The first workshop was then organized by NOAO at the Sun Space Ranch Conference Center in Oracle near Tucson, Arizona, from January 12 to 15 in 1987. Both organizations had invited in total 52 participants to this Joint ESO/NOAO Workshop on "High Resolution Imaging from the Ground Using Interferometric Techniques". The proceedings with the title "Interferometric Imaging in Astronomy" were published by NOAO in April 1987. During the workshop it became very clear that the topics addressed were of such interest to the astronomical community that the following meeting should be an open conference on high resolution imaging by interferometry and all researchers and scientists interested in this area should have the chance to participate. This time it was the task of ESO to organize a meeting in early 1988.

The second NOAO/ESO conference on "High Resolution Imaging by Interferometry" was held in Garching from March 14 to 18, 1988. The response was so large, that it had to take place in the lecture halls of the Technical University in order to accommodate all participants. Approximately 120 presenta-

tions were announced for this four-day conference, which took place just before the ESO-Conference on "Very Large Telescopes and their Instrumentation".

In addition, a one-day tutorial was arranged the day before the conference to teach scientists, researchers and students new in this area about the theory and experimental techniques of interferometry in optical astronomy. About 100 persons participated.

The conference itself was attended by 183 participants (including 24 from ESO and the ST-ECF). They came from more than 15 countries. The United States was represented by 46, followed by France with 41, and the Federal Republic of Germany with 26 scientists. A total of 20 invited talks, 97 contributed presentations (63 talks and 34 posters) and 1 special talk were given during the conference.

The programme was composed of papers covering the scientific needs for high angular resolution and interferometry, single aperture interferometry including speckle interferometry, pupil-plane interferometry, the Know-Thompson method, triple correlation methods, phase-closure methods and others, and multiple aperture interferometry with presentations on existing and future projects for long-baseline interferometers and related technologies. A special talk illustrated the progress of radio interferometry during the last decades and the way interferometry at infrared and visible wavelengths still has to go.

A large number of excellent and novel scientific and technical results were presented during this conference. The highlights included spectacular scientific results, improved algorithms and reconstructed images, advanced experimental set-ups, instruments and interferometers and plans and proposals for the next generation of interferometric equipment. The Proceedings, which will give a comprehensive overview of the area of high resolution imaging by interferometry in astronomy, are expected by end of July 1988.

The next ESO/NOAO meeting – on "Infrared Array Detectors" – will take place in Tucson in September or October 1989. *F. MERKLE, ESO*

VLT NEWS

The VLT Adaptive Optics Prototype System: Status May 1988

F. MERKLE, ESO

In 1987 ESO decided to develop and construct an adaptive optics prototype system. This initial step into the field of adaptive optics at ESO has been taken in collaboration with the French three institutions ONERA, CGE-Laboratoires de Marcoussis, and the Observatoire de Paris-Meudon (DESPA). The system is dimensioned for F/8 focus of the ESO 3.6-m telescope and the 1.52-m telescope of the Observatoire de Haute-Provence. It operates as a polychromatic adaptive system (see Fig. 1), i.e. it is equipped with an infrared camera for image detection in the 3 to 5 μm range while its wavefront sensor works in the visible. It uses a deformable mirror with 19 actuators while the wavefront is sensed at 10×10 subapertures. It serves as a testbench for the various elements of an adaptive system and the modal control algorithms.

The construction of the main elements of this adaptive optical system is basically finished and the first functional tests have already started. These elements are:

- the deformable mirror,
- the wavefront sensor, and
- the control computer.

For this prototype system a thin faceplate (0.7 mm) deformable mirror had been selected. It was developed at CGE-Laboratoires de Marcoussis in France (see Fig. 2). The 19 piezoelectric actuators are distributed over a circular area with 65 mm in diameter in a hexagon arrangement. The total diameter of the mirror is 130 mm. The maximum actuator stroke is in the range of ± 7.5 μm for a voltage of ± 1,500 V. The mirror itself is made of silicon which has been polished to better than half an interference fringe at the HE-NE-laser wavelength and is coated with silver.

For adaptive optics a Shack-Hartmann sensor seems to be the most adequate wavefront sensor. The lenticular arrays which are the key-components of Shack-Hartmann sensors have been

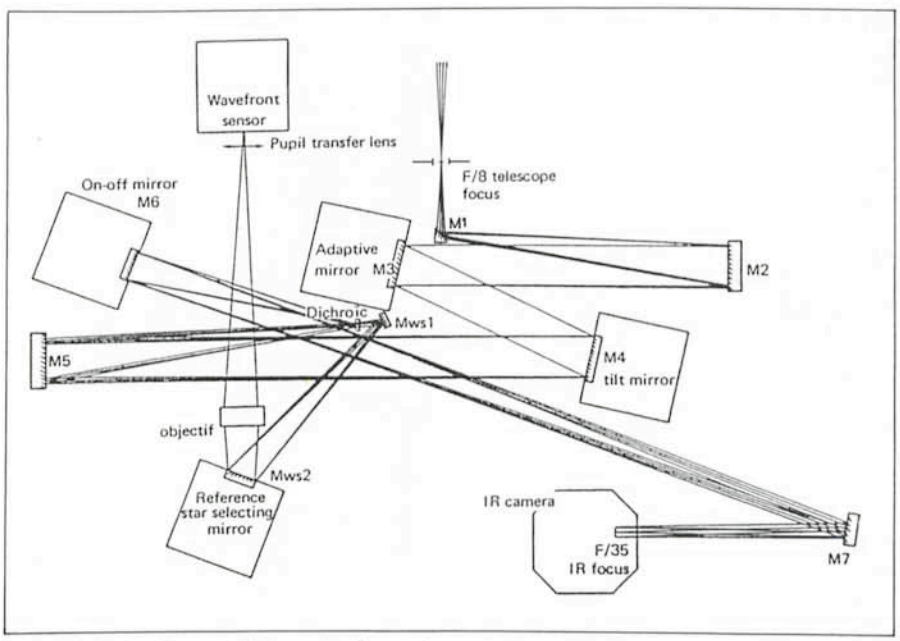

Figure 1: *Optical lay-out of the adaptive optics prototype system.*

Figure 2: *Deformable mirror developed at CGE-Laboratoires de Marcoussis with 19 piezoelectric actuators.*

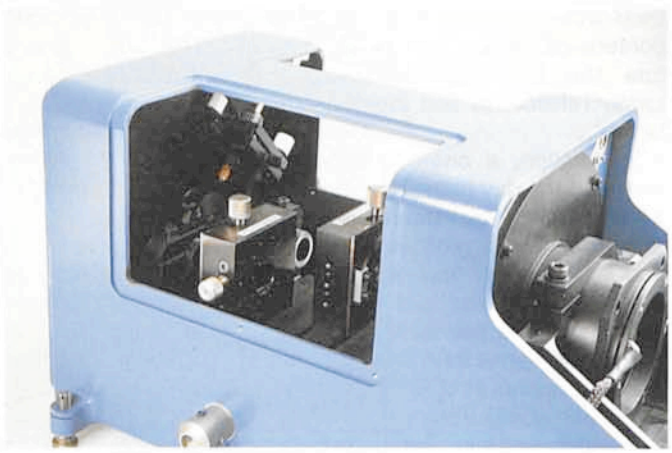

Figure 3: *Picture of the fast Shack-Hartmann sensor developed at ESO which is equipped with an intensified 100 × 100 Reticon array detector.*

developed at ESO already for the NTT. The individual lenses (in total 1,600) are 1 × 1 mm and have a focal length of 170 mm. They are manufactured by a replication technique using two crossed arrays of cylindrical lenses. A Reticon type array is used as detector to sense the position of the individual foci for the calculation of the centres of gravity within the subpupils. Combining the beam to be analysed with a reference beam, representing a plane wavefront, allows a self-calibration even during observation.

Figure 3 shows a picture of the fast ESO Shack-Hartmann sensor equipped with a 100 × 100 Reticon array detector. The spot pattern is intensified by a two stage proximity focus intensifier (Proxitronic). The intensifiers and the Reticon are coupled together by fiber plates. Two optical configurations can be selected, either 10 × 10 or 5 × 5 subapertures with 10 × 10 or 20 × 20 pixels, respectively. The maximum frame rate is 500 frames per second but in typical operation conditions it is limited to 200.

All slope-measuring wavefront sensors require a reconstruction of the wavefront itself. Normally, two orthogonal wavefront slope measurements are made for each subaperture. The reconstruction algorithms require very high computation powers in order to meet the temporal and spatial requirements. With special dedicated hardware or hybrid systems this problem is successfully approachable.

The prototype system is based on special hardware developments going on at ONERA and CGE in France. These systems use microprogrammable parallel structures, controlled by a general purpose host processor. The maximum pixel rate of the detector of the wavefront sensor is currently limited to 2 Megapixels per second which sets the maximum control loop rate to 200 cy-

Figure 4: *Wavefront computer developed at ONERA.*

cles per second due to the 10,000 pixels of the detector. The expected OdB-bandwidth of the system is approximately 30 Hz. This will allow a full correction for wavelengths greater 2.2 μm. At this wavelength the typical atmospheric correlation time is 35 ms.

The integration of the optomechanical system is planned for October and November. In December system tests with closed-loop operation will begin. First light is scheduled for March 1989 at OHP and at the 3.6-meter telescope later next year.

This development programme is carried out within the frame of the VLT project. It is intended to equip each individual VLT telescope with independent active and adaptive optical systems. The active optics will be used for the figure compensation of the telescope optics. The atmospheric compensation is foreseen in a separate adaptive optical system which will be installed in the Coudé beam. Active and adaptive optics will have separate wavefront sensors, due to the different isoplanatic angles and the different time constants for the corrections. At the moment, an adaptive system with 100 to 200 subapertures and 50 to 100 Hz operational frequency is the target for future investigations. By extrapolating currently available technology with piezoelectric material for the 100 to 200 actuators the diameter of this mirror will be approximately 300 mm. Future developments in mirror technology and special control electronics may lead to much more complex systems. It is envisaged to incorporate these developments after availability into the concept.

Acknowledgements

The author's thanks are due to many colleagues contributing to ESO's activities in the field of adaptive optics, particularly J.C. Fontanella (ONERA), J.P. Gaffard (CGE), P. Kern (Obs. de Meudon), P. Léna (Obs. de Meudon), J.C. de Miscault (CGE), G. Rousset (ONERA), and to many colleagues at ESO for stimulating discussions.

Latest Studies Lead to Revised Design of the VLT Enclosure

L. ZAGO, ESO

Like for many other systems of such an innovative project as the VLT, the design process of the enclosure is necessarily iterative. Those who have followed the evolution of the project from its beginning will remember the first concept which presented the arrangement of the four telescopes observing in the open air, behind a large wind shield and with mobile shelters for daytime and weather protection. Then inflatable domes were proposed: the resulting enclosure was certainly much lighter, more elegant and above all cheaper.

Now, in view of the latest studies and developments on both telescope and dome, we are coming to a further iteration (possibly not the last one) in the definition of the VLT enclosure. This is well illustrated by the latest model of the VLT, first shown at the Large Telescopes Conference of last March.

The new model shows one unit telescope of the VLT array, which is enclosed by a circular service platform supporting the inflatable dome. The telescope pillar is lower than in the previous designs, as measurements of atmospheric properties in the near ground layer at La Silla have shown that there is no advantage in having the opening of a telescope higher than 15 metres above the ground. While this conclusion may be revised for other sites, it has been included in the present baseline project. It is therefore now more convenient to base the gantry crane on tracks at ground level than to make a continuous

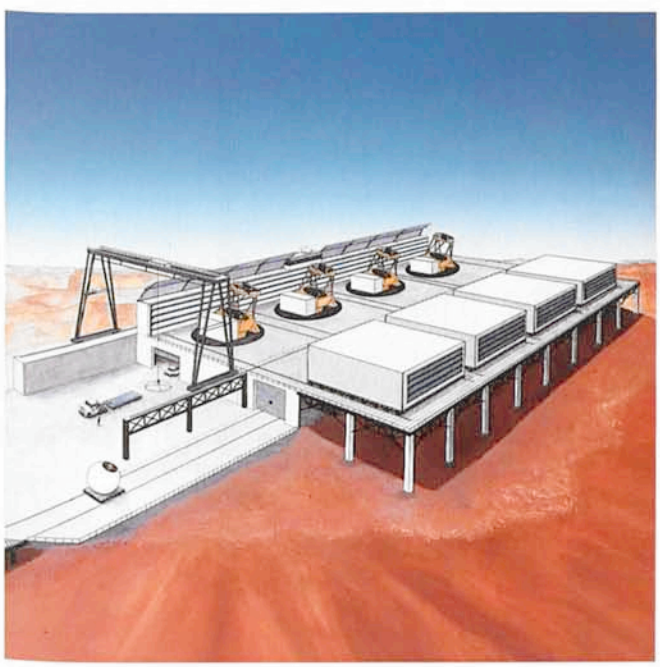

Figure 1: *The first VLT concept.*

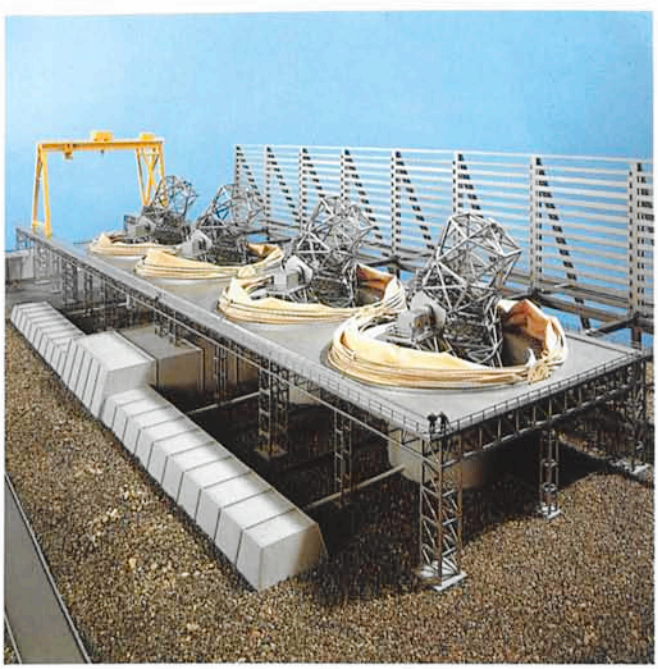

Figure 2: *Second iteration: inflatable domes, a lighter platform.*

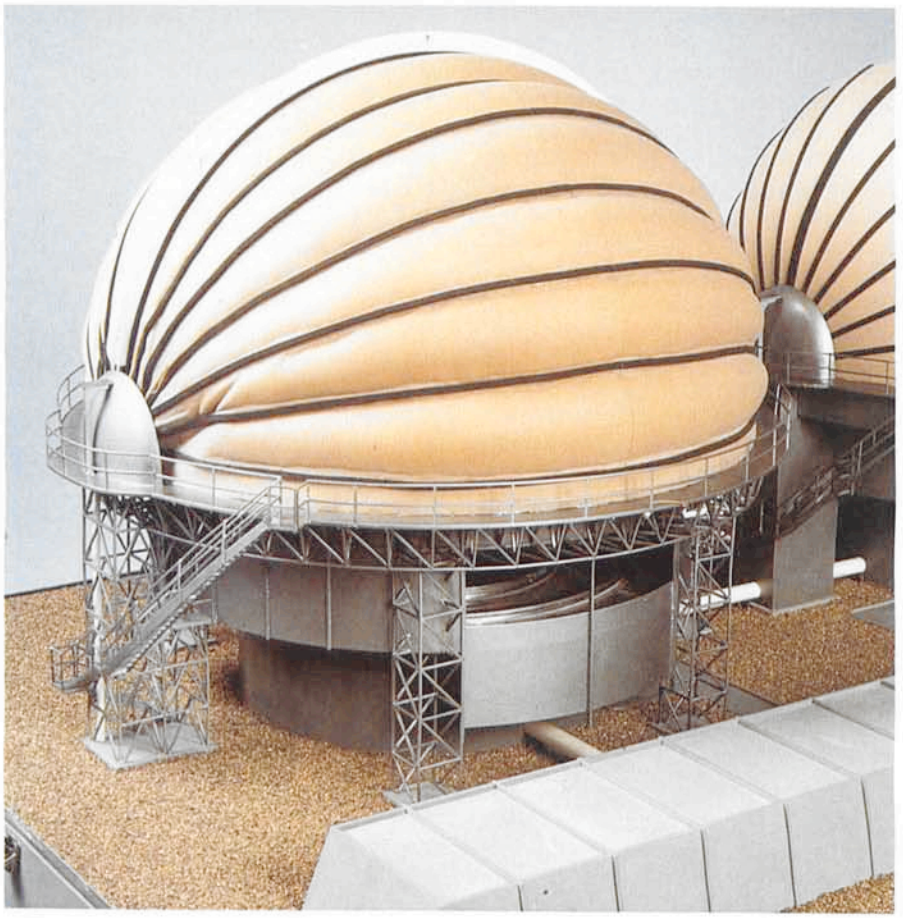

Figure 3: *The latest enclosure design for the VLT unit telescopes. The sliding door in the recess is used for natural ventilation. From another one at the opposite end it is possible to take the primary mirror out for aluminization.*

Figure 4: *The enclosure in open configuration.*

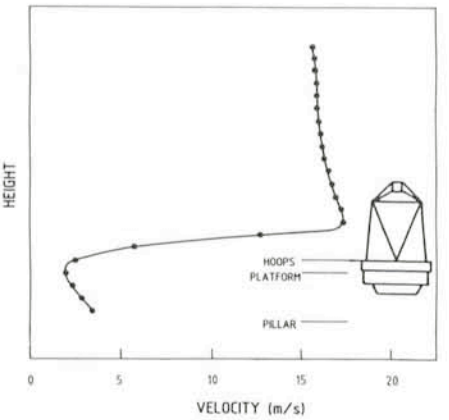

Figure 5: *Wind velocity profile along the azimuth axis measured during wind tunnel tests.*

platform for all four telescopes. A small crane will possibly also be included in each dome for minor handling operations.

The large wind screen present in the older versions has disappeared, as studies have shown that with the use of direct drives for the altitude motion and an active secondary mirror for correction of tracking errors it will be possible to achieve the specified tracking accuracy under wind buffeting.

Conversely, the lower part of the telescope is now imbedded in a recess made in the platform so that the primary mirror can be effectively protected from wind buffeting. Indeed the relative thinness of the primary mirror and the still preliminary status of the mirror support design led to assume conservatively that it will be necessary to shield the mirror from most of the wind loading. Several sliding doors in this recess will nevertheless allow complete ventilation of the enclosed volume when deemed convenient.

The dome in the model represents essentially a scaled-up version of the 15-metre prototype just erected at La Silla. The test and experimental phase which is beginning now will hopefully give many data for a refined design of the 30-metre domes for the VLT.

Inflatable VLT Dome Prototype Erected at La Silla

The 15-metre inflatable dome prototype has been erected at La Silla. First tests took place at the beginning of March and at the time these lines are written the dome is already sheltering a telescope, a new 40-cm seeing monitor which is being tested there previously to its installation at Cerro Vizcachas near La Silla.

The dome itself is not yet formally complete as the motorized system for lowering the auxiliary hoops and some minor items have still to be supplied by the contractor, but the planned test programme aiming at achieving the optimum design for the VLT has already started. The main functions of the dome (opening, closing, blowing) are success-

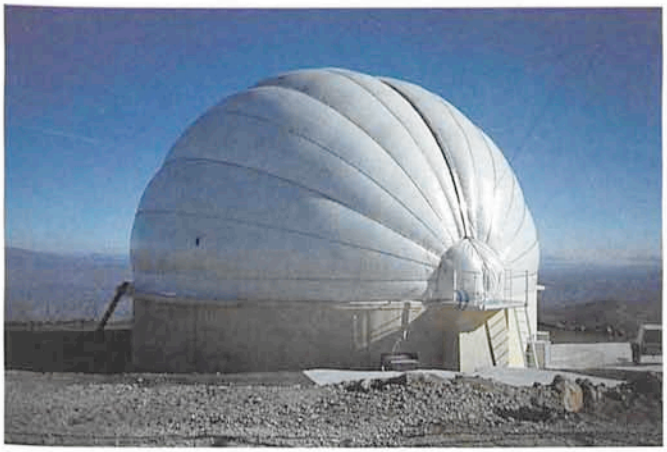

Figure 1: *The closed and inflated dome.*

Figure 2: *The open dome. The motor for lowering the auxiliary hoops has still to be installed.*

fully demonstrated so far, and now the work will concentrate on other aspects such as the thermal behaviour, safety devices, resistance to extreme conditions.

The safety and reliability aspects are particularly important. In this respect, the coming austral winter will represent a suitable test for the resistance to extreme environmental conditions. The dome was designed to withstand wind speeds of the order of 200 km/h, but with such a particular structure the calculations were inevitably approximate and, although large margins of safety were taken, it is always possible that an unthought-of problem appears. Furthermore, the actual effects and possible damages of a combination of extreme wind, ice and snow conditions can only be verified in reality. This also will be an objective of the present evaluation phase.

Another known major hazard to the dome may come from a prolonged electrical power cut-off as then the internal volume will be quickly depressurized, while the ribs will take 10–20 minutes to deflate, with serious loss in strength and stiffness. For the VLT, independent emergency power generators will be mandatory.

The experiments performed so far are already giving ideas for improvements and optimization in view of the VLT final design. Among the improvements already envisaged, we have the automation of the locking system which is now manual. More ambitious will be the replacement of the present closing/opening mechanisms constituted of winches, cables and auxiliary hoops with hydraulic actuators acting on the main hoops. This will allow the dome to serve also as a wind shield with variable height during observations. This is not possible now because of the auxiliary hoops.

L. ZAGO, ESO

Site Evaluation for the VLT: Seeing Monitor No. 2 Tested in Garching

M. SARAZIN, ESO

The ESO parking lot in Garching must be eliminated from the list of candidate sites for the VLT. During the night of April 19, the second seeing monitor (Fig. 1) underwent final full scale tests before being shipped to La Silla. It was an opportunity to verify that the seeing in Garching is not of the quality that the VLT deserves. During the few minutes we had before the instruments were covered with condensed water, an average seeing of 3 arcsec was measured. (Not all that bad for Europe, though!)

The seeing monitor No. 1 has now been sensing the atmosphere over Cerro Paranal, 2,700 m, for one year (*The Messenger* No. 49, September 1987, p. 37–39) and measurements will continue. In addition to seeing, many parameters are monitored simultaneously so as to acquire full understanding of the environment which a large telescope would meet if this site was chosen.

The summit of Vizcachas, 2,400 m, 5 km from La Silla, is now being prepared for seeing measurements. A road has been completed and a 5 m high tower is being built. The seeing monitor No. 2 will be installed there and will perform measurements in a way exactly identical to its Paranal counterpart. Detector and software are completely interchangeable, yet the telescope has been considerably improved in two ways.

The alt-alt mount has been modified for easier setup, it is now possible to start measurements less than one hour after arriving at a site, which is very convenient when several spots are to be probed or for temporary tests such as measurements inside the dome of a large telescope.

Secondly, autoguiding is now possible, using the same star as for seeing measurements. This, added to the computer control of the ICCD intensification level, provides the possibility to completely automatize seeing measurements in the near future.

For several future applications such as adaptive optics, dome and telescope thermal control, remote observing or flexible scheduling, modern large telescopes will need as much information as possible about their environment, and automatic seeing monitoring stations will soon be considered a vital necessity to boost the efficiency of the astronomical work.

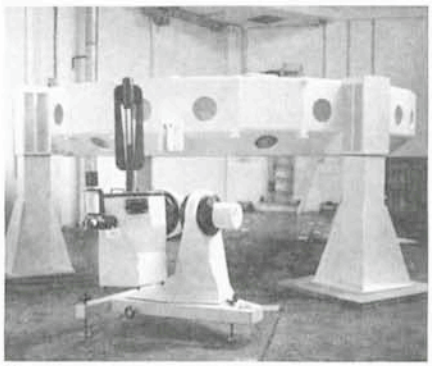

Figure 1: *A pilot fish for modern large telescopes: The Seeing monitor telescope close to the NTT primary mirror cell in the Assembly Hall at the ESO Headquarters in Garching.*

With its Optics Complete, the NTT Telescope Homes In

M. TARENGHI and R. WILSON, ESO

On 11 May 1988 an important event took place for the development of telescope technology at ESO: the NTT optics was successfully tested at Carl Zeiss, FRG. This means that the three mirrors (primary, secondary and Nasmyth) are finished and within specification. The interferometric data currently available for the primary refer to this mirror on its manufacturing support (see Fig. 1). A further series of tests of the primary is scheduled for 1 July on the actual NTT support in its cell. Final acceptance will take place in the finished, functioning telescope in La Silla at the beginning of March 1989.

These results will not only be a milestone in the history of ESO but also a milestone in the history of the reflecting telescope in general. The NTT will be the first telescope to go into operation with a complete active optics control system to maintain constantly an optical performance which will exceed by a clear margin that of any other telescope ever built with the possible exception of the 2.4-m Space Telescope.

To understand the manufacture of the NTT optics, we must look at its specification for the final Nasmyth image:

(a) 80% geometrical energy within 0.40 arcsec

(b) 80% geometrical energy within 0.15 arcsec if 5 terms, to be controlled actively, are mathematically removed from the combined image forming wavefront (Intrinsic Quality).

The active control gives a relaxation of certain errors (such as astigmatism) which enables the manufacturer to concentrate above all on specification (b) which ensures very smooth surfaces without high frequency errors such as "ripple", zones or local bumps. In function, specification (b) should then operate all the time and will be the working specification of the telescope. This is quite near the "diffraction limit" for such a telescope.

The blank with aspect ratio 1 : 15 (2½ × thinner than the blank of the ESO 3.6-m telescope) was delivered from Schott to Carl Zeiss in June 1986. The blank itself represents a great technical achievement by Schott in zero-expansion glass ceramic, Zerodur. Two years of intensive work at Carl Zeiss followed and are now drawing to completion. The NTT specification (b) has required, and resulted in, a remarkable technological development at Carl Zeiss both in figuring techniques and in test technology. With the practical development of "stabilized phase interferometry", Carl Zeiss is now in possession of an excellent and time-saving technology in the manufacture of large optics.

The results of the Carl Zeiss interferometric tests, established in a most rigorous way, are as follows for the whole optical train M1, M2, M3:

(a) 80% geometrical energy within ca. 0.30 arcsec

(b) 80% geometrical energy within ca. 0.125 arcsec for the Intrinsic Quality.

Both values are thus well within the specification. Cross checks with the ESO Shack-Hartmann (ANTARES) test procedure are still being carried out but are essentially in agreement with the interferometric results. However, for technical reasons, specification (b) probably exceeds our measuring precision with Shack-Hartmann in the workshop setup, though we expect to achieve the required precision in the actual, functional telescope.

Meanwhile, work on the NTT telescope and building is advancing rapidly both in Europe and on its location at La Silla, Chile.

The mirror cell is now in Garching for the integration of the active support system and the associated electronics prior to its transport to Zeiss.

The civil engineering work was completed in February 1988, followed by the start of the construction of the rotating building (Fig. 3). At the end of May the steel frame and the external panels were in place (see figure on page 1). Completion is expected by July 1988.

In February and March of this year the telescope's mechanical structure was dismounted and packed at INNSE Brescia (Italy) – where it was manufactured – and then shipped from Genova to Chile on 29 April 1988 (Fig. 2).

On 31 May 1988 the ship "ISLA BALTA" carrying the telescope arrived in the Chilean harbour Valparaiso, and a few days later, on 3 June, the boxes containing the NTT reached La Silla. The enormous task of erecting the telescope will take almost 7 months to complete, starting in June 1988.

Apart from the technical achievement, the NTT contracts have been marked by an excellent spirit of cooperation between industry and ESO.

Figure 1: *The 3.58-m NTT prime mirror at Zeiss with many of the Zeiss colleagues who were involved at various stages of the optical figuring work.*

Figure 2: *Loading of the NTT boxes onto the ship in Genova harbour, 29 April 1988. In the front of the picture the box containing the base of the fork is visible. This box weighs about 44 tons.*

Figure 3: *The rotating building under construction in April 1988.*

Speckle Masking Observations of the Central Object in NGC 3603, Eta Carinae, and the Seyfert Galaxies NGC 7469 and NGC 1068

G. BAIER, J. ECKERT, K.-H. HOFMANN, W. MAUDER, D. SCHERTL, H. WEGHORN, and G. WEIGELT,

Physikalisches Institut, Universität Erlangen-Nürnberg, F.R. Germany

Introduction

Speckle masking bispectrum processing yields diffraction-limited images in spite of image degradation by the atmosphere and by telescope aberrations. For example, with the ESO 3.6-m telescope a resolution of 0.″028 can be obtained at $\lambda \sim 400$ nm. The limiting magnitude is $\sim 18^{m}$.

In speckle masking the same speckle raw data (speckle interferograms) are evaluated as in speckle interferometry. Speckle interferograms are short-exposure images recorded with an exposure time of ~ 10 to 50 msec. Speckle masking consists of the following processing steps (Weigelt, 1977; Weigelt and Wirnitzer, 1983; Lohmann, Weigelt and Wirnitzer, 1983):

(a) calculation of the average bispectrum of all speckle interferograms,
(b) compensation of the photon bias in the average bispectrum,
(c) compensation of the speckle masking transfer function,
(d) derivation of modulus and phase of the object Fourier transform from the object bispectrum.

We will show applications of speckle masking to various types of objects. The speckle raw data were recorded with the 2.2-m ESO/MPG telescope, the Danish 1.5-m telescope, and the 2.2-m Calar Alto telescope.

Central Object in the Giant H II Region NGC 3603

NGC 3603 is one of the strongest H II regions in our galaxy. The central object in NGC 3603 is the star-like object HD 97950 AB. In various papers it has been discussed that this object may be of the same nature as R 136a in the 30 Doradus nebula. Figure 1 is the first diffraction-limited image which shows that the central object in NGC 3603 consists of six stars. In this experiment CLEAN was applied to the speckle masking reconstruction. The stars have magnitudes in the range of 12 to 14. The separation of the closest pair is ~ 0.09″. The image was reconstructed from 300 speckle interferograms recorded with the 2.2-m ESO/MPG telescope (filter RG 610). An image of the four brightest stars was reconstructed by Hofmann and Weigelt (1986).

Eta Carinae

η Carinae is one of the most peculiar objects in our galaxy. It underwent

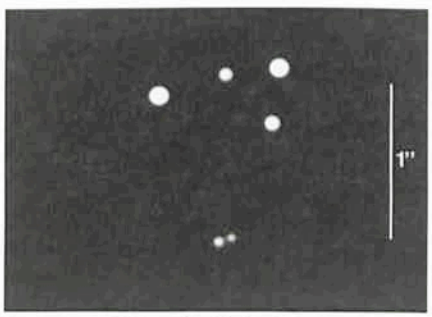

Figure 1: *Diffraction-limited image of the central object in the giant H II region NGC 3603 reconstructed by speckle masking (filter RG 610; North is at the top and East to the left).*

Figure 2: *Diffraction-limited image of η Carinae ABCD (filter RG 830; North is at the top and East to the left).*

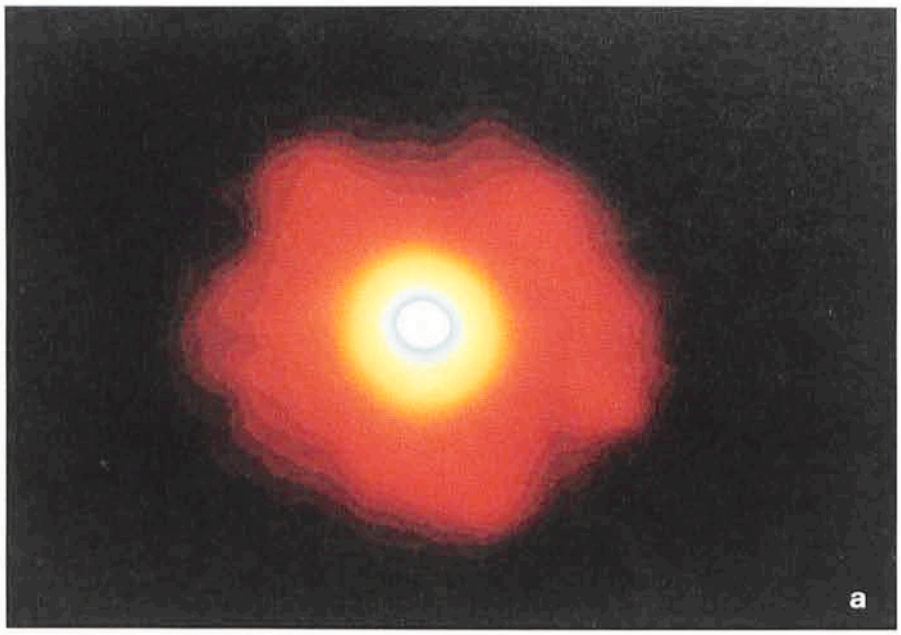

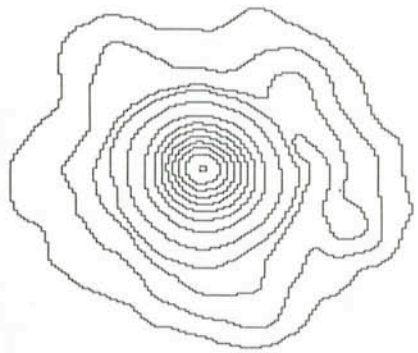

1"

NGC 7469 b

Figures 3a and b: *High-resolution image of NGC 7469 reconstructed by speckle masking (filter: $\lambda_c \sim 610$ nm/$\Delta\lambda \sim 118$ nm; North is at the top and East to the left; isophotes: 1.0, 0.9, 0.8, 0.7, 0.6, 0.5, 0.4, 0.3, 0.2, 0.15, 0.13, 0.11, 0.09).*

dramatic brightness changes during the last 300 years: 4^m in 1667, -1^m during the outburst in 1843, present magnitude $\sim 6^m$. It is surrounded by the homunculus nebula, which consists of material blown from the star during its strong eruption from 1830 to 1860. η Carinae is one of the most extreme IR sources in the sky at $\lambda \sim 20$ μm. Its mass is probably ~ 100 solar masses. Figure 2 is the first diffraction-limited image of η Carinae at optical wavelengths. The image shows that η Carinae consists of a dominant bright star and three faint, star-like objects at separations 0.11″, 0.18″, and 0.21″. The three faint objects are ~ 12 times fainter than the dominant star. The image of η Carinae was reconstructed from 300 speckle interferograms recorded with the 2.2-m ESO/MPG telescope at $\lambda_c \sim 850$ nm (filter RG 830). More details are described in a paper submitted to *Astron. Astrophys.* (Hofmann and Weigelt, 1988).

Seyfert I Galaxy NGC 7469

Figure 3 shows a speckle masking observation of the Seyfert I galaxy NGC 7469 (filter $\lambda_c \sim 610$ nm/$\Delta\lambda \sim 118$ nm). The image was reconstructed from 2,900 speckle interferograms recorded with the 2.2-m telescope at Calar Alto observatory in Spain. The image shows five clouds surrounding the central object. In the next few weeks we will improve the image by reducing additional 15,000 speckle interferograms.

Seyfert II Galaxy NGC 1068

Figure 4 shows an image of the Seyfert II galaxy NGC 1068 reconstructed from 2,400 speckle interferograms by

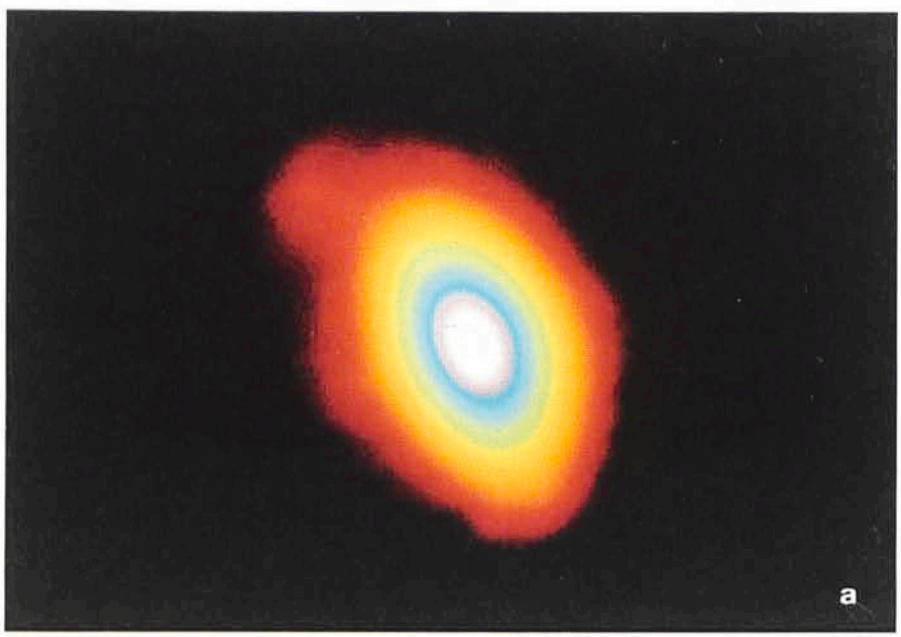

1"

NGC 1068 (O III) b

Figures 4a and b: *High-resolution image of NGC 1068 reconstructed by speckle masking (filter: $\lambda_c \sim 501$ nm/$\Delta\lambda \sim 25$ nm; North is at the top and East to the left; isophotes: 1.0, 0.9, 0.8, 0.7, 0.6, 0.5, 0.4, 0.3, 0.25, 0,20, 0.15)*

speckle masking. The speckle interferograms were recorded with the Danish 1.5-m telescope and an OIII filter ($\lambda_c \sim 501$ nm/$\Delta\lambda \sim 25$ nm). There is an interesting similarity between the OIII image and radio images.

References

Hofmann, K.-H., Weigelt, G., 1986, *Astron. Astrophys.* **167,** L 15.

Hofmann, K.-H., Weigelt, G., 1988, "Speckle masking observation of Eta Carinae" (submitted to *Astron. Astrophys.*).

Lohmann, A.W., Weigelt, G., Wirnitzer, B., 1983, *Appl. Opt.* **22,** 4028.

Weigelt, G., 1977, *Opt. Commun.* **21,** 55.

Weigelt, G., Wirnitzer, B., 1983, *Opt. Lett.* **8,** 389.

SN 1987 A (continued)

The study of SN 1987 A continues to occupy many astronomers at the major southern observatories. Some of the programmes have now settled down to routine, while others exploit new techniques, all in order to harvest as much information as possible from this rare event.

Since the last summary of recent developments in this journal (*The Messenger* **51,** 9), new and exciting observations at the European Southern Observatory have become available, which probe the interstellar space at different distances from the supernova by means of very different techniques.

On the smallest angular scale, *speckle masking observations* in the visual and near infrared spectral regions have been made in December 1987 by a group from the Erlangen-Nürnberg University, working at the ESO/MPG 2.2-m telescope. With this powerful method they are able to establish upper limits for the size of the expanding supernova shell, which was ejected at the time of the explosion last February. Their value is around 0.023 arcsec. They will report their results for the supernova in a future issue of the *Messenger.*

The summary about *infrared speckle observations* by Chalabaev and co-authors with the ESO 3.6-m telescope (*The Messenger* **50,** 21) has now been followed up by a comprehensive paper, which was submitted to the journal *Nature* in April 1988. The detection of an infrared light echo is confirmed with a radius of 0.350 arcsec on August 6, 1987.

This infrared echo is thought to result from the thermal re-radiation of the initial light flash by dust grains formed during a previous phase, when the exploding star Sanduleak −69°202 had been a red supergiant with a strong mass loss. From the date of the first detected infrared light echo, the size of the dust-free shell can be estimated. Knowing also the outward velocity of the material, it would appear that the red supergiant mass loss phase ended only a few thousand years before the explosion.

This is also a result of *high-resolution spectral observations* by Wampler and Richichi, reported in this *Messenger* issue. This paper shows for the first time an image of the shell of material from the mass loss phase, measuring about 2 arcsec across. The observations were made in 1988 with the CES and the 1.4-m CAT telescope. A more detailed report has now been submitted to the journal *Astronomy and Astrophysics.*

On a still larger scale, a *double, visible light echo* has recently been detected. Contrary to the infrared echo referred to above, this echo arises from the reflection of the bright supernova light in interstellar clouds much farther away from the exploded star.

Astronomers had been searching for this phenomenon since last year. A detection on March 3, 1988, was announced by A. Crotts from McDonald Observatory, Texas, USA. However, by inspection of earlier images made at the European Southern Observatory, it was seen on CCD frames made on January 25 by H. Pedersen with the Danish 1.5-m telescope and also on February 13, by M. Rosa with the ESO 3.6-m telescope. Later, it was also found that the outer echo can be seen as early as in August 1987, on EFOSC CCD frames obtained by S. D'Odorico, and also on a dozen Schmidt photographic plates after November 1987. Further observations were made in mid-March, with the

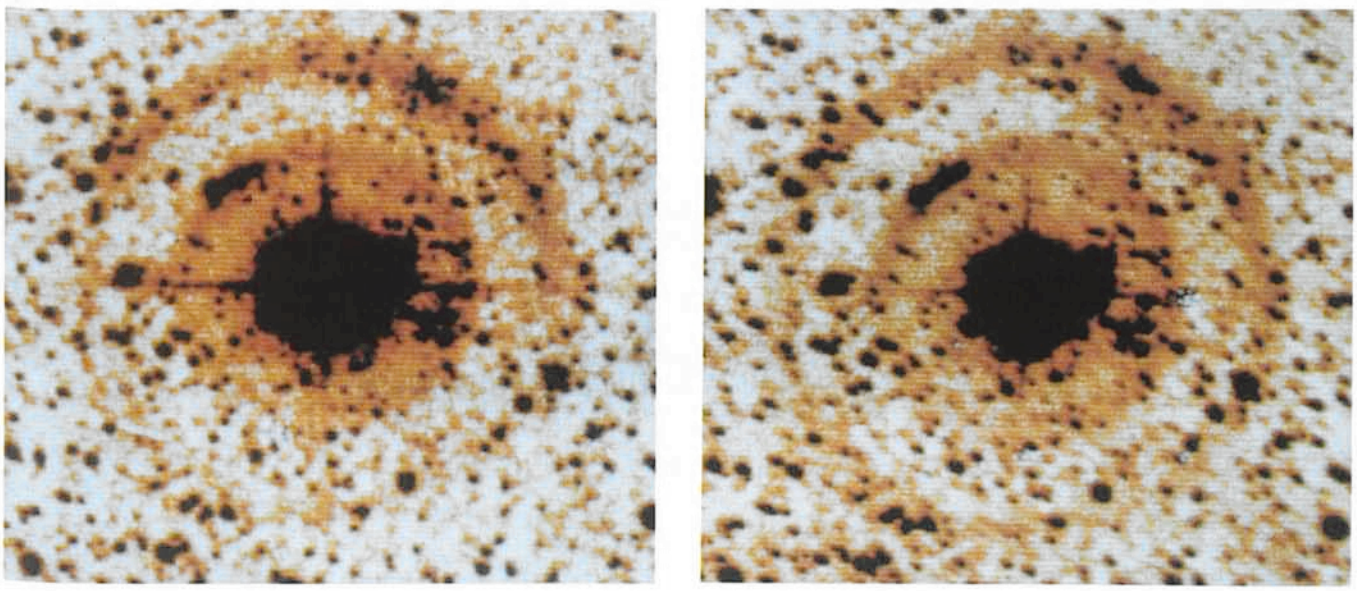

CCD images of the double light echo around SN 1987A, as observed with the ESO 3.6-m telescope and EFOSC with a coronographic mask on February 13, 1988 (left) and March 16, 1988 (right). A 6 nm wide filter at wavelength 470 nm suppressed the light from the emission nebulae in this region. Observers: M. Rosa, Chr. Gouiffes and M.T. Ruiz. A careful comparison shows the expansion, at present about 3 arcsec/month.

EFOSC instrument at the 3.6-m telescope, see the figure. A team of nine astronomers have now submitted a Letter to the Editor of *Astronomy and Astrophysics*, with expected publication in the June(I) 1988 issue. This paper is also available as ESO Preprint no. 591.

For these exposures, the bright light from the supernova itself was dimmed by the insertion of a small, obscuring disk into EFOSC. Two almost concentric rings are clearly visible. On February 13, the radii were 32 and 52 arcseconds. The rings are brighter towards North, because there is more interstellar matter in this direction. The integrated intensity of the light echo is about 2,000 times fainter than the current brightness of the supernova and is in agreement with the predicted intensity.

EFOSC spectra of the rings were also obtained, proving that they are the reflected supernova light from the time of the maximum, in May 1987. From the time delay and the angular dimensions of these rings, it can be inferred that the reflecting clouds are at distances of approximately 120 and 315 pc in front of the supernova, respectively.

Continued observations of these light echoes will allow to determine the three-dimensional structure of the interstellar clouds near the line-of-sight to the supernova (like a movie). The rings currently expand by about 3 arcsec per month and variations in the brightness along the periphery will indicate variations in the density of the reflecting material.

Among the other observations of SN 1987A during the past three months, there is a notable activity around the infrared spectra being obtained with the Kuiper Airborne Observatory; they show important and rapid changes, while the total infrared intensity decreases as the supernova fades. In early May 1988, the visual magnitude was around 7.5, or almost 100 times fainter than at maximum last year.

Several successful observations of SN 1987A during balloon flights with γ-ray detectors have been reported. One of these instruments, the Caltech Imaging Gamma-Ray Spectrometer, was flown from Alice Springs in Australia and yielded some of the first γ-ray pictures ever taken of any celestial object. *R. M. WEST (ESO)*

Observations of the Antique Wind of SN 1987A

E. J. WAMPLER and A. RICHICHI, ESO

In the last days of 1987, green spectra of SN 1987A obtained with the ESO Cassegrain Echelle Spectrograph (CASPEC) and the 3.6-m telescope, show strong, narrow lines of forbidden [OIII]. These [OIII] lines are very narrow, in marked contrast to the wide emission lines emitted by the expanding supernova shell. In fact, their observed width is largely determined by the resolution of CASPEC (about 12.5 km/sec). For comparison, the strongest lines in the expanding supernova envelope, such as Hα, show velocity widths of several thousand km/sec. And the narrowest features that can be associated with the envelope itself, such as the substructure seen in the [OI] $\lambda\lambda$ 6300, 6364 lines, have velocity widths of several hundred km/sec. Thus the [OIII] lines point to an ionized region associated with the supernova but distinct from the expanding envelope.

We describe here our observations and give the arguments for believing that we are seeing fluorescence radiation caused when the ultraviolet flash of SN 1987A ionized a shock front that had previously been generated in the progenitor wind when the star switched from a red to a blue supergiant. From the diameter of the nebula we can estimate the duration of the blue supergiant phase that culminated in the explosion of SN 1987A. This age is less than 10,000 years. We have, therefore, decided to call the red supergiant wind an "antique" wind to emphasize that it stopped blowing on a time scale comparable to the age of human civilization.

Using CASPEC with the 31.6 ℓ/mm grating, SN 1987A was observed at the end of October and again at the end of December. The wavelength interval 3700 Å–9500 Å was covered. Following the discovery of [OIII] λ 5007, the supernova spectrum was searched for other identifiable narrow features. In addition to [OIII] λ 5007, we have found [OIII] λ 4959 and λ 4363, together with Hβ, Hγ and, possibly, Hδ and HeII λ 4686. None of these features, which are present in the December spectra, are seen in the October spectra of the supernova. Of course, the supernova was much brighter in October than it was in December. Also, the spectra we obtained in October have a lower S/N ratio than those obtained in December. Thus it is not surprising that we did not see the weaker lines which are near the limit of detection even in the December data. But we also failed to detect [OIII] λ 5007 in October, a line that is very strong in December. We estimate that we would have clearly seen a feature if it had been $\frac{1}{2}$ as strong in October as in December. While it is difficult to set a precise upper limit to the October line strength, it does appear that [OIII] λ 5007 increased substantially in strength between October and December.

Figure 1 shows the lines that we found in the December spectra of SN 1987A. The peak intensities of the individual lines are given in fractions of the continuum intensities. Note that many of the lines have peak intensities only a few per cent above the local continuum. The equivalent widths ranged from about 5 to about 50 milli-

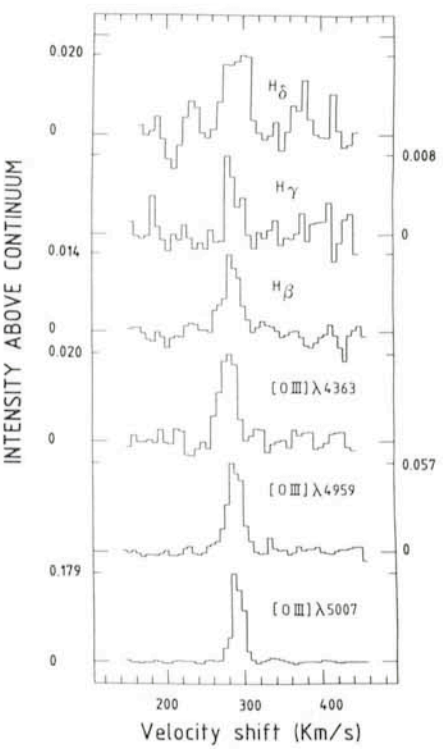

Figure 1: *CASPEC observations of narrow emission lines in SN 1987A. The intensity of the peak of each line, in units of the fractional intensity above the continuum, is given.*

angstroms. The velocity widths (~ 15 km/sec) of the observed lines are appropriate for galactic HII regions or the velocities of outflowing winds from red supergiant stars. Other types of stellar winds, such as found for blue supergiants, WR stars, etc. have wind velocities one to two orders of magnitude greater than the velocities seen here. The possibility that the nebula is a normal galactic HII region can be ruled out as it is very highly ionized. The ratio of the O^{++} lines to Hβ is much higher than is seen in HII regions or even planetary nebulae. Also, the ratio of [OIII] λ 4363 / [OIII] λ 5007, which is temperature sensitive, gives a gas temperature of about 55,000°K instead of the 9,000–10,000°K expected for HII regions.

As the CASPEC data did not have sufficient resolution to determine the velocity structure of the [OIII] λ 5007 line and also because the CASPEC spectra were trailed in order to improve the signal-to-noise ratio, we decided to obtain untrailed spectra of SN 1987A using the ESO 1.4-m CAT together with the CES. The peak intensity of [OIII] λ 5007 was quite strong relative to the local continuum so that observations with CES at a spectral resolution of about 60,000 were relatively easy. H. Schwarz, D. Gillet, P. Molaro, S. D'Odorico and U. Munari very generously shared some of their CES time so that we could obtain a series of high resolution spectra of the λ 5007 region during the January-March 1988 interval. Figure 2 shows the results obtained from a spectrum taken on March 25, 1988. The line is clearly resolved. The full-width-half-maximum is about 14.5 km/sec and the heliocentric velocity is 286.3 ± 0.8 km/sec. This is in agreement with the idea that the line comes from a shell within the red giant wind.

Starting in late May 1987, IUE spectra of SN 1987A showed lines of HeII, CIII, NIII, NIV, and OIII which increased in strength with time (Fransson et al. 1988). These line widths were narrower than the IUE instrumental profile (ca. 30 km/sec). Their mean velocity, 284 ± 6 km/sec, agrees with the velocity of the optical emission lines seen in the CES spectra as well as a 284.8 km/sec component of the interstellar absorption lines (Vidal-Madjar et al. 1987). Thus it would appear that all of these features come from the same ionized cloud. While the IUE data do not provide an accurate estimate of the gas temperature, the ratio of CIII] λ 1906.7 to CIII] λ 1908.7 does give the density. Using the temperature determined from the optical [OIII] lines and the λ 1906.7/ λ 1908.7 ratio given by Fransson et al. (1988), we find that $N_e \approx 3\times10^4$ cm^3. In addition it is possible to use the IUE data to study the abundances in the nebula. A preliminary estimate (Fransson et al. 1988) indicates that nitrogen is very much over-abundant relative to carbon and oxygen.

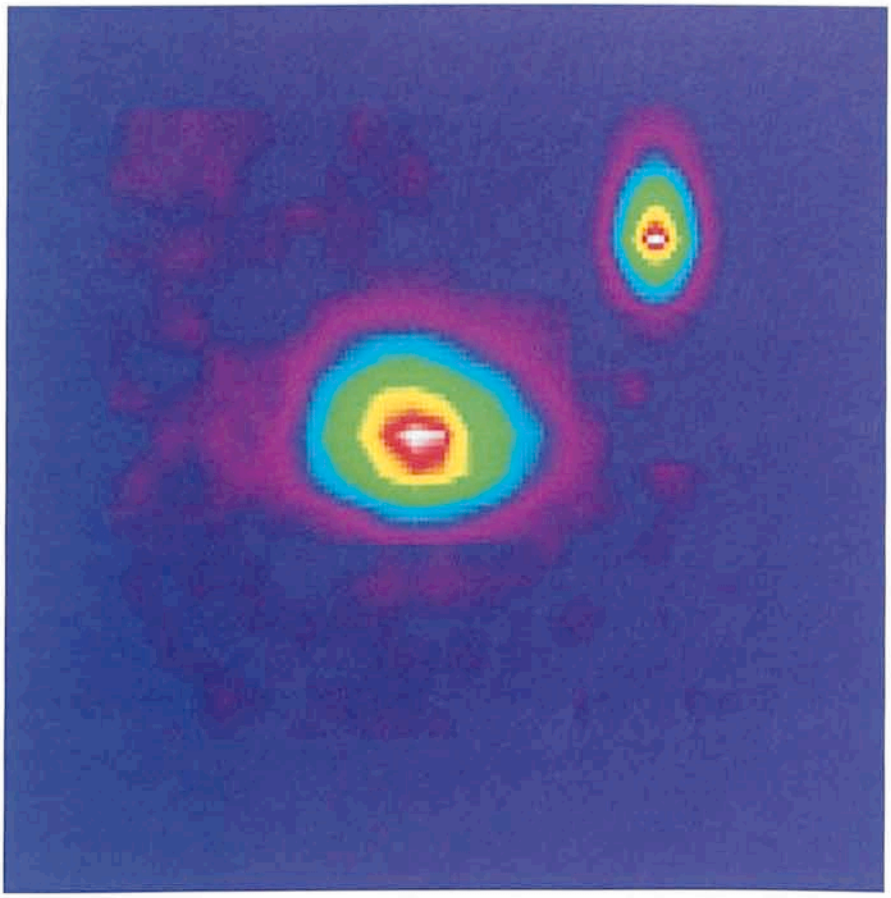

Figure 2: *The smoothed structure of [OIII] λ 5007 from a March 26, 1988 CES spectrum (centre). The image in the upper right is the instrumental profile for this observation. The position along the slit (ordinate) is given as a function of wavelength (abscissa). The outer, deep blue, contour of the instrumental profile image measures 10.4 km/sec by 3.2 arcsec. The asymmetry of the instrumental profile in the slit direction was caused by imperfect telescope tracking.*

Taken together, all the available data suggest that the narrow lines originate from a slow moving, heavy element enriched, remnant stellar wind that is near the supernova. The most plausible origin for this wind is that it came from the supernova's progenitor during an earlier, red giant phase in its evolution. Enough material was removed from the progenitor during this phase that a substantial amount of the end products of nuclear burning were ejected along with the hydrogen rich portion of the envelope. Then, when the supernova progenitor switched to a blue supergiant, the high velocity blue supergiant wind expanded into the older antique red supergiant wind and compressed the gas to the observed density of about 3×10^4 cm^{-3} behind the expanding shock front. The shock interface between the red and blue supergiant winds is expected to expand with a velocity of 50–100 km/sec, depending on the relative strengths of the two stellar winds. When SN 1987A exploded, the initial ultraviolet flash from the explosion ionized this compact nebula and drove the temperature to at least 55,000°K. We are now seeing it as it cools down. The diameter of the nebula gives the position of the shock front and therefore an estimate to the amount of time that has passed since the blue supergiant wind started blowing. By deconvolving the two-dimensional line profile of Figure 2 with the measured instrumental profile shown in the upper right corner of the figure, we find that the nebula extends about 2 arcseconds along the spectrograph slit. This is surprisingly small. At the distance of the LMC one arcsecond corresponds to 1 light-year. A shock front travelling at 50 km/sec can cover that distance in less than 7,000 years. Thus the progenitor could only have remained in the penultimate, blue supergiant, phase for a similar time. This suggests that the supernova exploded only a short time after it became a blue supergiant.

If it had been a blue supergiant for a

longer time, the shock front should have progressed much further into the antique red supergiant wind and the nebula would have been much larger. It is not likely that we are seeing only part of a much larger nebula: first, it has been over a year since the supernova exploded. But the angular radius of the nebula is only about one light-year. Thus, we are not seeing the apparent superluminal expansion that would be expected if the actual size of the nebula was much larger. And second, the detected flux of [O III] λ 5007 has remained approximately constant since February 1, 1988. Therefore we are not seeing the rapid increase in flux that would signal an expanding linear radius of the nebula.

It is also not likely that we are witnessing the interaction of the fast moving outer parts of the supernova envelope with the surrounding medium. In this case the nebula that we see is rather large to be produced by particle interaction from the expanding outer shell of the supernova and, in addition, the X-rays that would be expected to accompany the collisions should be rapidly increasing in strength as the density of particles increases. This is not happening.

Model calculations (Woosley, 1988) show that the final blue supergiant lifetime implied by the diameter of the nebula is the same as the time for the outer stellar envelope to reach equilibrium. But, to explode, the progenitor must form a massive iron core. If, as the Woosley models suggest, the star returns to the blue part of the H-R diagram after helium exhaustion, the mass of the helium core determines the length of time for carbon, neon, oxygen and silicon burning before the final collapse of the iron core to produce the supernova event. This time is dominated by the helium core collapse and the carbon burning lifetime. Woosley finds that stellar models that have about 19 solar masses of material when they are on the main sequence end up with helium cores in about the right mass range to power the SN 1987A explosion. An 18 $M_\odot$ star ends up with a helium core near 5 $M_\odot$. This star would explode 70,000 years after it switches to the blue supergiant phase. A 20 $M_\odot$ star produces a 6 $M_\odot$ helium core and explodes after 20,000 years.

These calculations suggest that it will be possible to construct a model that will be a good fit to all the observational data. Rotation, the $^{12}C\ (\alpha,\delta)\ ^{16}O$ reaction rate, convection, etc. can all affect the lifetime of the last stages of stellar evolution. And, observationally, the radius of the nebula is still somewhat uncertain. The important point to make is that observations of this nebula together with theoretical calculations are likely to provide important additional constraints on SN 1987A models. It is probably fortuitous that the first estimate of the duration of the blue supergiant wind is comparable to the Kelvin Helmholtz contraction time for the progenitor envelope. We observers, therefore, don't have to worry too much about the details of the helium core. The contraction of the outer envelope is decoupled from the details of the inner core physics. We need only to model the outer envelope contraction to obtain the time dependence of the progenitor radiation field that drives the shock wave into the red supergiant wind. This, in turn, will lead to a more accurate velocity for the shock and, hence, a better estimate for the time interval between the time of helium core collapse and the supernova explosion.

Finally, of course, the very existence of the nebula shows that there *was* a red giant phase for the progenitor of SN 1987A. This by itself eliminates all those models that explode before they reach a red giant phase.

This small nebula from the antique red giant wind has proven to be an important new clue for understanding SN 1987A. As the supernova fades, the contrast of the nebula will increase and the spatial information will be easier to obtain. Then the observational constraints can be greatly improved.

References

Fransson, C., Cassatella, A., Gilmozzi, R., Panagia, N., Wamsteker, W., Kirshner, R.P. and Sonneborn, G. 1988, *Astrophys. J.* (in press).

Vidal-Madjar, A., Andreani, P., Cristiani, S., Ferlet, R., Lang, T. and Vladilo, G. 1987, *Astron. Astrophys.* **177,** L 17.

Woosley, S.E. 1988, *Astrophys. J.* (in press) and private communication.

Deep Photometry of Supernovae

M. DELLA VALLE[1], E. CAPPELLARO[2], S. ORTOLANI[2], and M. TURATTO[2]

[1] Dipartimento di Astronomia, Padova, Italy; [2] Osservatorio Astronomico, Asiago, Italy

1. Introduction

Supernovae are among the more exciting transient astronomical phenomena. Unfortunately the interest for them appears to fade faster than their luminosity. Only for one fifth of the 637 confirmed supernovae discovered up to the end of 1987, there are sufficient data to describe the photometric evolution; moreover, the majority of the published light curves are limited to the first two or three months after the maximum. On the other hand, the knowledge of the faintest tail of supernova light curves can give useful constraints in the discrimination among different theoretical models (Sutherland et al., 1984). The analysis of data available in literature, allowed Barbon et al. (1984) to investigate the behaviour of the late decline of supernovae. They showed that the late light curves can be described by a single exponential decay with different rates of decline, $< \gamma^B_{200^d} > \simeq 1.52$ mag/100^d for type Ia SNe (half-life 49^d.5) and $< \gamma^B_{200^d} > \simeq 0.81$ mag/100^d for type II SNe (half-life 93^d), favouring therefore the possibility that the $Ni^{56}-Co^{56}-Fe^{56}$ radioactive decay is the main energy source up to these stages. More recently the bibliographical material of type II SNe has been used by Schaefer (1987a) to test the effect of light echoes in the B-band light curves, but the shortage of observations compelled him to include objects not observed at very late stage. He claimed to find different decline rates and argued that scattered light echo in the circumstellar dust can dominate the shape of the light curves of supernovae. To progress on this subject we decided to start photometric observations of supernovae at intermediate and late stages, extending to much fainter limits the extensive SN survey carried out at Asiago Observatory in the last thirty years by Rosino and collaborators.

2. Observations

The first observing session was performed at the 1.5-m Danish telescope equipped with RCA 320 × 512 #3 CCD on 17–19 January 1988. The sample of

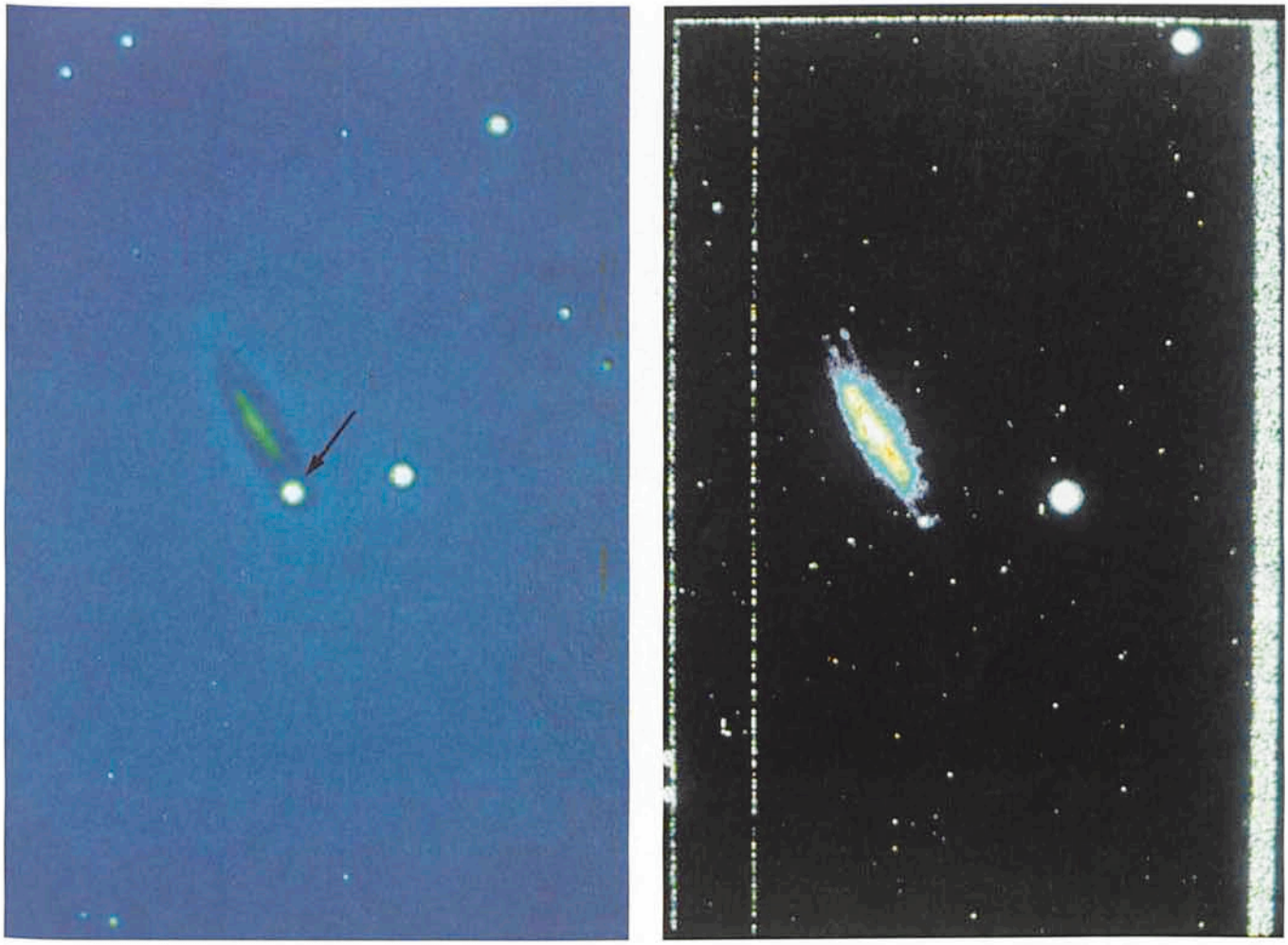

Figure 1. *On the left (Fig. 1a) is represented a V frame of MCG +00-32-01 obtained at the end of April, 1987, when the SN 1987d was at its bright stage. The image on the right (Fig. 1b) shows the same object at the time of our last observation. In both cases North is on the top and East is on the right.*

objects investigated was selected according to the following requirements:

- magnitude in the 19–23 range, estimated by means of the average light curves, for the first decline, and via linear decay rates (Barbon et al. 1984) for the late decline;
- availability of a detailed map of the field containing the supernova at its bright stage;
- existence of photometry at early stages.

For each object B, V and R frames were obtained with 40, 25 and 20 minutes typical exposures, which allowed to reach a S/N $\geq$ 10 for a V = 23 supernova with a typical seeing of 1.2 arcseconds. Preliminary reduction of the B and V frames, including de-biasing, flat-fielding and flux measurements, was carried out with MIDAS package at the Observatory of Padova. The calibrations were performed using Landolt's standard stars, obtaining colour terms remarkably similar to previous determinations at La Silla. The inspection of the material has pointed out that, for the determination of the magnitude, each object has to be treated individually, and moreover that particular care has to be devoted to the subtraction of the local galaxy contribution, which, at low level, can affect strongly the measurement. When possible, for objects visible also in the northern latitude, the maps of the SNe were secured at Asiago, in other cases, good quality maps of supernovae kindly provided by B. Leibundgut, C. Pollas, R. Evans and M. Wischnjewsky have been very useful. In fact, even for objects with precise absolute position it is very difficult to go back to the position of the supernova at this faint stage when no other bright stellar objects are present on the frame, an accurate determination of the galaxy centre being usually very difficult. The easiest identification was that of 1986e in NGC 4302 for which King (IAU Circ. 4206) reported the position relative to a near foreground star. Therefore, for such a programme it should be recommendable that astrometrists give positions relative to near stellar objects.

Table 1 reports the list of objects, their type, the phase at the time of the observations and the preliminary determinations of the magnitude in the B and V systems. The typical magnitude at maximum light for all our objects was B = 14 ÷ 15. We estimate the accuracy of our measurements to be about 0.1 mag. for objects brighter than 21 mag. located in regions with smooth and uniform background, rising up to 0.5 mag. in the most unfavourable cases, i.e. 23 mag. objects situated in very confused regions. In the last column we report the expected magnitude of each object at the time of observation assuming the linear decline determined by Barbon et al. (1984) for the corresponding supernova type. At the time of the preparation of this communication, no detailed investigation on such objects is available, so the date and magnitude at maximum light are not accurately known. The predictions are then thought to bring an indetermination of 0.3 magnitudes in the expected value of the magnitude of the supernova at the phase of the observations.

3. Discussion

From the inspection of Table 1 two facts appear evident:

Figure 2. *V frame of SN 1986e in NGC 4302. North is on the top and East on the left.*

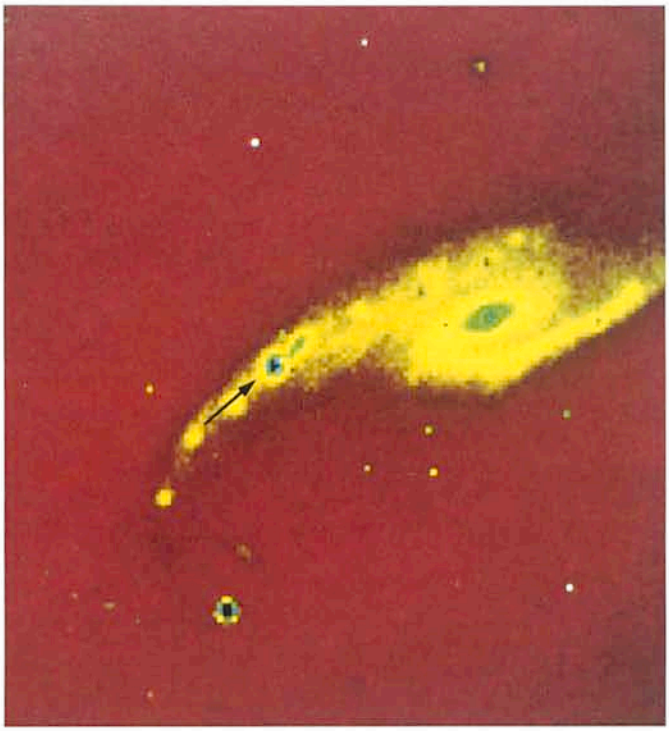

Figure 3. *The arrow indicates the SN 1987f in NGC 4615 on a (B-V) frame. North and East as in Fig. 2.*

– The correspondence between the observed and the estimated magnitudes via linear decline for the objects of the sample is fairly good. A slight systematic trend to increase the previous value of the slope at the late decline stage may exist. Therefore, the input of energy from light echoes seems to play a minor role compared to the supply from radioactive decay (at least for the objects of the sample).

– The value of the colour index must be taken with care; before discussing the intrinsic properties of the objects, the reddening due to the galactic and internal absorption of the parent galaxy has to be taken into account. Nevertheless, even without the correction, it appears that SN Ia colour curves tend to stabilize around (B-V) $\simeq$ 0 in analogy to the SN Ia 1972e in NGC 5253 (Ardeberg and de Groot, 1974). The situation for the type II SNe is less clear because the observed B-V colour index could be strongly contaminated by the underlying HII region. A more complete analysis of data after the reduction of photometry at intermediate stages and of the R frames at late stages, will make possible to account for reddening and to determine accurately the individual fading rate, thus providing better constraints to SNe evolutionary models.

4. SN 1986g in Cen A

Finally we spend a few words on SN 1986g in NGC 5128, which recently has been pointed out as one of the best candidates (Schaefer 1987b) for the detection of light echoes. A V frame was obtained on May 20, 1987 with the same equipment as for the other objects, and with similar conditions. The precise position has been determined by means of a previous frame, obtained when the SN was near maximum light and the magnitude has been carefully measured via Daophot and Inventory programmes. The calibration of the frame has perfectly confirmed the magnitudes of the field stars used for relative photometry by Phillips et al. (1987) and Schaefer. Since the colour index of the type Ia SNe during the late decline is almost constant, one might expect that $\gamma^B \approx \gamma^V$ and in fact, from the last tail of the V light curve (Phillips et al.) and our measurement (at phase 374^d), we obtain a rate of decline, $\gamma^V \simeq 1.77$ mag/100^d, which is comparable to both the γ^B, $\simeq$ 1.88 mag/100^d by Phillips et al., and with the quoted $< \gamma^B >$ decline rate. Even in this case, hence, our results show no significant effects due to echoes (at this stage). The only indication, in this sense, seems to come from Schaefer's B estimate of June 1987, that induces to look at the SN 1986g as the only doubtful case among the observed ones.

References

Ardeberg, A.L., de Groot, M. 1974, *Supernovae and Supernova Remnants* ed. C.B. Cosmovici, Reidel, Dordrecht **45,** 103.

Barbon, R., Cappellaro, E., Turatto, M., 1984, *Astron. Astrophys.*, **135,** 27.

Phillips, M.M., et al. 1987, *Pub.A.S.P.*, **99,** 592.

Schaefer, B., 1987a, *Ap.J.*, **323,** L51.

Schaefer, B., 1987B, *Ap.J.*, **323,** L47.

Sutherland, P.G., Wheeler, J.C. 1984, *Ap.J.*, **237,** 541.

TABLE 1

List of objects

Supernova		Type	Phase days	Observed		Expec.
				B	V	B
1985p	NGC 1433	II	820	22.5	22.4	22.1
1986e	NGC 4302	II	645	22.3	21.9	22.4
1986i	NGC 4254	II	610	–	23.4	23.4
1986l	NGC 1559	II	470	19.8	–	20.2
1986o	NGC 2227	Ia	390	23.0	23.0	22.4
1987d	MCG + 00-32-01	Ia	270	20.3	20.4	19.9
1987f	NGC 4615	II pec	290	20.0	18.7	20.2
1987k	NGC 4651	II	180	20.0	19.6	19.4
1986g	NGC 5128	Ia	374	–	20.3	V 20.1

A Hole in the Hat or Evidence for a Black Hole in the Sombrero Galaxy?

B. J. JARVIS, P. DUBATH, Observatoire de Genève, Switzerland

1. Introduction

Studies of the nuclei of normal galaxies have received renewed interest in the past few years partially due to new detector technology, particularly CCD's, used in both direct imaging and spectroscopic modes. This has led to the understanding that the nuclei of some of these galaxies are dynamically complex systems exhibiting unusual kinematic and photometric behaviour compared to the surrounding bulge. The most notable examples are M87 (eg. Sargent et al., 1978), M31 (eg. Kormendy, 1988) and M32 (Dressler and Richstone, 1987). High spatial resolution kinematic data of the nuclei of these galaxies revealed the presence of large increases in velocity dispersion and large velocity gradients over the central few arcseconds. Both of these studies concluded that a central black hole most adequately explained the very large increase in central mass-to-light ratio.

The likely presence of black holes in two of the closest galaxies with bulge-like components compels us to look at the nuclei of other nearby or large galaxies to see if they also show evidence for supermassive objects. We report here the initial results of new kinematic data for the major axis of NGC 4594 (M104) which are shown to have large kinematic similarities with those galaxies already believed to possess black holes.

2. Observations and Reduction Procedures

The long-slit spectroscopic data were obtained with the Boller and Chivens spectrograph attached to the 3.6-m telescope at La Silla, Chile. The detector was an RCA CCD (512 × 320 pixels) with pixel sizes of 1.74 Å by 1.″17. We used a grating with a dispersion of 59 Å mm^{-1} which gave an instrumental dispersion of 60 km s^{-1} with a 2″ slit. Our spectra covered about 900 Å centred on the Mg b absorption lines at 5175 Å. See Jarvis et al. (1988) for a more detailed description of the instrumental setup. We observed a total of 5 × 1,020 s (= 5,100 s) exposures with the slit aligned along the major axis of the galaxy passing through the nucleus at a position angle of 270°. The reduction and analysis followed now fairly standard procedures for this type of data and the reader is again referred to Jarvis et al. (1988) for details.

Our final absorption line velocity and dispersion data are shown in Figure 2. The major axis kinematic data obtained by Kormendy and Illingworth (1982; hereafter KI) are also plotted for comparison as open circles. In an attempt to preserve the signal-to-noise ratio of the data with increasing r, we have averaged together groups of adjacent rows in the outer parts of the galaxy. These are shown as horizontal bars in the figure.

3. Discussion

The first point to note is the overall excellent agreement between the independent data sets of KI and that of this paper. This was our original and only motivation for observing this galaxy, to check our reduction and analysis techniques against those of others before proceeding on another programme. We have arbitrarily assigned a radius of zero to the brightest row in our spectra which due to the large spatial scale of 1.″17 $pixel^{-1}$ probably accounts for most of the difference between the velocity of the inner rotation peaks at $r \simeq \pm 15''$. Previous independent measurements of the central velocity dispersion of NGC 4594 range from 215 ± 35 km s^{-1} by Williams (1977) to 263 ± 32 km s^{-1} measured by Whitmore et al. (1979). In comparison, Schechter (1983) found 248 ± 29 km s^{1} and KI found 256 ± 22 km s^{-1}. Our final value of 249 ± 15 km s^{-1} is in good agreement with both these last measurements. In view of the rapid decrease of velocity dispersion within the central few arcseconds, it is apparent that the major sources of difference between the above measures are probably due to small centring errors of the spectrograph slit and seeing differences. We conclude, therefore, that our measurement of the central velocity dispersion is likely to be a lower limit due to our mediocre seeing, fairly large slit width and coarse spatial scale.

There appears to be at least two distinct dynamical components in both the rotation and dispersion profiles. It is clear that exterior to $|r| \simeq 15''$, where the bulge is dominating the observable light, we are measuring the rotational motion of the large spheroidal bulge component. Interior to $|r| \simeq 15''$, the situation is more complex. It appears that the kinematics are dominated by a rapidly rotating nucleus which has a fairly constant velocity gradient of 38 km s^{-1} $arcsec^{-1}$ for $|r| \leq 3.''5$. Additional information on the detailed shape of the nucleus requires kinematic data at different position angles.

The most striking feature of the velocity dispersion profile is the sharp increase in the central few arcseconds.

Figure 1: *The Sombrero galaxy, photographed in the prime focus of the ESO 3.6-m telescope. Observer: S. Laustsen. Colour composite of three B/W exposures.*

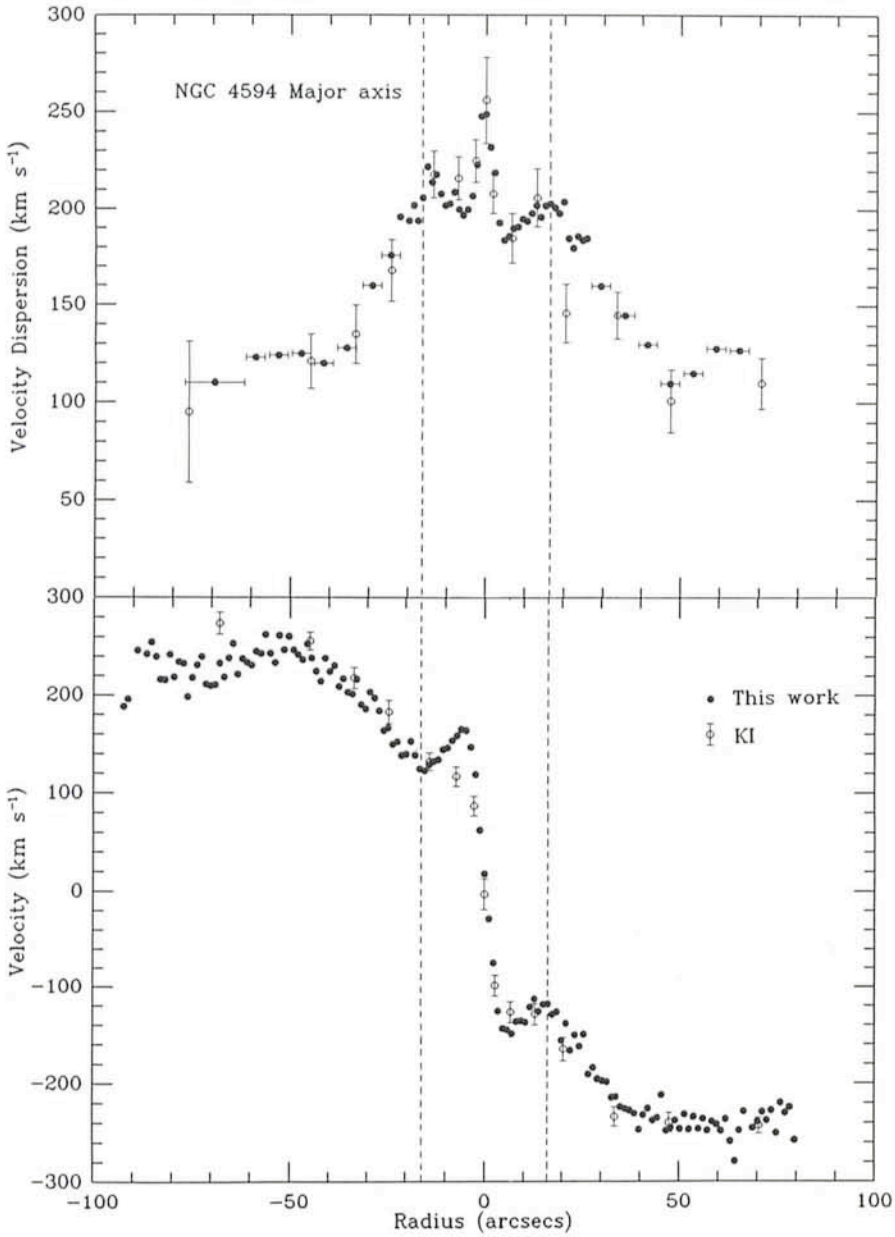

Figure 2: *Major axis rotation (lower panel) and velocity dispersion (upper panel) profiles for NGC 4594. Negative radii denote points east of the nucleus. Units of velocity and velocity dispersion are km s^{-1}. The horizontal bars in the dispersion profile show the extents of averaging adjacent rows to increase the signal-to-noise ratio. Overplotted as open points are the data from Kormendy and Illingworth (1982) for comparison.*

The dispersion rises by at least 65 km s^{-1} on the west side of the nucleus and 52 km s^{-1} on the east over a distance of about 4″.5, much wider than the seeing point-spread-function (PSF). Again, these are probably lower limits due to the finite seeing PSF and the fairly large slit width used. This rapid increase in dispersion is similar to what has been observed in M31 and M32 by Kormendy (1988), Dressler and Richstone (1988) and others. They concluded that the sharp increase in velocity dispersion and the large velocity gradient indicated a significant increase in M/L above that of the surrounding bulge. Moreover, for M31, Kormendy concluded that a central black hole as large as 10^7-10^8 $M_\odot$ was the most likely alternative although a very massive star cluster could not be completely ruled out. Little or no conclusive evidence exists for a corresponding sharp increase in the observed nuclear luminosity of NGC 4594. However, Burkhead (1986) visually observed a bright compact nucleus but this requires quantifying by observation in good seeing.

Unfortunately, a full and complete analysis of the data is hampered by the lack of a good measurement of the seeing during our observation, since there were no observable stars near the slit. However, we estimate that the seeing was between 1″.2 and 1″.5 based on reports from other telescopes on La Silla observing at the same time. Some simple experiments involving the convolution of infinitely sharp jumps in simulated rotation profiles with the seeing PSF showed that the observed velocity gradient is not significantly affected by the seeing but more likely due to the low spatial resolution of the instrument (1″.17 pixel^{-1}) and the relatively large slit-width. Again, we stress that no attempt was made to optimize the instrumental setup for high spatial resolution observations.

An estimate of the total mass inside a radius r can be calculated from the Vlasov equation,

$$M(r) = \frac{V^2 r}{G} - \frac{r^2}{\varrho G}\frac{d}{dr}(\varrho\sigma^2)$$

where ϱ is the stellar volume density, V is the rotation velocity, σ is the radial component of the velocity dispersion and G is the gravitational constant. If we assume that the mass distribution is spherical, the mean rotation is circular and the stellar motions are isothermally distributed, then this equation yields a total mass of about 1.3×10^9 $M_\odot$ within r=3″.5 of the centre for an assumed distance of 18.2 Mpc (Schweizer, 1978). This mass is at least an order of magnitude greater than that observed in M31 (Kormendy, 1988).

What is the true nature of the central mass concentration? A detailed discussion of this is beyond the scope of this note. The two most likely candidates are a massive black hole or massive star-cluster like object. A mass of 1.3×10^9 $M_\odot$ contained within 3″.5 of the centre of NGC 4594 implies an average density of only 10 $M_\odot$ pc^{-3} at a distance of 18.2 Mpc. Such densities are still consistent with globular cluster like systems. A massive star cluster may be revealed through a colour change or an observable change in the line strength in the nuclear spectrum. A small colour change has already been observed (Burkhead, 1986) but the true magnitude of which must wait for higher resolution data. However, the formation processes of such systems with the required mass remain uncertain. Secondly, if the stars in this cluster are akin to those in globular clusters of our own galaxy, we would expect to see a significant light cusp at the centre of NGC 4594. If future high resolution surface photometry does not reveal such an increase, then this mass must reside within objects of high M/L. A system of degenerate stellar remnants or a black hole would therefore be the most likely candidates. Further constraints on the true nature of the central mass concentration in NGC 4594 must await the availability of more suitable high resolution photometric and kinematic data.

4. Conclusions

The major new finding of this study is the discovery of a large mass concentration at the centre of NGC 4594. Our strongest evidence is the detection of a sharp rise in the observed velocity dispersion of at least 59 km s^{-1} within the central 3".5, although this is probably a lower limit. Under the assumption of spherical symmetry and an isotropic velocity distribution, the mass contained within r = 3".5 of the centre of NGC 4594 is $M \simeq 1.3 \times 10^9 M_\odot$. Higher spatial resolution kinematic and surface photometry of the nuclear region of NGC 4594 in good seeing are urgently needed to put new constraints on this problem.

Acknowledgements

We gratefully acknowledge the ESO telescope time that has been allocated to this project.

References

Burkhead, M.S.: 1986, *Astron. J.* **91,** 777.

Dressler, A., Richstone, D.O.: 1987, *Astrophys. J.* **324,** 701.

Jarvis, B.J., Dubath, P.: 1988, *Astron. Astrophys.*, in press.

Kormendy, J.: 1988, *Astrophys. J.* **325,** 128.

Kormendy, J., Illingworth, G.: 1982, *Astrophys. J.*, **256,** 460, KI.

Sargent, W.L.W., Young, P.J., Boksenberg, A., Shortridge, K., Lynds, C.R., Hartwick, D.A.: 1978, *Astrophys. J.* **221,** 731.

Schechter, P.L.: 1983, *Astron. J. Supp.* **52,** 425.

Schweizer, F.: 1978, *Astrophys. J.* **220,** 98.

Whitmore, B.C., Kirshner, R.P., Schechter, P.L.: 1979, *Astrophys. J.* **234,** 68.

Williams, T.B.: 1977, *Astrophys. J.* **214,** 685.

Physical Studies of Asteroids

C.-I. LAGERKVIST, G. HAHN, M. LINDGREN and P. MAGNUSSON,
Astronomiska Observatoriet, Uppsala, Sweden

Introduction

Photometric and spectroscopic observations of asteroids give important information on the physical properties of these bodies and increase our understanding of the origin and evolution of the asteroids. The 50-cm, 1-m and 1.5-m telescopes and the Schmidt telescope at ESO, Chile, have for almost ten years been used by us for such observations. These observations have so far resulted in more than 20 scientific papers. References to these may be found in (1). Here only a short summary of these results will be given.

Spin Properties of Asteroids

The ESO 50-cm telescope has been used for UBV and UBVRI photometry of asteroids with the intention of deriving lightcurves and broadband colours. These lightcurves give information about spin rates, and the lightcurve amplitudes give a hint of the asteroidal shapes. The study of colours and magnitudes as a function of solar phase angle (phase curve) give important constraints to the light scattering properties of the surface material. One night or a few consecutive nights of observations usually give a full coverage over all rotational phases and enable an unambiguous construction of a composite lightcurve. The amplitude of this curve, which can amount to several tenths of a magnitude, gives important statistical information on asteroid shapes and albedo variegation (1, 4). Scenarios for the collisional evolution of the asteroid belt in general, and asteroid dynamical families and other subclasses in particular, may be tested against the wealth of spin rates that have been obtained from photometry. If observations of an object are carried out at several oppositions, the differing viewing geometry gives three-dimensional information which enables us to derive the axis and sense of rotation (6). Such pole information is of importance in the interpretation of most physical observations of asteroids (e.g. radar, infrared, etc.) as soon as the "spherical-featureless-nonrotating-model" is abandoned. One goal with these observations is to obtain an inversion of the full photometric information to interpretable constraints on shape and albedo variegation.

The M-type asteroids have attracted special attention from us in Uppsala since they seem to have different rotational properties from asteroids of other types (1, 5). In this report only the variation of spin rate with the mean distance from the sun will be discussed briefly. Figure 1 shows this variation for asteroids of type S and C. We use only data for asteroids smaller than 140 km in diameter since larger objects show a

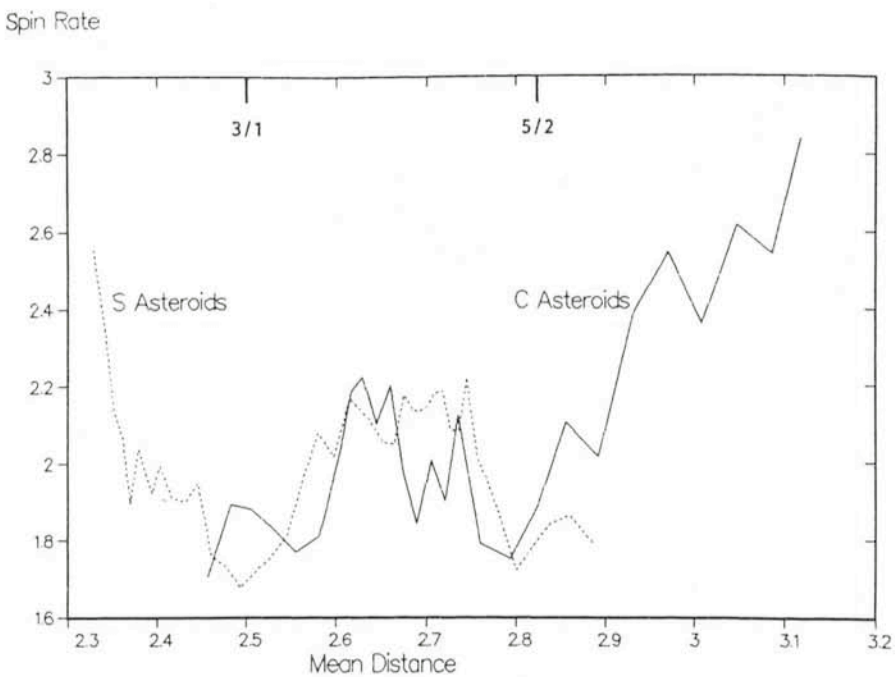

Figure 1: *Running mean of spin rate (rev./day) versus mean distance from the sun (AU) for S and C asteroids. The bin sizes are 15 and 10 objects, respectively.*

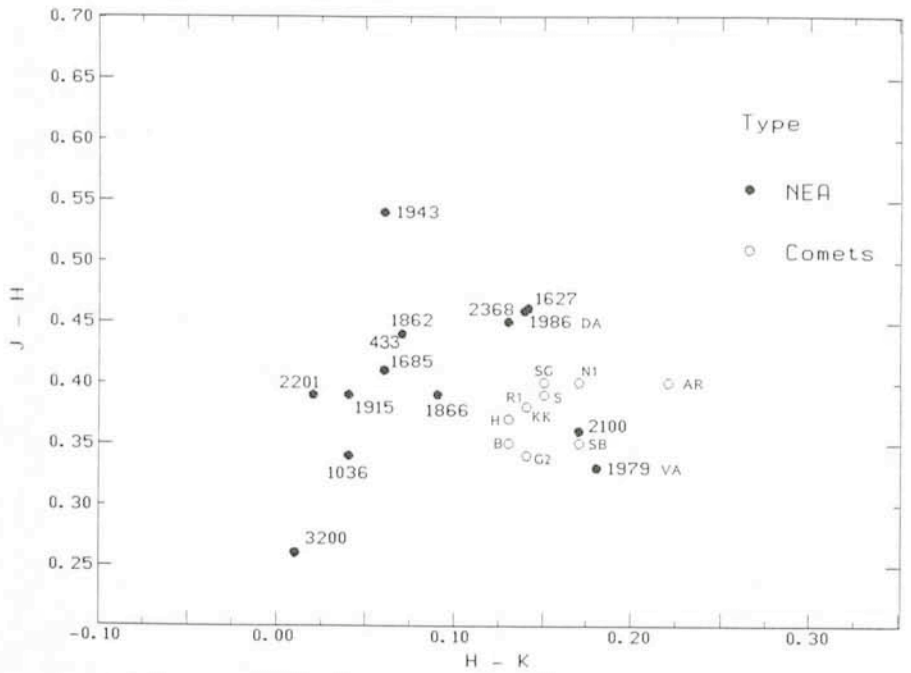

Figure 2: *JHK colours in magnitudes for Near-Earth asteroids and comets. (G2: Gehrels 2, SG: Swift-Gehrels, H.: Howell, B: Bowell, SB: Slaughter-Burnham, KK: Kearns-Kwee, R1: Reinmuth 1, S: Shoemaker, N1: Neujmin 1, AR: Arend-Rigaux).*

strong correlation between spin-rate and size (1). The running means of spin rate has been plotted using data for 36 C-type asteroids and 55 S asteroids with well determined periods. There is a peculiar trend for the S group which shows a steep rise of spin rate towards the inner edge of the main asteroid belt and a minimum (though statistically uncertain) near the 3 : 1 Kirkwood gap at 2.5 AU. Possibly a second minimum may be present at 2.8 AU where the 5 : 2 resonance gap is located. The general trend for the C-type asteroids seems to be the same but more data are needed to confirm these findings. Both data on small asteroids, asteroids at the resonances, and data for distant asteroids are desireable and will hopefully be obtained in the near future.

JHK Photometry

Broadband photometry gives colour indices which may be used for dividing asteroids into different taxonomic classes. An extension of the classification criteria into the infrared region of the spectrum is important since several absorption features that are characteristic for the various taxonomic types are present at these wavelengths. JHK observations of asteroids give thus a possibility to improve the definition of the taxonomic types and to look for interesting absorption features. The 1-m telescope was used during 1984–1986 to obtain JHK colours for 74 main belt asteroids

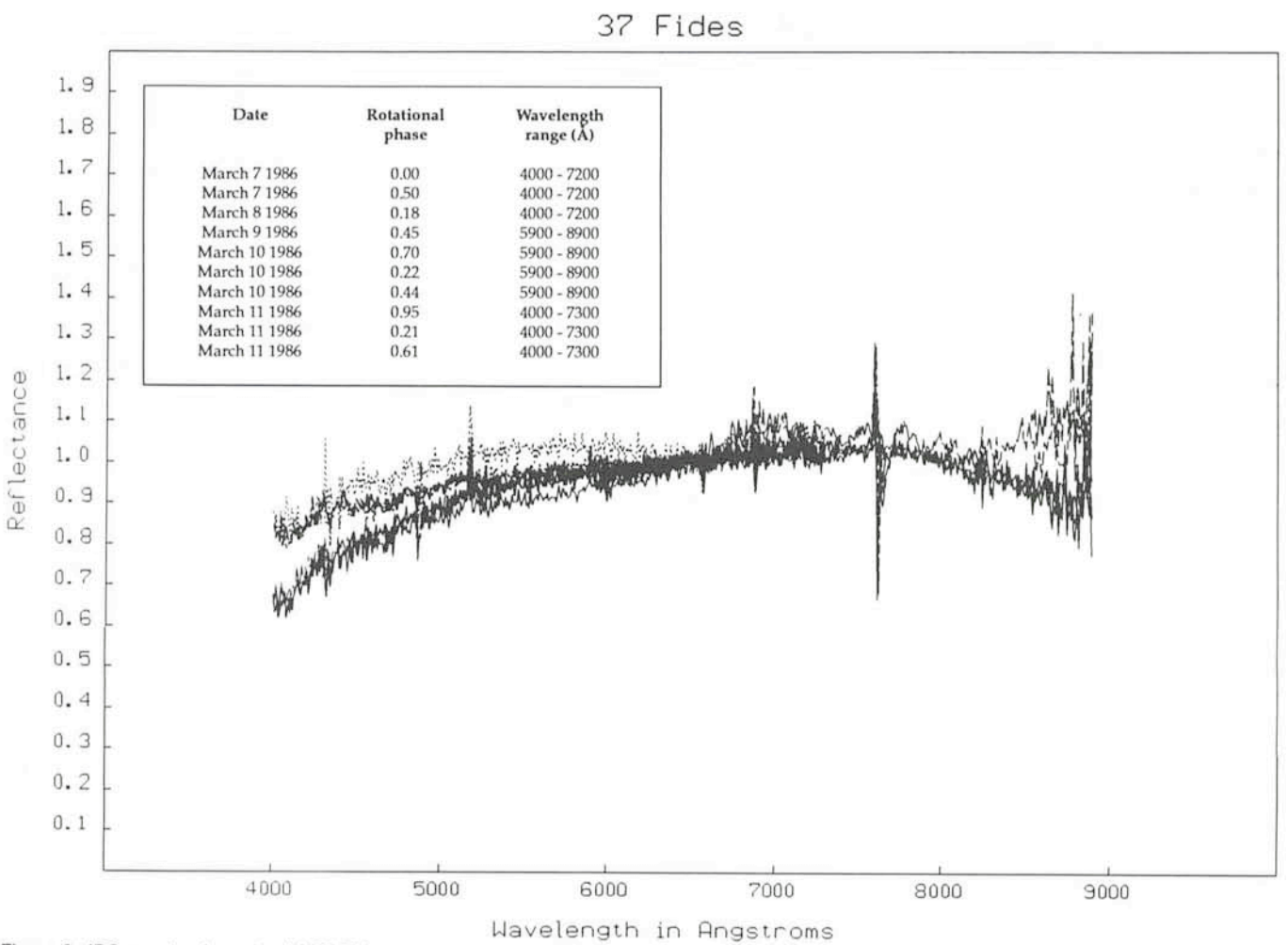

Figure 3: *IDS spectra for asteroid 37 Fides.*

and 3 Apollo asteroids. Combined with previously published observations this gives a total sample of 151 asteroids with known JHK colours (2). Here we discuss only the results concerning the Apollo asteroids. Figure 2 shows J-H versus H-K for near-Earth asteroids and for comets. From the figure may be seen that there is a large spread in the JHK colours for these asteroids, maybe reflecting a variety of surface materials and different origins. Almost half the objects fall into the S-type domain which long seemed to be the dominating type among this kind of asteroids. The asteroids 1627 Ivar, 2368 Beltrovata and 1986 DA have almost identical JHK colours and lie in the part of the diagram where D-type asteroids and comets are found. These results are even more evident for the asteroids 2100 Ra-Shalom and 1979 VA rendering them candidates for being extinct cometary nuclei.

Figure 4: *The first picture of asteroid 2100 Ra-Shalom was taken with the ESO Schmidt telescope on October 2, 1975 (see also the* Messenger *No. 15, page 17). During the 60-min exposure, it moved more than 5 arcminutes. By coincidence, it was seen in front of the Sculptor dwarf galaxy.*

IDS Spectra of Asteroids

Spectra of asteroids give important contributions to the knowledge about the composition of the surfaces of the asteroids and a possibility to study albedo variegations. IDS and Reticon spectra were obtained with the ESO 1.5-m telescope during 1985–1986 and a total of 148 spectra of 45 asteroids were obtained. Additional CCD spectra have also been obtained. The spectral range was normally 3800–9000 Å and a typical resolution was 172 Å/mm. The intention was to cover as many asteroid types as possible in order to make it possible to draw conclusions about the surface composition and to improve the definitions of the taxonomic types. Some asteroids were also observed quite frequently in order to get spectra at different rotational phases for studies of surface variegations. In this short report we will only discuss some of our investigations of surface variegation (8).

For 37 Fides, an asteroid known to have quite complex lightcurves (3), we obtained 10 spectra. These are shown in Figure 3. As seen from the figure there are good reasons to believe that for 37 Fides we have albedo variegations over the surface. Another indication for albedo variegation comes from the unusually high odd Fourier terms in the lightcurves of Fides (4). With further UBV observations of Fides an accurate determination of the sidereal rotation period will be possible and thus a determination of the absolute rotational phase at the time of the spectroscopic observations.

Although we now have lightcurve information about more than 500 asteroids (7) there are still many interesting questions that are not settled yet. We still lack data on small asteroids to draw conclusions about spin properties of these asteroids. Outer-belt asteroids and Trojans are still a fairly unknown population although there are reasons to believe that these asteroids have a quite different evolution from that of main-belt asteroids. Data on more family asteroids are also higly warranted as are further studies on spin properties of different taxonomic types. More high-precision UBV photometry of already well-observed asteroids is needed in order to increase the knowledge about the pole orientations. Observations in order to improve asteroid magnitudes, and thus the sizes are also needed as well as studies of phase variations of magnitudes and colours. Further infrared observations and spectra will help to improve the definition of the taxonomic types and the knowledge about how common surface variegations are. Target asteroids for space projects such as VESTA, a proposed space mission to the asteroids by ESA, CNES and Interkosmos, should be studied extensively from the ground in order to complement space observations and to calibrate the ground data-base on asteroids in general.

References

(1) Lagerkvist, C.-I., Hahn, G., Magnusson, P., Rickman, H.: 1987, "Physical studies of asteroids XVI: photoelectric photometry of 17 asteroids", *Astron. Astrophys. Suppl. Ser.* **70,** 21–32.

(2) Hahn, G., Lagerkvist, C.-I.: 1988, "Physical studies of asteroids XVII: JHK photometry of selected main-belt and near-Earth asteroids", *Icarus,* in press.

(3) Lagerkvist, C.-I., Barucci, M.A., Capria, M.T., Fulchignoni, M., Guerriero, L., Perozzi, E. and Zappala, V.: 1987, *Asteroid Photometric Catalogue,* Consiglio Nazionale Delle Ricerche, Rome.

(4) Lagerkvist, C.-I., Magnusson, P.: 1988, "An investigation of asteroid lightcurve shapes", *Icarus,* in prep.

(5) Hahn, G., Lagerkvist, C.-I.: 1988, "Ephemerides of asteroids of type M and related types", Uppsala Astron. Obs., Rep. No. 46.

(6) Magnusson, P.: 1986, "Distribution of spin axes of rotation for 20 large asteroids", *Icarus* **68,** 1.

(7) Lagerkvist, C.-I., Harris, A.W., Zappala, V.: 1987. Asteorids II machine-readable data base: March 1988 version, National Space Science Data Center, Greenbelt MD, USA.

(8) Hahn, G., Lagerkvist, C.-I., Magnusson, P., Rickman, H.: 1986, "Physical Studies of Asteroids XIII: IDS spectra of selected asteroids", in *Asteroids, Comets, Meteors II.* Eds. C.-I. Lagerkvist, B.A. Lindblad, H. Lundstedt, H. Rickman, Uppsala University, p. 93.

Are Bulges of Disk Galaxies Triaxial?

Evidences from the Photometry and the Gas Dynamics

*F. BERTOLA[1], M. VIETRI[2], and W. W. ZEILINGER[1]**

[1] Dipartimento di Astronomia, Università di Padova, Italy; [2] Osservatorio Astrofisico di Arcetri, Firenze, Italy

Introduction

It is now generally accepted that elliptical galaxies are triaxial in shape. There are at least two strong observational hints that this is indeed the case: the first one is the well-known fact that elliptical galaxies are, normally, slow rotators (Bertola 1972; Bertola and Capaccioli 1975; Illingworth 1977) whose shape is not due to rotation and therefore must be due to the flattening of their velocity dispersion ellipsoids. This makes it likely that the dispersion velocity tensor is flattened also along the intermediate axis, so that the resulting galaxy's figure is triaxial, rather than oblate. Secondly, elliptical galaxies show radial variations in ellipticity and position angle of their apparent major axis (Bertola and Galletta 1979), a phenomenon that cannot occur if their shape is prolate or oblate. This observational evidence is supported by theory: we know now that several galaxy-formation scenarios (Aarseth and Binney 1978; see also Lake, and White 1987 for reviews) exist where collapse of the proto-cloud in its three main directions occurs on different timescales, making a triaxial object the most likely end-product of the scenario. Also, we know that triaxial stellar-dynamical models exist, which are stationary (except for perhaps a slow figure rotation), and stable to at least the grossest instabilities (Schwarzschild 1979).

However, although much circumstantial evidence exists in many different cases to indicate that a given elliptical galaxy is indeed triaxial, it is difficult to find a clear-cut example of an isolated galaxy which we are sure is triaxial. In fact, projection on the plane of the sky of a triaxial object involves four, a priori unknown, parameters: two viewing angles, θ and φ, and the two intrinsic axial ratios, b/a and c/a, while observations provide, as the only constraint, the apparent axial ratio ε. So, if we want to prove that a given elliptical galaxy is triaxial, recourse has to be made to more complicated, dynamical arguments; such is the case, for instance, of the galaxy studied by Davies and Birkinshaw (1986), and of NGC 5077, an elliptical with a gaseous disk, where these four parameters were determined in a straightforward way (Bertola, Bettoni, Danziger, Sadler and de Zeeuw, 1988, in preparation).

The situation for bulges of disk galaxies is, however, completely different: Lindblad (1956), arguing on the basis of purely geometrical arguments, proved that the bulge of M31 cannot be oblate, and it is now known (Stark 1977) that it is unlikely to be prolate also. The similarity of bulges of disk galaxies and ellipticals is now well-established, once objects of equal luminosity are compared. There seems to be, in fact, a continuum spectrum of properties which extends from giant elliptical galaxies down to small bulges (Davies 1987), the latest property to be studied being the existence of "normal" exponential disks in SOs and elliptical galaxies (Capaccioli and Vietri, 1988).

In the past, however, this continuum has been taken to imply that, since bulges seem to be oblate, so should be the small ellipticals. Here we argue the other way round: we show that a fair fraction of bulges (for which a deprojec-

* Affiliated to the Astrophysics Division, Space Science Department, European Space Agency.

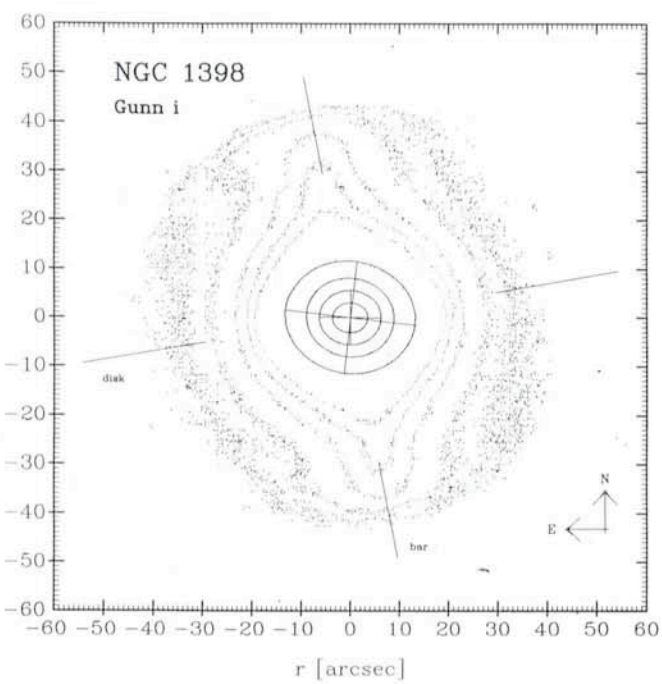

Figure 1: *Contour plot of the Gunn i frame of NGC 1398. On the inner four isophotes the fitted ellipses together with the respective major and minor axes are superimposed. The position angles of the bulge (PA = 89° and PA = 83°), bar (PA = 11°) and disk (PA = 100°) are indicated. The latter value was taken from Lauberts (1982).*

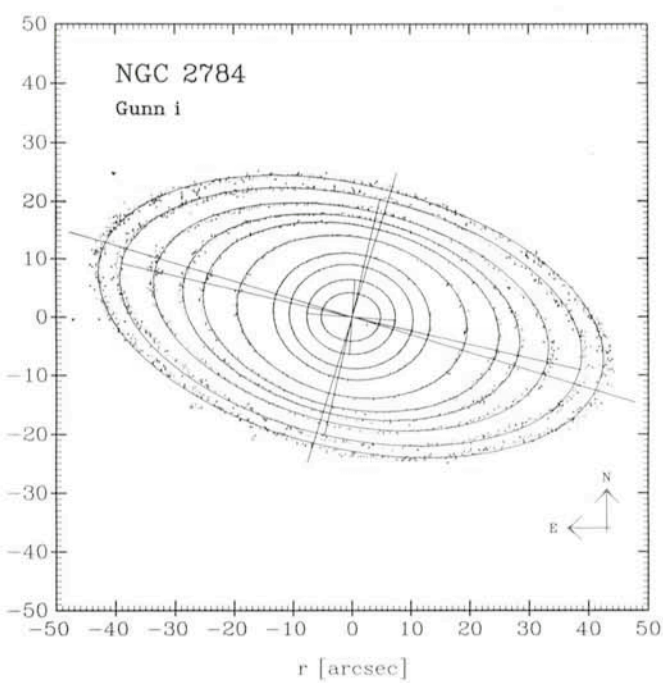

Figure 2: *Contour plot of the Gunn i frame of NGC 2784. The fitted ellipses are superimposed to the isophotes. In order to make the variation in position angle more evident, three major and minor axes at different radii are plottet, the last one representing the disk.*

tion is easier than for ellipticals) are triaxial, and we take this to imply that small ellipticals too are, most likely, triaxial. We stress here, furthermore, that our argument does not depend upon uncertain dynamical interferences, but exclusively on straightforward geometrical evidences. We will examine some dynamical evidence in the last section of this paper. In the next section we extend Lindblad's arguments to a large sample of spirals' bulges.

The Photometric Evidence

Lindblad's argument, in dealing with M31, was simple: he noticed that the apparent major axis of the bulge was misaligned with the apparent major axis of the disk by $\gamma = 12°$. He correctly reasoned that, if the bulge is oblate and its true minor axis coincides with the disk's axis of symmetry, one should have $\gamma = 0°$. He then deduced that the bulge could not be oblate but triaxial. This argument is not peculiar to M31, of course. So we decided to investigate photometrically a large number of spiral galaxies, hoping to find cases analogous to the Andromeda nebula.

In the period from December 31 to January 2, 1987 we obtained CCD pictures of 28 disk galaxies during an observing run at the ESO/MPI 2.2-m telescope equipped with the RCA CCD camera. We selected objects of various Hubble types ranging from S0 to late spiral type. For each galaxy at least two frames were obtained in the Gunn r and Gunn i filters in order to emphasize the older stellar population in the bulge region.

The frames were calibrated using standard techniques of normalized flat field division and bias correction. The galaxy images were analyzed using an ellipse fitting algorithm yielding the position angle PA of the galaxy's isophotal major axis and apparent ellipticity ε. The accuracy in determining these quantities is not limited by method since the formal errors would be of the order $\sigma(\mathrm{PA}) \simeq \pm 1°$ and $\sigma(\varepsilon) \leq \pm 0.01$. The influence of the disk component's dust absorption on the isophotes poses much severer limits on the accuracy. Dust tends to mimic flatter isophotes which appear also to be twisted by several degrees. In order to minimize these effects we used therefore filters in the redder wavelength region where the light from the bulge is predominant. For the most part of the Galaxies observed we found in the bulge region no significant disturbance due to dust. For the remaining objects we applied appropriate masks on the affected regions and performed a reasonable interpolation of the isophotes. Because of the limited size of the CCD frames we used also position angle measurements of the disk's major axis from the sky survey prints.

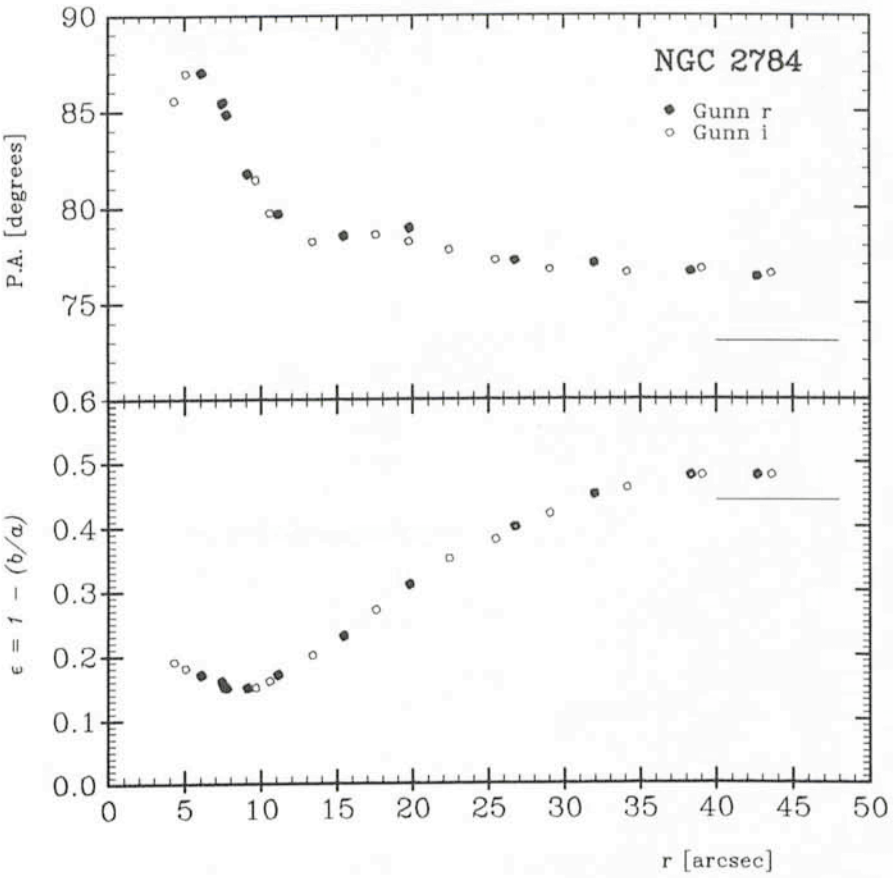

Figure 3: *Profiles of ellipticity and position angle as a function of radius for NGC 2784. The line indicates the respective values for the disk (Lauberts 1982).*

As a comparison, we included also a few barred galaxies in the programme, which do show the effect of a misaligned bulge with respect to the disk and the bar. One such case, NGC 1398 is shown in Figure 1. For this class of galaxies, the fact that the bulge is triaxial is well-known (Kormendy 1982); it has been ascribed to the dynamical interaction of the bulge with their prominent bars. As a further indication of the bulge's triaxiality an evident twisting of the isophotes ($\Delta \mathrm{PA} \simeq 6°$) in the inner bulge region ($r < 13''$) was detected. Other non-barred examples have been mentioned in the literature, albeit never properly discussed (Boronson 1981; Gamaleldin and Issa 1983). Zaritsky and Lo (1986) concluded already, however based on a fairly small galaxy sample, that non-axisymmetric nuclear bulges should be generally anticipated.

In our survey, we have detected several possible cases of misaligned galaxies out of a total sample of 13 non-barred galaxies studied so far. The best case is represented by the S0 galaxy NGC 2784, which is very probably an almost dust-free system and whose isophotal twisting was also noticed by Gamaleldin and Issa. A contour plot of NGC 2784 is shown in Figure 2, together with the fitted ellipses. In order to make the variation in position angle more evident, three major and minor axes at different radii are superimposed. The outmost position angle indicated was taken from Lauberts (1982) since his measurements, based on sky survey prints, refer always to the disk region of the galaxy. The ellipticity and position angle profile is shown in Figure 3. The photometry in the Gunn i band yields exactly the same results, showing that we are not seeing any dust-related phenomenon. Figure 3, together with Figure 4, the ESO (B) Sky Survey print, show that the disk's major axis position angle is well-defined, and not due to the presence of spiral arms. Figures 2, 3 and 4 clearly show the existence of a misalignment by $\gamma = 14°$.

Could this misalignment have another cause? Once dust has been ruled out, the only remaining possibility is that the disk itself be flattened in its own plane (oval distortion). However, given the disk's apparent flattening of $\varepsilon \simeq 0.5$, one can show that the disk's true flattening in its own major plane needed to explain away $\gamma = 14°$, is $b/a \simeq 0.75$, a value that is probably inconsistent with the observations of most face-on disks. We be-

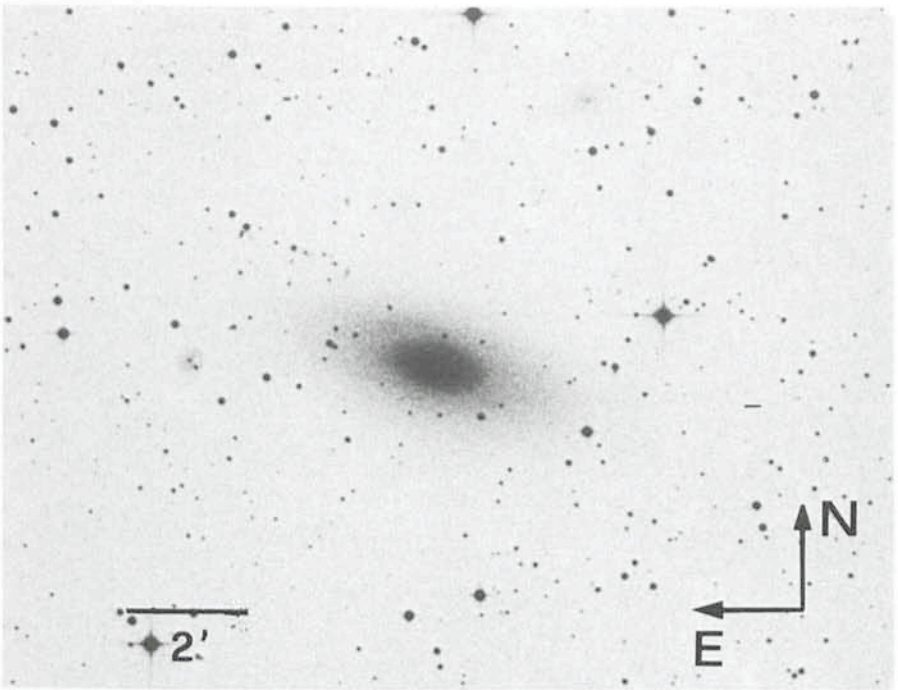

Figure 4: *NGC 2784. Reproduction from the ESO (B) Sky Survey print.*

lieve that this conclusively shows that *the bulge of NGC 2784 cannot be oblate.*

Could it be *prolate?* Stark (1977) has shown how this can be ascertained. If we again assume that disk and bulge have coincident minor axes (an assumption supported by observations of edge-on disk galaxies), then he showed that there are three constraints on the four free parameters of the projection: the disk's and bulge's apparent flattenings, and the angle γ. Basically, the disk's flattening gives us immediately one of the viewing angles, while the other two constraints are more complicated functions of all four unknown parameters. One can then find a one-parameter family of solutions for the projection equations, where the free parameter can be taken as the bulge's major axis position angle in the disk's plane, from the line of nodes. This exercise can be carried out for NGC 2784. The solution is shown in Figure 5. We see that all angles $\varphi > 142°$, lead to a c/a > b/a, which is an unlikely solution (when seen edge-on, such a bulge would look like a rugbyball with its major axis sticking out of the disk plane). Also, as expected, we see that a prolate solution is not very likely on statistical grounds, since it corresponds to a small range of position angles: only angles $142° > \varphi > 136°$ are consistent with this galaxy being roughly prolate, within the range of observational errors. Lastly, in this fortunate case, since the most likely distribution of values for φ is casual, i.e. flat, we see that *the most likely solution is a mildly triaxial bulge,* with axial ratios c/a $\simeq$ 0.4, and b/a $\simeq$ 0.6.

The Dynamical Evidence

Far from being unexciting, such mildly triaxial bulges may give rise to a deeply non rotationally-symmetric gas velocity field, as shown by Gerhard and Vietri (1986) in the case of the Milky Way, by Gerhard and Vietry (1987) in the case of an arbitrary bulge, and by Bertola, Gerhard, Rubin and Vietri (1988, work in progress) in the case of NGC 4845. The main effect that we expect, dynamically, from a flattened bulge, is that the gas orbits will be slightly elongated, with their longest axis pointing along the potential's intermediate axis. As a consequence, the gas velocity at the point closest to the galaxtic centre will be (considerably) higher than the velocity at the most distant point on the same orbit. Thus, depending on the viewing angle, the rotation curve may appear to have a hump (as in the case of the Milky Way, Gerhard and Vietri 1986), or may seem to be abnormally slowly rising. For bulges with de-Vaucouleurs-like luminosity profiles, velocity perturbations of over 100 km s^{-1} are expected. When observations of the whole velocity field are available, we can thus use the photometrically-determined parameters, plus the angle φ as fitting parameters of the whole field. In other words, by combining photometry and spectroscopy, we can find the angle φ and, thus, by looking at Figure 5, we can determine the intrinsic axial ratios of the bulge. It is exactly this exercise that has been carried out for NGC 4845, and, although in this case the photometric

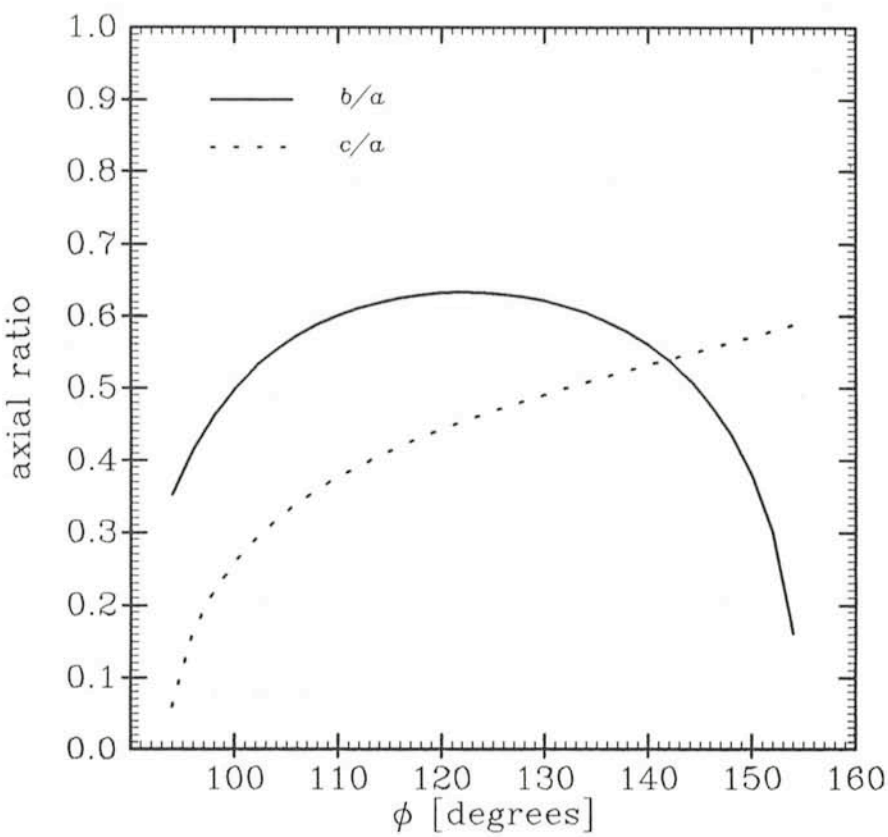

Figure 5: *Solution for the axial ratios b/a and c/a at different position angle φ with respect to the major axis for the bulge of NGC 2784 in the disk plane.*

observations are marred by a large amount of dust, making the determination of the galaxy's axial ratios somewhat unreliable, still these arguments have received considerable support by the ability of the triaxial-bulge model to explain the gross departures from the axially-symmetric rotational velocity field observed in this galaxy.

In conclusion, we have shown that purely geometrical evidence shows that bulges are triaxial, a conclusion also supported by dynamical evidence, which re-establishes the similarity between bulges and elliptical galaxies.

Acknowledgement

W.W.Z. acknowledges the support of this project by the Austrian *Fonds zur Förderung der wissenschaftlichen Forschung* (project P 5529).

References

Aarseth, S.J. and Binney, J.J., 1978. *Mon. Not. Roy. Astr. Soc.*, **185,** 227.

Bertola, F., 1972. in *Proc. 15th Meeting of the Ital. Astron. Soc.*

Bertola, F. and Capaccioli, M., 1975. *Astrophys. J.*, **200,** 439.

Bertola, F. and Galletta, G., 1979. *Astron. Astrophys.*, **77,** 363.

Bertola, F., Bettoni, D., Danziger, J., Sadler, E.M. and de Zeeuw, T., 1988, in preparation.

Boronson, T., 1981. *Astroph. J. Suppl. Ser.*, **46,** 177.

Capaccioli, M. and Vietri, M., 1988. *Mon. Not. Roy. Astr. Soc.*, in press.

Davies, R.L., 1987. in *Structure and Dynamics of Elliptical Galaxies,* I.A.U. Symp. 127, ed. T. de Zeeuw (Dordrecht:Reidel) p. 63.

Davies, R.L. and Birkinshaw, M., 1986. *Astrophys. J.*, **303,** L45.

Gamaleldin, A.I. and Issa, I.A., 1983. *Astron. Nachr.*, **304,** 21.

Gerhard, O. and Vietri, M., 1986. *Mon. Not. Roy. Astr. Soc.*, **223,** 377.

Gerhard, O. and Vietri, M., 1987, in *Structure and Dynamics of Elliptical Galaxies,* I.A.U. Symp. 127, ed. T. de Zeeuw (Dordrecht:Reidel) p. 399.

Illingworth, G., 1977. *Astrophys. J.*, **204,** 73.

Kormendy, J., 1982. *Astrophys. J.*, **257,** 75.

Lake, G., 1987, in *Structure and Dynamics of Elliptical Galaxies,* I.A.U. Symp. 127, ed. T. de Zeeuw (Reidel) p. 331.

Lauberts, A., 1982. *The ESO/Uppsala Survey of the ESO (B) Atlas* (ESO).

Lindblad, B., 1956. *Stockholm Obs. Ann.*, **19,** No. 2.

Schwarzschild, M., 1979. *Astrophys. J.*, **232,** 236.

Stark, A.A., 1977. *Astrophys. J.*, **213,** 368.

White, S., 1987, in *Structure and Dynamics of Elliptical Galaxies,* I.A.U. Symp. 127, ed. T. de Zeeuw (Dordrecht:Reidel) p. 339.

Zaritsky, D. and Lo, K.Y., 1986. *Astrophys. J.*, **303,** 66.

Simulations of High Redshift Galaxies and Observations with the Hubble Space Telescope

T.J.-L. COURVOISIER, ST-ECF, and A. LAUBERTS, ESO*

The high angular resolution of the Hubble Space Telescope (HST) will allow the observations of the structure of small but extended objects. Prime candidates for this type of research are galaxies at moderate or high redshifts. These galaxies are approximately 1″ in diameter and will contain many resolution elements of the space telescope. The exact resolution will depend on the wavelength of the observation and on the mode in which the observations will be made, the highest resolution being obtained with the faint object camera in the f/288 mode. Since most imaging modes will provide a resolution better than ~0.″1, galaxies at large redshift will cover more than ~100 resolution elements. The Wide Field Camera (WFC) with a field of view of 3′ × 3′ is well suited for statistical studies of the properties of field galaxies, although its spatial resolution will be limited by the pixel size to .1″. The number of galaxies that can usefully be studied in each exposure naturally depends on the depth of the exposure, at V ~25 it is expected to be of the order of 100 galaxies.

In order to assess the potential of HST-WFC for the observation of random fields, we conducted a programme of simulations of galaxies and their "observations" with the WFC simulator developed at the ST-ECF (Rosa and Baade 1986). The starting point of our simulations was a set of 14 nearby galaxies of all Hubble types observed with the ESO Schmidt telescope, in the colours B and R, digitized and calibrated. U and V images were computed using a linear combination of the B and R images with coefficients based on a sample of multi-aperture photoelectric UBVR photometry. We shifted the galaxies to different distances, constructed a field of galaxies (3′ × 3′) and "observed" this field with the HST simulator.

Individual Galaxies

We shifted the galaxies to different distances, scaling the angles as appropriate for a Friedmann cosmology with $q^o = 0$. The K-correction which needs to be applied to take the redshift into account was applied locally, pixel by pixel. This was done by calculating the colour of the individual pixels (the images were all shifted so that the centroid of the galaxy corresponded on all the frames taken for each galaxy). This colour was compared with the integrated colour of galaxies for which K-corrections are available (Coleman et al. 1980), and the K-correction of the standard galaxy with colour closest to the pixel colour was applied for the desired redshift. This procedure allows to correct the individual features of a galaxy, and hence to study the apparent evolution of the galaxy with redshift. No intrinsic evolution has been taken into account for the time being.

Our scheme to apply K-corrections has several shortcomings: Ideally the K-correction should be calculated for the individual components of a galaxy and applied to each component separately, the components being identified by their colour and location in the galaxy. In addition, reddening by dust in the galaxy modifies the spectrum of individual features and therefore the K-corrections that ought to be applied. Our procedure identifies the different

(continued on p. 30)

* Affiliated to the Astrophysics Division of the Space Science Department of ESA.

The centerfold shows a highly structured molecular cloud which is located in the southern constellation Norma, a region with many dark clouds. The cloud is clearly divided in two parts, a large irregular "head" and a long, thin "tail". The almost complete extinction of the rich background star fields in the Milky Way indicates that the clouds are very dense. Star formation is taking place at various points in the cloud, and two Herbig-Haro objects, HH 56 and HH 57, are found in the head. The energy source of HH 57 erupted just a few years ago in a so-called FU Orionis outburst, and is now a bright infrared source. This is one of the first star-forming

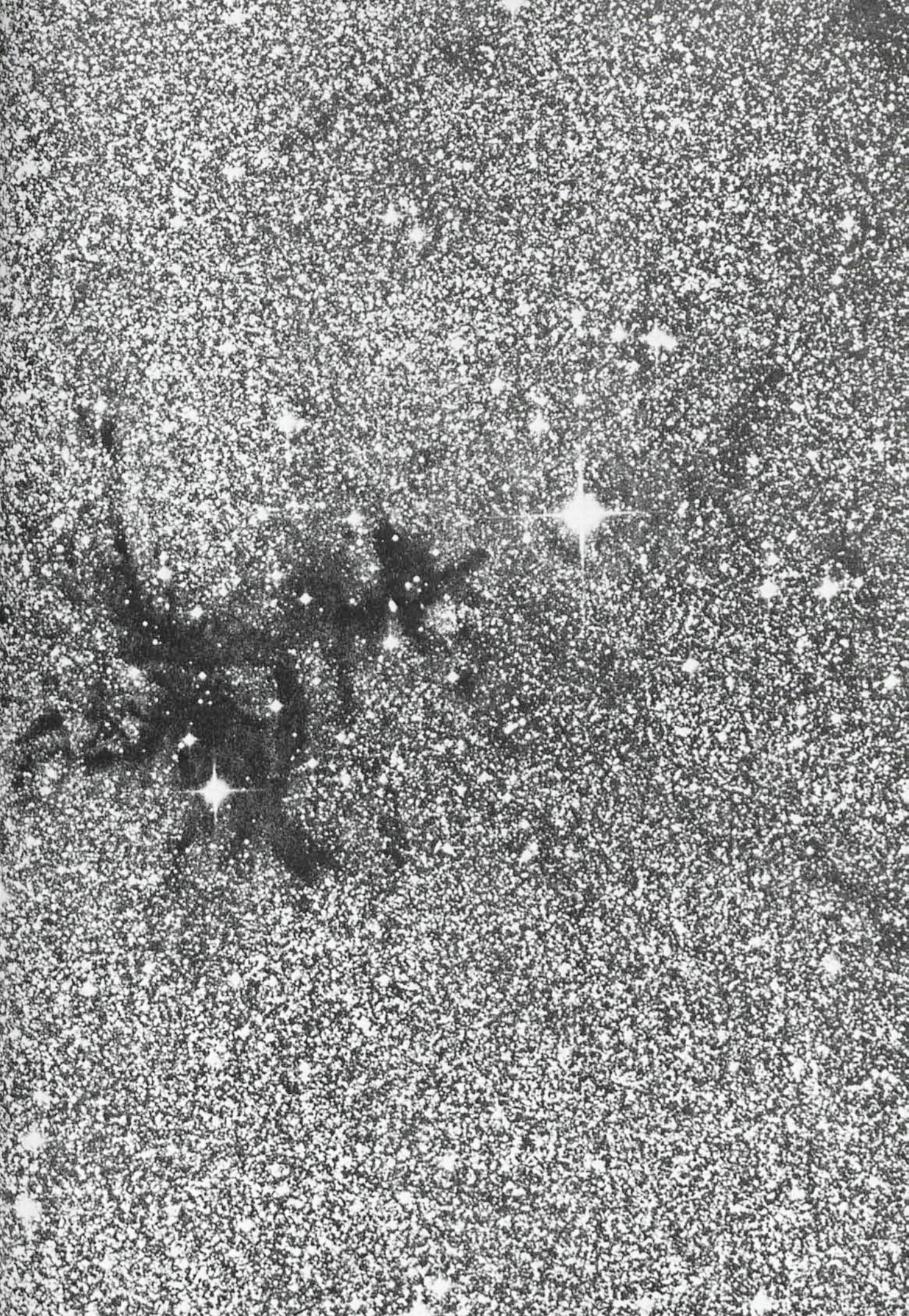

regions observed with the new SEST millimetre-wave telescope at La Silla. The observations revealed the presence of a large bipolar outflow, formed by energetic stellar winds from energy sources of the Herbig-Haro objects. All young stars are believed to pass through early phases with strong stellar winds, which will clear away the ambient material left over from the birth of the stars. To reveal the details of this highly structured cloud, the original plate was subjected to a combination of unsharp masking and diffuse-light amplification.

The smaller photo on this page shows the surroundings of the cloud. Here the reproduction is negative to bring out the nearby structures, which are somewhat less dense.

From a deep, red-sensitive ESO Schmidt plate (150 min; IIIa-F + RG630). Observers: H.-E. Schuster and G. Pizarro. Text by B. Reipurth; photographic work by C. Madsen.

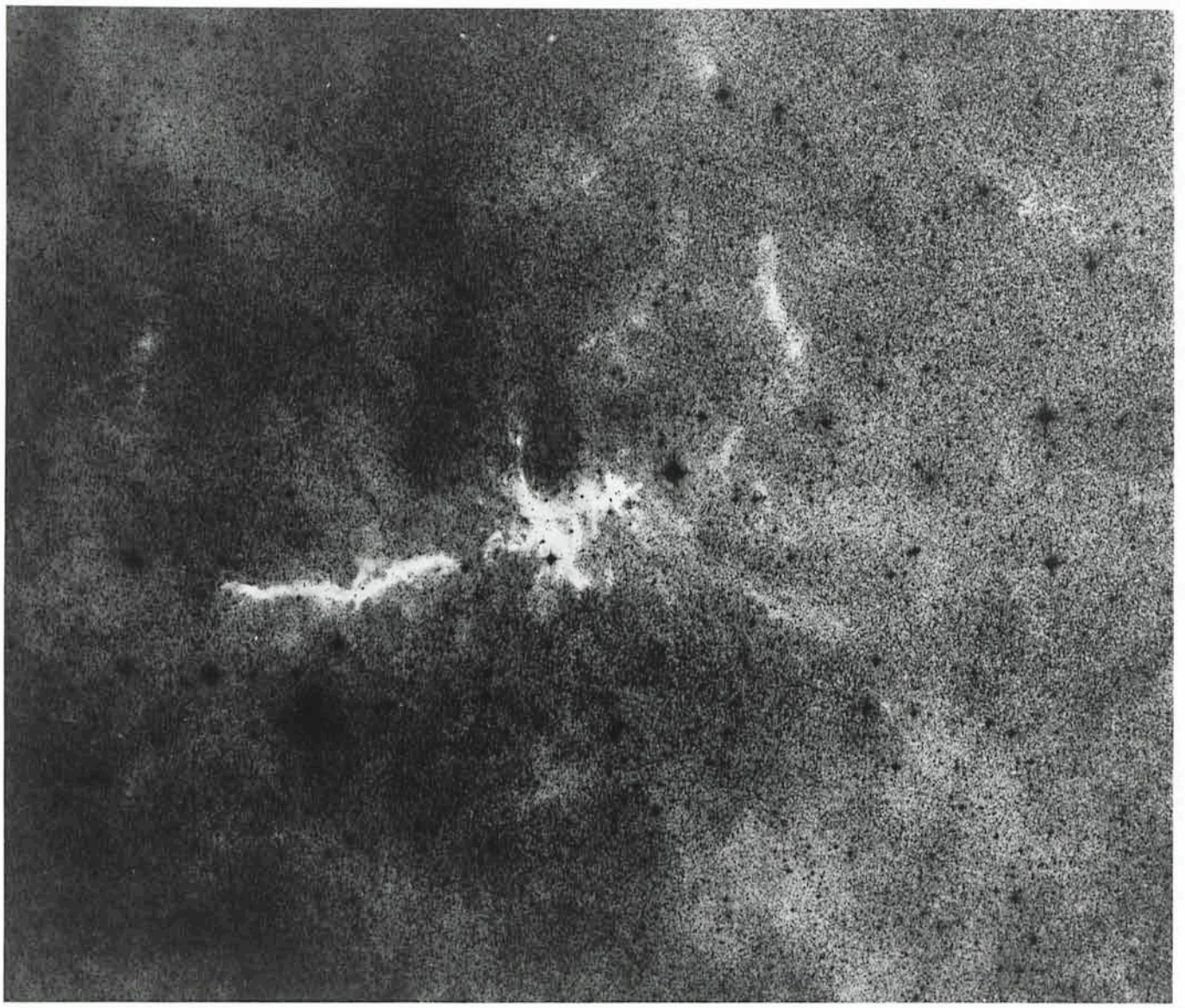

(continued from p. 27)

components of a galaxy on their colour only and approximates the K-correction by assuming that the typical galaxies for which K-corrections are given in the literature correspond to these single components.

Since our original images had been well exposed, the signal-to-noise ratio is good in all the galaxies and we do not expect that random colour fluctuations have had any impact on the resulting frames. This can be seen in that the K-corrected images look as smooth as the original images (Fig. 1, 2 and 3). Where the signal to noise per pixel did not allow to determine a colour (sky), no K-correction was applied. In the outer parts of the galaxies, where the galaxy signal is between 10 % and 50 % of the sky level, the colour of the pixels used in the K-correction procedure was calculated using the average colour of the complete galaxy.

Figure 1 gives the late type galaxy NGC 1365 at a redshift of 0.0054 in the U, B, V and R filters. Figures 2 and 3 give the same galaxy in the same colours but with the K-correction applied as described above for a redshift of $z=0.5$ and $z=1$. It is immediately apparent that the structure of the galaxy has changed in that the arms become more prominent in the $z=0.5$ and $z=1$ U images than in the original image, to the point that the brightest parts of the galaxy are to be found in the arms and not in the nucleus as is the case at low redshift. In the red image, the bar and bulge disappear at $z=1$, leaving a structure dominated by the nucleus and the arms.

Elliptical galaxies, having no azimuthal colour structure at $z=0$ keep this symmetry also at high redshift. Therefore, early type galaxies show less morphological changes with redshift than late type galaxies. In general, the bar of barred galaxies decreased in relative intensity in U and B with increasing redshift. This tendency is less pronounced in V and R.

In summary, the galaxies at high redshift appear to be of later type than at low redshift. This trend is more pro-

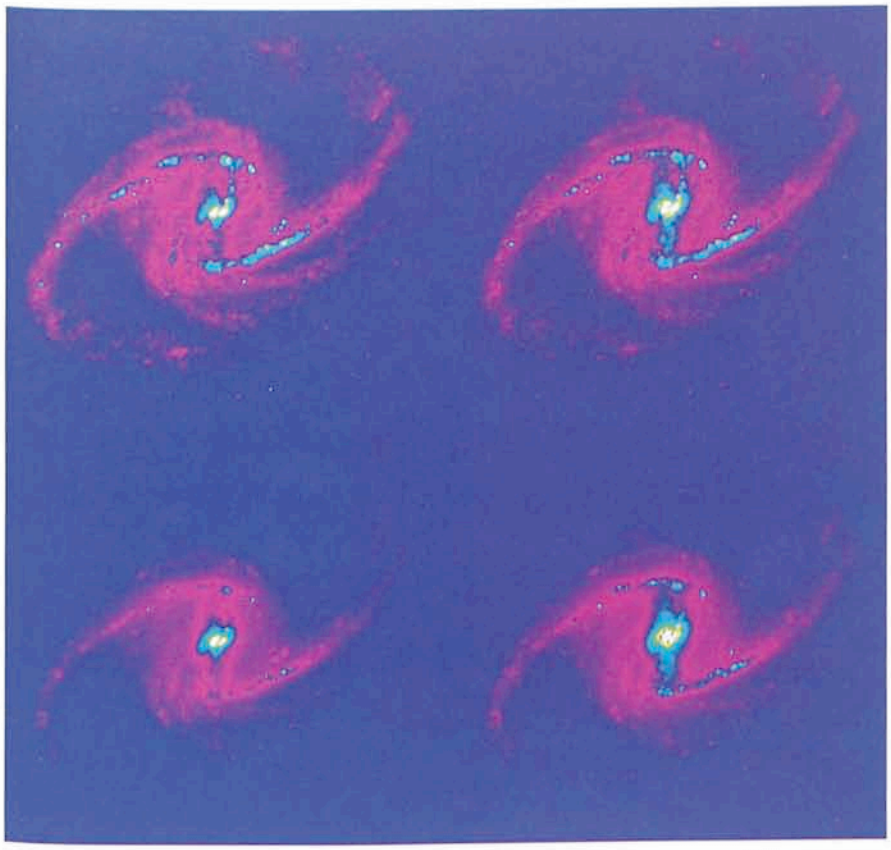

Figure 1: *The Galaxy NGC 1365 at the redshift z=0.0054. The upper right panel gives the B image, upper left panel the U image, the lower left panel the V image and the lower right panel the R image.*

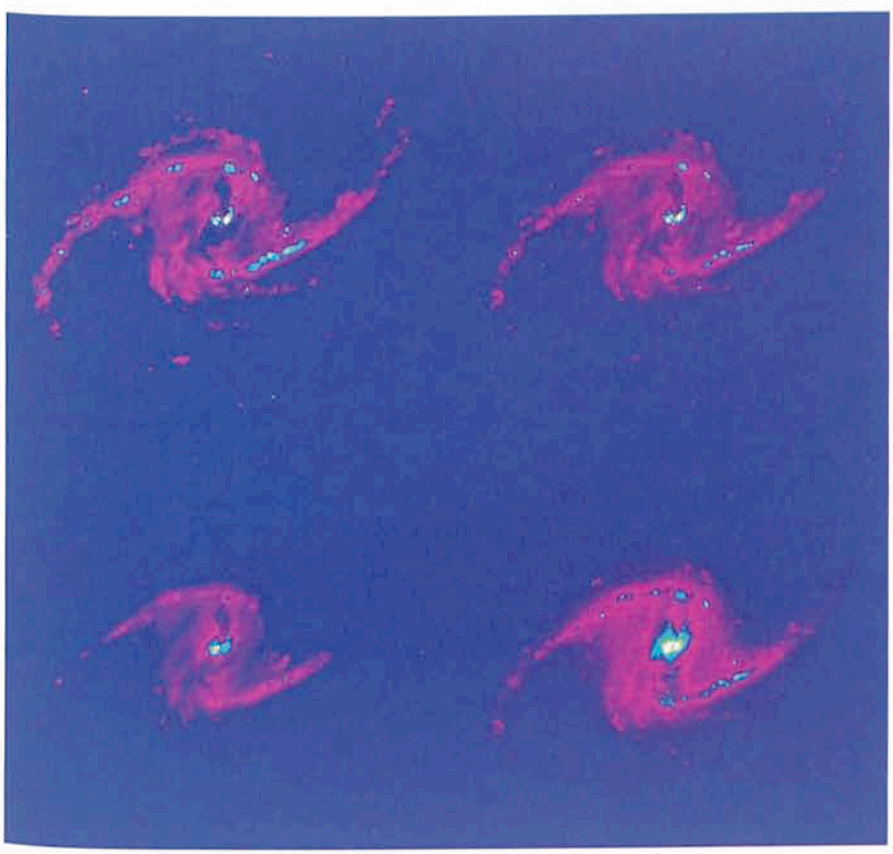

Figure 2: *Same galaxy and colours as Figure 1 but at a redshift z=0.5. The image was shifted as described in the text.*

nounced for already late type galaxies and for U and B images than for early type galaxies and V and R images. The Hubble classification of galaxies also doesn't match the high redshift galaxies as well as it matches the low z observed galaxies.

Field of Galaxies

The galaxies we used to study the effect of redshift on the morphological type were also used to construct a $3' \times 3'$ field of the sky. This was done using a random distribution of galaxies in 3 dimensions, characterized by a mean galaxy surface density of ~ 800 galaxies per $5' \times 5'$ and no clustering. The galaxy types were matched with our sample galaxies, the K-corrections applied as described above and the galaxies randomly flipped and rotated. The resulting frame is given in Figure 4. The resolution of the display used to generate Figure 4 is limited to 512×512 pixels, so that Figure 4 has only ⅓ of the WFC resolution.

A $51\farcs2 \times 51\farcs2$ part of this frame (lower left of Figure 4) was then "observed" with the WFC HST simulator of the ST-ECF. The effects of seeing were approximated by the re-binning of the frame to the pixel size of the WFC ($0\farcs1$) as this is the dominant effect of the instrument resolution. Several noise effects were taken into account in the simulations: photon noise, preflash electrons, deferred charge and read out noise. The signal was calculated using the magnitude of the galaxies at the corresponding redshift, the effective surface of HST, the filter transmission and the detector quantum efficiency. The integration times were chosen to correspond to realistic exposures. The images were expressed in ADU counts and a bias was added to the images.

Several effects of real images were not simulated, these include the presence of point sources in the field (expected to amount to 10% of the sources at high galactic latitude), cosmic rays and the lack of uniformity of the detector sensitivity (flat fields).

Figure 5 gives the resulting V-image following a 2,500-second integration.

Galaxies down to V mag of ~ 24 integrated magnitude can still be seen. The brightest galaxy has an integrated V magnitude of 19.6. The limiting surface brightness for which useful morphological information can still be obtained will depend on the procedure used to analyse the images. The nucleus of an Sc galaxy at $z=0.98$ can still be seen on the image. More detailed analysis of the image will be performed by different groups using several algorithms and software in order to test the analysis

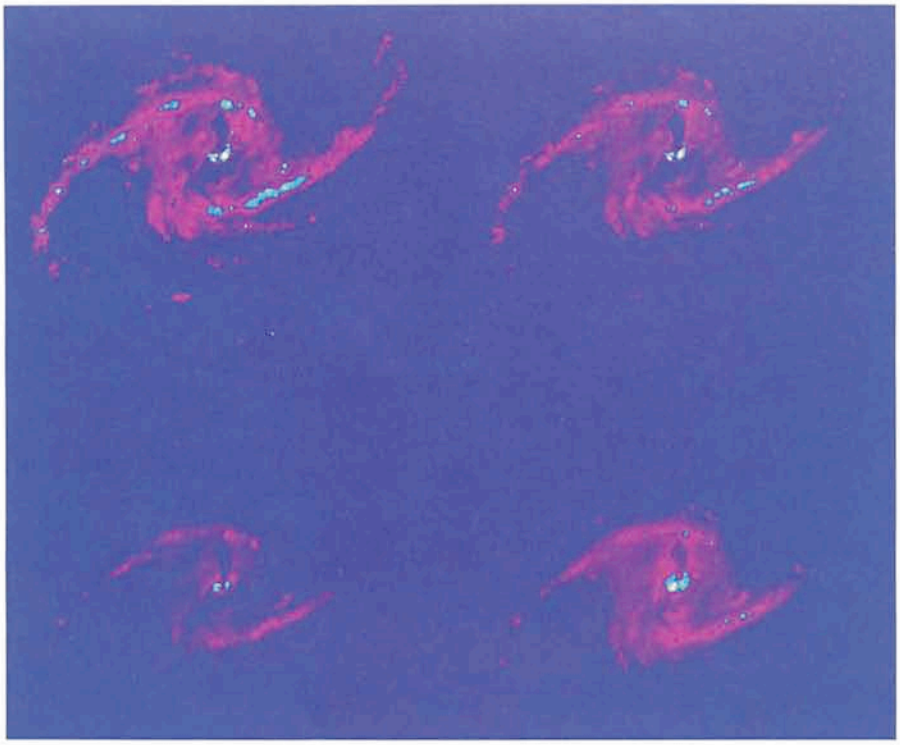

Figure 3: *Same galaxy and colours as Figures 1 and 2 but at z = 1.*

methods and show to which extent the information content of the image can be recovered.

Figure 6 gives the resulting B image after a 5,000-s integration. On this image, only the brightest features can still be distinguished. This shows the great difficulty to obtain colour information using U and B filters for extended objects with the WFC. In this wavelength domain, the faint object camera is expected to be more sensitive. Its smaller field of view will however reduce the sample of objects available in random fields.

We thank P. Vettolani for providing us with one of his simulations of the location, redshift and magnitudes of a random field of galaxies.

References

Rosa and Baade 1986, *The Messenger* **45.**
Coleman, Wu and Weedman, 1980, *Ap. J. Supp.* **43,** 393.

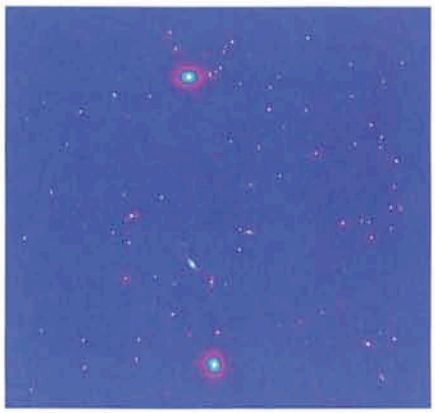

Figure 4: *Simulated field of galaxies 3′ × 3′. The galaxy distribution is a 3-D random distribution without clustering.*

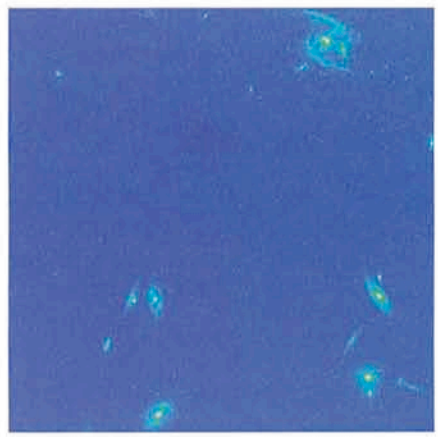

Figure 5: *Simulated "observation" of the 51.″2 × 51.″2 lower left part of Figure 4 with the WFC of HST. The image is in a wide band filter approximating the V band, the exposure time of 2,500 s.*

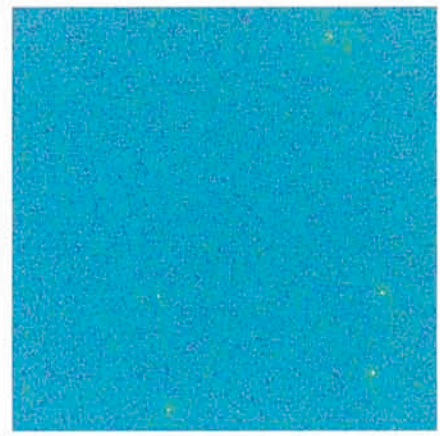

Figure 6: *Same as Figure 5 but through a filter approximating the blue band and with an exposure time of 5,000 s.*

List of ESO Preprints

(March–May 1988)

573. F. Matteucci and G. Vettolani: Chemical Abundances in Galaxy Clusters: a Theoretical Approach. *Astronomy and Astrophysics.*
574. A. Iovino, J. Melnick and P. Shaver: The Clustering of HII Galaxies. *Astrophysical Journal,* Letters.
575. H.-M. Adorf and E.J.A. Meurs: Supervised and Unsupervised Classification – The Case of IRAS Point Sources. F. Murtagh: Multivariate Analysis Methods: Background and Example. Papers presented at the Bad Honnef meeting on "Large Scale Structures in the Universe – Observational and Analytical Methods". December 1987. In press, Springer-Verlag.
576. G. Meylan: On the Individual Masses of Globular Clusters in the Magellanic Clouds: NGC 1835. *The Astrophysical Journal.*
577. F. Verbunt and G. Meylan: Mass Seggregation and Formation of X-ray Clusters. *Astronomy and Astrophysics.*
578. R. Arsenault and S. D'Odorico: Medium Resolution Spectroscopy of the Supernova 1986 O in the Spiral Galaxy NGC 2227. *Astronomy and Astrophysics.*
579. M. Pierre, P.A. Shaver and A. Iovino: Void Structure in the Lyman alpha Forest. *Astronomy and Astrophysics,* Letter.
580. F. Matteucci and A. Tornambè: Theoretical Supernova Rates in the Galaxy and M31. *Astronomy and Astrophysics.*
581. M.H. Ulrich and T.J.-L. Courvoisier: Short and Long Term Variations of the Ultraviolet Spectrum of 3C 273. *Astronomy and Astrophysics.*
582. G. Contopoulos: Qualitative Characteristics of Dynamical Systems. In press in: A. Roy, "Long Term Behaviour of Natural and Artificial N-Body Systems", Reidel.
583. G. Contopoulos: Critical Cases of 3-Dimensional Systems. *Celestial Mechanics.*

584. G. Contopoulos: The 4 : 1 Resonance in Barred Galaxies. *Astronomy and Astrophysics.*
585. T. Le Bertre: Optical and Infrared Observations of IRC + 10216 and Related Objects: Dust Shells Modelling. *Astronomy and Astrophysics.*
586. G.A. van Moorsel: A Neutral Hydrogen Study of Interacting Galaxies in the NGC 697 Group. *Astronomy and Astrophysics.*
587. N. Bergvall and L. Johansson: Detection of Molecular Hydrogen in Two Merging Galaxies. *Astronomy and Astrophysics.* Letters to the Editor.
588. A.F.M. Moorwood and E. Oliva: Infrared Spectroscopy of [FeII], H_2 and H Line Emission in Galaxy Nuclei. *Astronomy and Astrophysics.*
589. Bo Reipurth: Herbig-Haro Objects in Flows from Young Stars in Orion. *Astronomy and Astrophysics.*
590. O.-G. Richter and M. Rosa: On Supernova Rates and Bursts of Star Formation. *Astronomy and Astrophysics.*
591. C. Gouiffes et al.: Light Echoes from SN 1987A. *Astronomy and Astrophysics.*

Large Scale Deviations from the Hubble Flow

J. HESSELBJERG CHRISTENSEN, The Niels Bohr Institute, University of Copenhagen, Denmark

Introduction

All standard Big Bang cosmologies have one thing in common. The initial state from which the Universe has developed, was homogeneous and isotropic to a "very high degree". Indeed we now observe that the distribution of galaxies is very homogeneous and isotropic when smoothed over a suitable large area of the sky. Also we observe that galaxies recede from one another in a universal manner described by the Hubble law, and this law is considered as valid on sufficiently "large scales". There is additional observational evidence in the "very high degree" of isotropy of the microwave background radition, neglecting the very well understood dipole anisotropy for the moment.

As the observational techniques have improved tremendously in recent years, the time has also come for the observers to quantify statements like "large scales" and "very high degree". It seems that the determination of the values of these poorly determined quantities finally are approaching the situation, where it is no longer the equipment of the observer but rather the adopted analysis of the observations, which is the crucial factor.

Such quantities have turned out to be some of the most desired physical parameters for tests of cosmological models, and we are now very close to getting important insights into cosmological phenomena. As the accuracy of observationally determined parameters increases, the number of models which can match them all decreases. The gain is therefore twofold. We can increase our knowledge of the present Universe and at the same time reduce the number of theories which claim to describe the evolution of it. The big trouble of course is that human beings can invent new theories all the time, so in reality it is only the former of these two statements which is true.

Previous Work

Almost since the discovery of the microwave background radiation, a dipole anisotropy has been noticed. It can be rather precisely accounted for if the Sun moves at 377 $\pm$ 14 km s^{-1} towards (l, b) = (267°, 50°) (Fixen et al. 1983), where (l, b) are galactic coordinates. With the standard de Vaucouleurs convention for the motion of the Sun relative to the Local Group, this means that the Local Group moves at 614 $\pm$ 14 km s^{-1} towards (l, b) = (269°, 28°).

In 1976 Rubin and Ford (Rubin et al. 1976) measured the velocity of the Local Group with respect to ScI galaxies in the redshift range from $\approx$0.01 to $\approx$0.02, corresponding to 3,000 – 6,000 km s^{-1} in the Hubble flow. They considered these galaxies to be standard candles and found a significant motion of the Local Group of 454 $\pm$ 125 km s^{-1} towards (l, b) = (163°, −11°). This implied a motion of the frame defined by the ScI galaxies relative to the microwave background of 862 $\pm$ 125 km s^{-1}. Ten years later, Aaronson et al. (1986) found no evidence for any net motion with respect to the microwave background for a sample of cluster spirals in the ring of sky accessible to the large Arecibo radio telescope. Their analysis was based on distances estimated from the infrared Tully Fisher relation. A programme designed to estimate distances to a sample of elliptical galaxies performed by a group of seven collaborators (Lynden-Bell et al. 1988) has changed the game somewhat. This group has demonstrated that the situation is much too complicated to be described by a simple motion of our Local Group towards a system of galaxies as defined above. They have shown that a model in which the bulk flow of galaxies is replaced by the flow generated by a mass concentration centred on (l, b) = (307°, 9°) at a distance corresponding to 4,350 km s^{-1} in the Hubble flow, now baptized "the great attractor", gives a much better understanding of the situation.

Determining Distances to Spiral Galaxies

The original Tully Fisher relation is a correlation between total B magnitude corrected to face-on and the 21 cm linewidth corrected to edge-on. In order to minimize the uncertainties in deprojecting the linewidth, one has to stick to highly inclined galaxies. This on the other hand increases the uncertainties in the estimated total B magnitudes. When the photometry is done in the infrared (H band at 1.6 μm), this problem is expected to be reduced considerably. There is however one disadvantage in using H band photometry. H magnitudes are measured within a standard aperture A, which is determined by the condition that $\log A/D_0 = -0.5$, where D_0 is the isophotal diameter at 25 B mag $arcsec^{-2}$ for the galaxy seen face-on. This choice of aperture has been made primarily because of historical lack of a suitable devise to make detailed surface photometry of galaxies in the near infrared. A nice demonstration of the somewhat complicated situation can be found on one of the figures in Giraud (1987).

The combination of the optical and infrared Tully Fisher relations has suggested another distance indicator. This is an infrared colour-magnitude (C-M) relation which is based upon an observed correlation between $(B\text{-}H)_{-0.5}$ colour and $H_{-0.5}$ magnitude (Wyse 1982), where the subscript$_{-0.5}$ refers to the standard aperture described above. This relation has the advantage over the Tully Fisher relation that galaxies, which are seen face-on, can be used and thereby reduce the uncertain correction procedures for deprojecting inclined galaxies to face-on. However small

these corrections at first may seem to be in the infrared, one can forsee that there are at least three potential problems. The aperture is related to D_0, and this parameter becomes still more badly determined the more inclined the galaxy is. And secondly, it is not simple to deproject a spiral galaxy to face-on, when it is seen through a relatively small aperture. At least to my knowledge it has in theoretical work only been studied in detail how one can hope to deproject a whole galaxy. Finally the majority of galaxies with $H_{-0.5}$ photometry only have B magnitudes at large apertures, and, therefore, extensive use of mean growth curves in order to extrapolate to the required $B_{-0.5}$ magnitudes, increases the uncertainties in the $(B-H)_{-0.5}$ colour further.

Modelled Inclination Effects

I have tried to investigate some of the effects induced by corrections for inclinations. This is done on the basis of a simple model for an exponential disk galaxy, which includes absorbtion.

The change of the modelled B and H observations with inclination, within 5 different standard apertures for a model galaxy is shown in Figure 1. The apertures chosen correspond roughly to 1, 2, 3, 4 and 5 times the standard aperture diameter previously defined. From the figures we see that although the galaxy at the largest aperture appears monotonically fainter with increasing inclination, the situation is more complicated at the smaller apertures. One should naturally take into account that this simple model only emphasizes the problems. In particular it is worth mentioning that the influence of a bulge component is totally neglected here. The model may only be a good approximation for Sc-Sd galaxies.

The curves in the two plots are the result of two effects: optical thickness and geometry. For an optically thin system, as a galaxy is expected to be in the H band, we will get more and more light from the outer part of the galaxy into the fixed aperture as we turn it towards edge-on. This explains most of what is seen on Figure 1a. An optically thick system will, due to inner absorption, lack this effect, and at the same time the amount of light coming from the internal parts will be reduced with increased inclination. Therefore, in a system with a moderate optical thickness, as is expected to be the situation in the B band, these two effects will compete. This is seen on Figure 1b.

As mentioned earlier there are problems with the analysis of existing $B_{-0.5}$ and $H_{-0.5}$ photometric data. To achieve some insight on their importance, I have tried to model them. In Figure 2 I have shown how a model galaxy by an inadequate treatment of the inclination corrections, that is without any correction for any of the mentioned effects, will be shifted from its locus in the C-M diagram for different inclinations, as indicated by the labels. Notice that for a face-on galaxy the shift is purely due to the use of mean growth curves. To see how this can influence the distance estimate to a cluster, I have simulated "observations" of cluster spirals. The spatial orientations were chosen at random – although all inclined more than 50° to be comparable with existing observations, see next section. The B-H magnitudes were chosen at random between 2.0 and 4.0 and the H magnitudes were generated from a linear C-M relation. Figure 3 is a plot of these observations. Also shown is the linear C-M relation from which the galaxies have been generated. It is evident that the data points still are in agreement with a linear correlation but the intersection differs from the original by a few tenths of a magnitude. This results in an error in the distance estimate of the order of 10–20%, which is crucial for the study of large scale motions.

Observations

Existing data on B and H magnitudes are biased towards highly inclined galaxies. This is because until now H band photometry has been focused on applicability to Tully Fisher. Thus select-

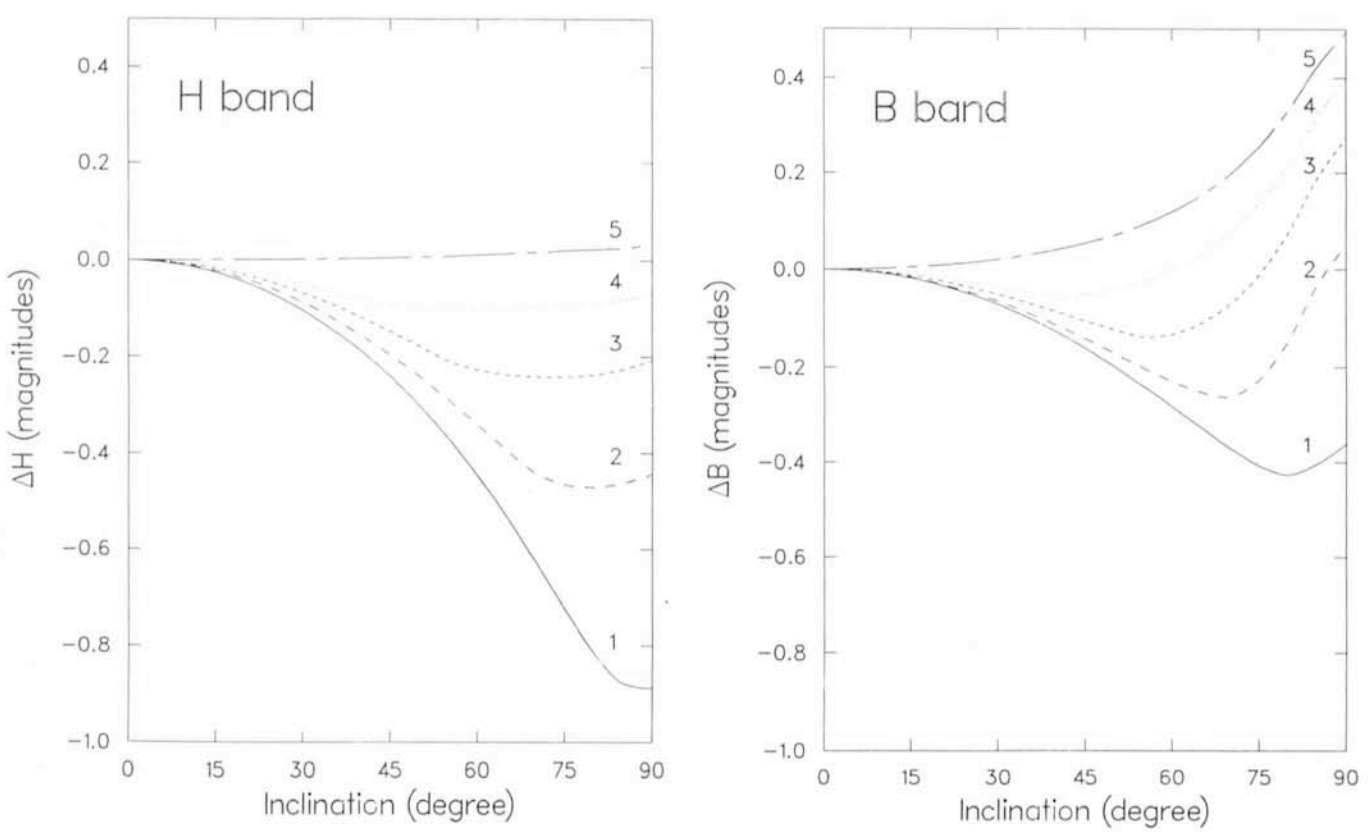

Figure 1: *(a) Change in "observed" H magnitude with respect to inclination for an exponential disk model, including absorbtion. Labels refer to aperture size, see text. (b) The same for B magnitudes.*

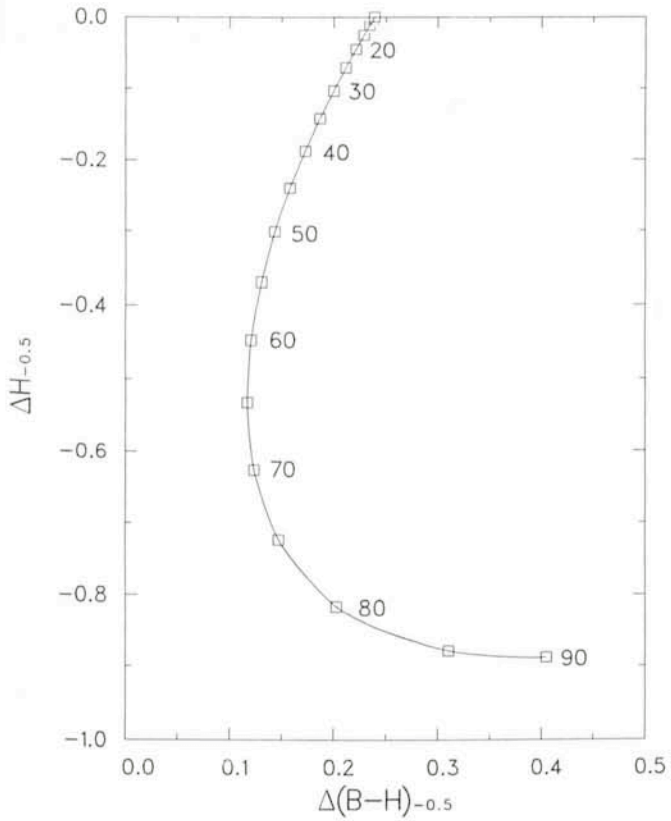

Figure 2: *Displacement in (B-H) and H due to the inclination effects at log $A/D_0 = -0.5$, and extrapolation of $B_{-0.5}$ from large aperture photometric data by means of mean growth curves.*

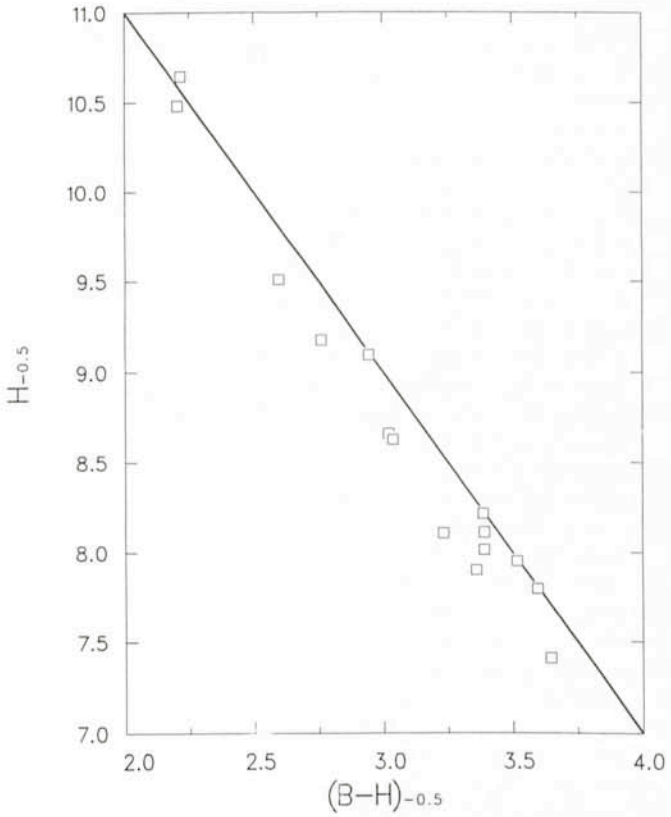

Figure 3: *Simulated $(B-H)_{-0.5}$–$H_{-0.5}$ relation for a sample of model galaxies, when no corrections for inclinations are made. Straight line shows the C-M relation from which the data has been generated.*

ing a sample of primarily face-on galaxies for observations in B and H, at apertures near log $A/D_0 = -0.5$, would seem to be a good opportunity to study the C-M relation in more detail. When at the same time one chooses to use galaxies with known redshifts, the full step of making a contribution to our further understanding of "large scale deviations from the Hubble flow" is within reach.

Thirteen nights in two runs (September/October 1987 and May/June 1988) at the ESO 1-m telescope have until now been allocated to a project, where this is the main goal. The data were acquired using a single channel photometer with the "Quantacon" in the B band, and after a change of setup to infrared in the middle of the observing period, with an infrared photometer using an InSb detector for the H band photometry. Unfortunately, very poor weather conditions were encountered during the major part of the first observing period. Useful observations under photometric conditions could be performed in B for less than 1 night and in H for 1 night so far. Since each galaxy has to be observed through a couple of apertures in each band, only observations of an uninterestingly small number of galaxies have been finished so far. Thus there is hardly enough to comment on yet. Hopefully I shall be in a better position after my next run at La Silla.

References

Aaronson, M., Bothun, G.D., Mould, J.R., Huchra, J., and Schommer, R.A., 1986. *Ap. J.* **302,** 536.

Fixen, D.J., Cheng, E.S., and Wilkinson, D.T., 1983, *Phys. Rev. Lett.* **50,** 620.

Giraud, E., 1987. *The Messenger* **No. 49,** 20.

Lynden-Bell, D., Faber, S.M., Burstein, D., Davies, R.L., Dressler, A., Terlevich, R.T., and Wegner, G., 1988. *Ap.J.* **326,** 19.

Rubin, V.R., Thonnard, N., Ford Jr., W.C., and Roberts, M.S., 1976. *Ast. J.* **81,** 719.

Wyse, R.F.G., 1982, *M.N.R.A.S.* **199,** 1P.

Searching for Double Degenerates

A. BRAGAGLIA, L. GREGGIO, A. RENZINI, Dipart. di Astronomia, Università di Bologna, Italy
S. D'ODORICO, ESO

The Elusive Progenitors of Type I Supernovae

The majority of stars are members of binary systems; this is a frequently referred aphorism. The majority of stars also terminate their evolution as white dwarfs (WDs), as only few stars are born massive enough to experience a supernova explosion. We can easily conclude that the majority of binary systems must at some stage become a double WD binary, and that a good fraction of the stars listed in our catalogues as WDs may indeed be double.

Very few WDs, however, are known for being double, and indeed Greenstein (1986) lists just six such objects. These are very wide pairs, visual double degenerates, in which each component has evolved independently of the other, as if it were a single star. An example of this kind may be provided by the Sirius system: in less than one billion years also Sirius A will be a WD, and Sirius A+B will become a wide double degenerate (DD) system. But in *close* binaries the evolution of each component is severely affected by the presence of the companion: The system can experience

common envelope phases during which first the envelope of the primary, and subsequently that of the secondary, are expelled from the system thus leaving bare, WD cores. The energy required for such an ejection is supplied (via friction) by the orbital motion of the binary: The orbit then shrinks during the common envelope stages, and at the formation of the second WD the separation can be much smaller than the original separation, when both stars were on the main sequence. This is just contrary to the evolution of wide binaries, where mass loss from the system leads to even larger final separations.

The relation between initial and final separation is theoretically very uncertain, an uncertainty which follows primarily from the hydrodynamical complexities of the common envelope stages which prevent a secure estimate of the efficiency (α) with which the orbital energy is converted into energy of the ejected envelope (Iben & Tutukov 1984). The smaller this efficiency, the closer the two WDs as the second WD is formed, i.e. the smaller the *initial* separation of the DD phase in the evolution of the binary system.

The duration of this phase, unlike the previous *nuclear* phases of stellar evolution, is controlled by a new *clock:* gravitational wave radiation. The fate of DD systems is then to spiral in, until the less massive WD fills its Roche lobe and the two components merge. If the initial semimajor axis of the DD is smaller than a critical value, then merging will occur within a time less than the Hubble time, and merging itself will become an astrophysically interesting event. Indeed, if the DD consists of two carbon and oxygen WDs and its combined mass exceeds the Chandrasekhar limit ($\sim 1.4\ M_\odot$) then either a thermonuclear explosion (carbon deflagration) destroys the star completely (Iben and Tutokov 1984), or the collapse of the merged object leads to the formation of a neutron star (Nomoto and Iben 1985), depending on the uncertain timescale of the actual merging process. Both possibilities are astrophysycally very interesting, as either a type I supernova event or a millisecond pulsar would then respectively be produced (Iben and Tutukov 1984, Saio and Nomoto 1985). The former case is perhaps more exciting, due to the strong impact that type I SNe have on the evolution of galaxies. Type I SNe, in fact, are thought to generate most of iron-peak elements produced in galactic nucleosynthesis (e.g. Greggio and Renzini 1983, Matteucci and Greggio 1986) as well as most of the heating required to maintain the interstellar medium of elliptical galaxies to the observed high temperature inferred from their strong X-ray emission (Fabbiano 1986, Canizares et al. 1987, Loewenstein and Mattews 1987). Clearly, the understanding of important aspects of galactic evolution requires a kowledge of the rate of type I SNe over cosmological times, which in turn depends on the detailed distributions of binary parameters, like masses and separations. Still, the mentioned theoretical uncertainty in the efficiency parameter α prevents a deterministic estimate of SNI rates as a function of population age, and at this point only dedicated observations of SNI candidate progenitors could help passing beyond this bottleneck.

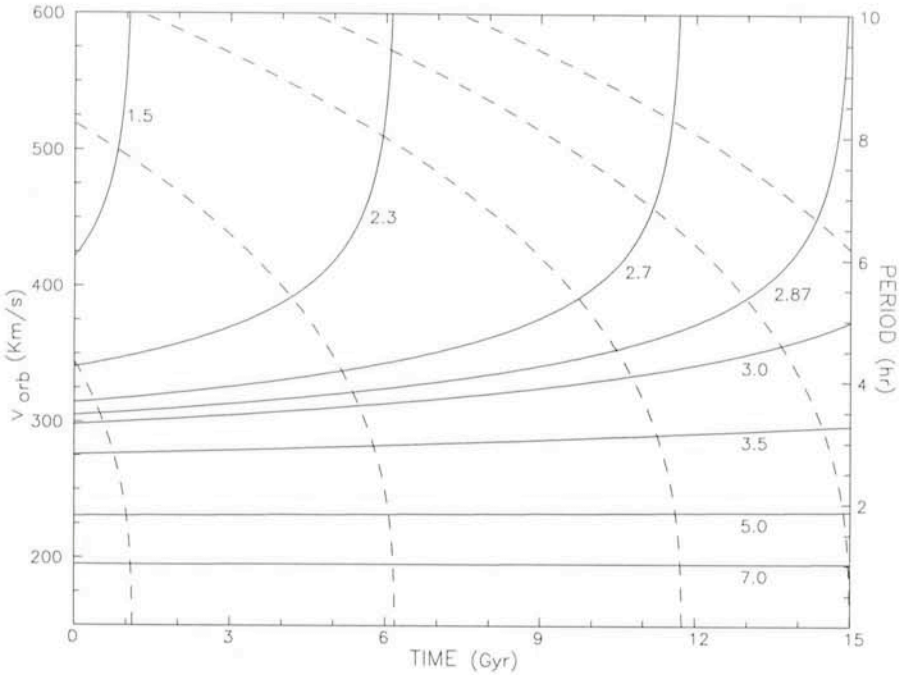

Figure 1: *The evolution of the period and orbital velocity of a double degenerate system of two 0.7 $M_\odot$ white dwarfs, as angular-momentum losses by gravitational wave radiation progressively shrink the orbit. Each curve is labelled with the initial semi-major axis in $R_\odot$ units. Note how the merging time is strongly sensitive to the initial separation of the DD system. Note also that objects with initial orbital velocity in excess of ~ 300 km s^{-1} merge in less than one Hubble time (assumed to be $\sim 15 \times 10^9$ yr).*

In this frame, we have started an observational programme aimed at reducing the uncertainties still enshrouding both the final stages of binary evolution and the nature of SNI progenitors. The questions we aimed to answer are basically two: (1) How frequent are DD systems among known white dwarfs? and (2) what is the fraction of such systems that will likely merge in less than one Hubble time? Figure 1 shows the computed evolution of the period and orbital velocity of DD components, as gravitational wave radiation progressively shrinks the orbit. One sees that the initial orbital velocity of the DD must exceed ~ 300 km s^{-1}, if merging is to take place

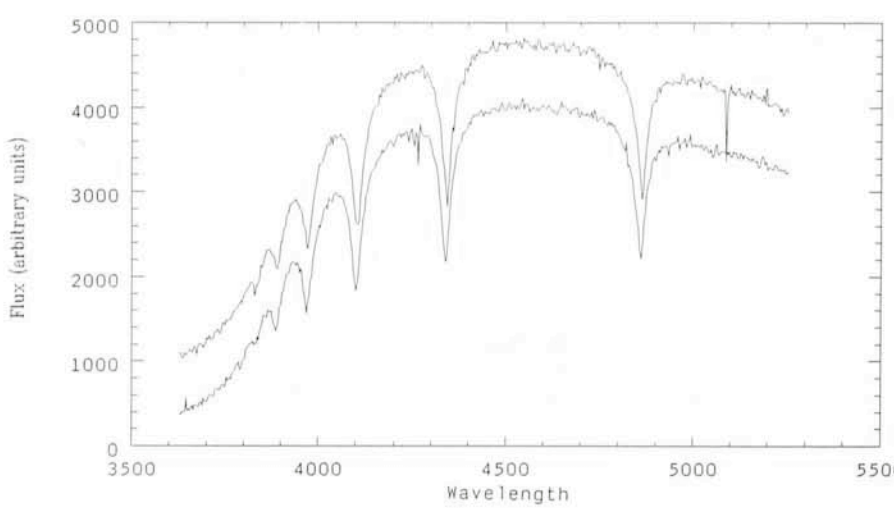

Figure 2: *Two spectra of WD-17 taken 25 hours apart. The flux scale is arbitrary. Note the shift of the Balmer lines, which corresponds to a radial velocity change of ~ 220 km s^{-1}.*

within one Hubble time. In this example, this corresponds to an initial period of ~12 hours. Therefore DD systems in which we are interested should exhibit radial velocity variations of a few hundred km s^{-1}, that can easily be detected using modern instrumentation. Correspondingly, our observational strategy has been to start a spectroscopic survey of catalogue WDs, with the aim of finding high orbital velocity DD pairs. We stress that theory cannot really predict what fraction of WDs are actually DD systems: This is in fact the main motivation for undertaking such a search, that ultimately we would like to extend to ~100 WDs, so as to ensure some statistical significance of the sample.

Hunting White Dwarf Binaries with EFOSC

Our target objects were chosen from the *Catalogue of Spectroscopically Identified White Dwarfs* of McCook and Sion (1984). The selection criteria of our choice have been very simple: We wanted the WDs to be relatively bright in order to minimize the observing time required to get a high S/N spectrum, and we further restricted to WDs of the DA variety in order to achieve the highest possible accuracy in radial velocity determinations, thanks to their prominent Balmer lines. Basically, our observational strategy has been to take several spectra of the same WD, a few hours apart (in practice, intervals between 2 and 25 hours), and then look for any radial velocity change. This should be most efficient in the case of DDs with components of very different luminosity (very different cooling time), while old DDs should rather have similar luminosity, and then exhibit variations in line profile, rather than in line position. EFOSC at the 3.6-m telescope was chosen as this provides the optimal observing configuration: thanks to its high efficiency, high S/N multiple spectra of several objects can indeed be obtained in one night. Moreover, each spectrum is obtained with a relatively short exposure (<~15 min), which then ensures adequate time resolution also in the case of short-period objects. Our observational strategy is very different from others that have been unsuccessful in singling out DD candidates that may be SNI progenitors. In particular, we are not bound only to short-period systems as in the case of the survey of Robinson and Shafter (1987).

Till now we had two observing runs at the ESO 3.6-m telescope, respectively in September 1985 (2 nights) and in January 1988 (3 nights). A total of 20 WDs have been observed at least twice and possibly three times, always using EFOSC with the B150 grism (spectral range 3600–5590 Å) giving a resolution of ~6.5 Å.

The reduction was carried out with the IHAP system in Garching. The spectra were wavelength calibrated with a helium lamp generally taken at the same telescope position of the target object. This data base allows to test the limiting accuracy of EFOSC for radial velocity determinations. By comparing the different calibration exposures taken through the night at different zenithal distances (from 1 to 2 air masses) we note that the lines fall in the same position on the CCD to within ~0.15 pixels, which would correspond to a systematic shift of ~35 km s^{-1} at λ = 5000 Å. The accuracy of the dispersion curves fitting the calibration lines of an individual exposure is somewhat better, giving an RMS of ~0.3 Å (or ~20 km s^{-1} at λ = 5000 Å). Our velocity determinations are based on several absorption lines, and hence we estimate that the error is actually smaller than 20 km s^{-1}. For the objects observed in the first run, we used a single calibration exposure taken at the beginning of the night. This leads to a larger uncertainty in the velocity determinations for the first run objects, that we then estimate to be at least of the order of ~60 km s^{-1}.

Given the main goal of the project, we are primarily interested in the actual value of the v_r differences between two or more spectra of the same star, taken at different times. To get such differences, we use a programme whose original version had been written by Pier (1983) and which has been adapted to work on WDs, where generally lines are very broad so that the wings are very important. The programme uses one spectrum as template; after normalizing, flattening with continuum subtraction, and rebinning, the programme computes the cross-correlation of this template with a second spectrum of the same star. The position of the cross-correlation peak gives immediately the velocity difference between the two spectra.

Two Good Candidates and Two WDs with Red Dwarf Companions

We have determined v_r variations for the 20 programme stars for which we have at least two spectra. Among these WDs two turned out to have red dwarf (RD) companions, and these two interesting objects are discussed below. Of the 18 residual dwarfs 9 were observed in the first run, and 9 in the second. All the first run objects show Δv_r values between ~50 and ~150 km s^{-1}, just consistent with all being the result of our poorer accuracy during that run. The situation is far more exciting for the second run objects: here seven dwarfs exhibit Δv_r consistent with 1σ errors ~20 km s^{-1}, one WD has $\Delta v_r \simeq$ 70 km s^{-1}, and for the last dwarf (WD-17, in our list of targets) the cross corre-

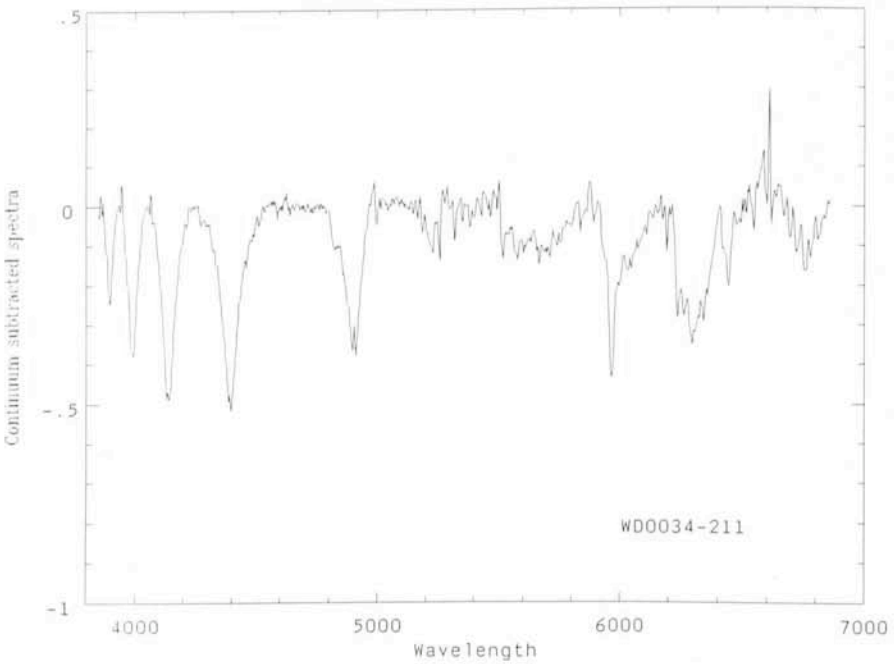

Figure 3: *Continuum subtracted and flattened spectrum of WD 0034-211; this is a composition of one blue and one red spectrum, taken respectively with the B 150 and O 150 grisms. Shortward of ~5000 Å the WD component dominates the light, while the red companion dominates at longer wavelengths. The faint emission core in the Balmer lines suggests the presence of an accretion disk. In the red side of the spectrum the most prominent features are the narrow Na absorption, several TiO bands, and the strong Hα emission.*

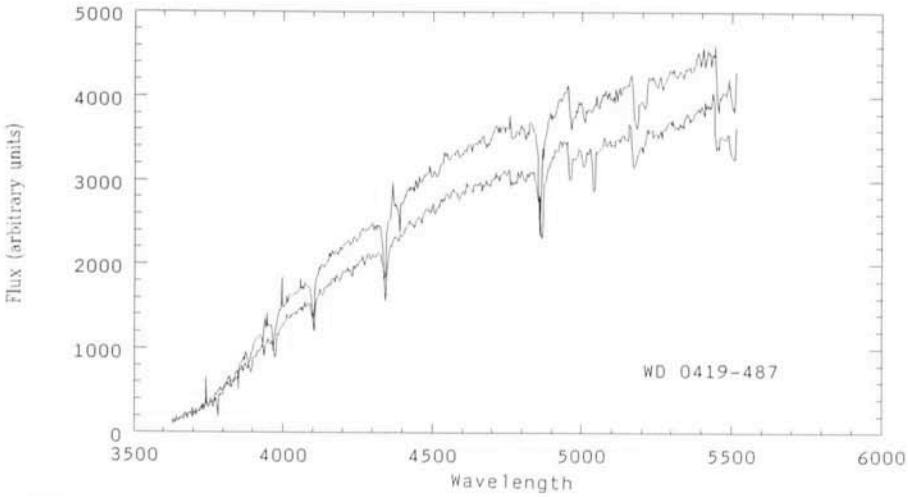

Figure 4: *The blue spectrum of WD 0419-487; note that also in this case the lines of the red companion are prominent in the red side of the spectrum. The Balmer lines are much narrower than in the case of the two other WDs; this is indeed a low surface gravity WD with a mass of only* $\sim 0.29\ M_\odot$.

lation between the three available pair of spectra gives Δv_r = 220, 176, and 45 km s^{-1} respectively, well above our estimated errors. Figure 2 shows two spectra of WD-17, where the shift in line position is also apparent. We conclude that two new DD systems may have been discovered, one of which exhibits radial velocity changes which are interestingly close to those expected for SN I progenitors. Clearly, further observations are required to confirm these preliminary results, and to determine the full Δv_r amplitude and period of the two DD candidates.

We now turn to the dwarfs with composite spectra. The spectrum of two programme WDs showed in fact clear signs for the presence of a RD companion. These two WDs were indeed already listed by Probst and O'Connell (1982) among the seven WD+RD pairs that they have discovered photometrically, thanks to their IR excess. The inclusion of these two objects in our programme was however unbiased, and then we can refer to a spectroscopic *rediscovery* of their binary nature. This will be relevant for the statistical aspects of the present research. In any event, the spectroscopic study of the two pairs is revealing some very interesting properties of the systems.

In one of them (WD0034-211, observed in the first run) a faint emission core was evident in all the Balmer lines, possibly indicative of an accretion disk originated by transfer of material from a nearby companion. In the second run we have then reobserved this object in the red spectral range (5000–7000 Å), using the O150 grism and calibrating with the He+Ar lamp. The composite spectrum (from 3600 to 7000 Å) is shown in Figure 3: Note the presence of several TiO bands typical of M-type stars, as well as the prominent Hα emission. The two blue spectra that are available do not indicate an interesting change in the radial velocity. However, the Balmer emission suggests that the RD component may be filling its Roche lobe, in which case the system should be very close. Orbital shrinking by both a common envelope stage and subsequent gravitational wave radiation might be blamed for the present configuration of the system, which appears to have the characteristics expected for a cataclismic binary caught in quiescence.

The other WD+RD pair (WD0419-487) is also an exciting object. Its spectrum is shown in Figure 4, where TiO bands are also evident at longer wavelengths where the RD light dominates. We have then applied the cross correlation technique separately for the blue (3850–4650 Å) and yellow parts of the spectrum (5000–5500 Å), so as to obtain the Δv_r of the WD and of the RD, respectively. This gives Δv_r = −124 km s^{-1}, and +232 km s^{-1}, indicating that the mass ratio is close to 0.53. Since the mass of the WD primary is known from surface gravity determinations to be $\sim 0.29\ M_\odot$ (Koester et al. 1979), we can then estimate the mass of the RD secondary as $\sim 0.15\ M_\odot$. The system appears to have evolved through a Case B Roche-lobe overflow, when the primary was experiencing its red giant phase of evolution, with a $0.29\ M_\odot$ helium core. We can then guess the approximate dimensions of the original orbit, and when knowing the present dimensions we could obtain a lower bound to the crucial efficiency parameter α.

Two very important applications of the WD+RD pairs can then be anticipated: First, we can check the mass-luminosity relation for RDs, which theoretically is extremely uncertain (cf. Liebert & Probst 1987, Renzini & Fusi Pecci 1988) while its knowledge is fundamental for the derivation of the low end of the initial mass function, and then for assessing the baryonic contribution to dark matter. Second, the determination of the masses and separation of WD+RD pairs can help setting constraints on the dynamical parameter α, and then help a better understanding of binary evolution, with implications also for the DD systems that may lead to a supernova explosion, and in which we are most interested.

The Perspectives

Our spectroscopic study of WDs has so far singled out four very interesting objects: The two WD+RD pairs and the two WDs with large radial velocity differences. This is quite a high proportion when we consider that just 20 objects have been investigated so far. The natural developments of this project are then both extensive as well as intensive: On the one hand we need in fact to enlarge the sample of observed WDs, on the other hand, we would like to obtain further data for those systems which are found to exhibit special characteristics. For example, we need to determine spectroscopic periods, as well as whole radial velocity curves. In particular, the system WD-17 deserves further study. Its large radial velocity variation makes it the best DD candidate for a SN I progenitor, comparable to WD0135-052 whose DD nature had been anticipated by Greenstein (1986) and spectroscopically confirmed by Saffer et al. (1987). In conclusion, modern instrumentation and techniques allow a fresh approach to apparently unconspicuous objects such as white and red dwarfs. Although certainly all WDs had a bright past, most will just fade away as time goes by. Few among them, however, might have an explosive future. Time is ripe for a closer look on these dwarfs.

Acknowledgements

We would like to thank Dr. Luciana Federici, Paola Focardi, and Bruno Marano for a preliminary manipulation of the spectra obtained in 1985, and for their introduction to the use of the cross-correlation programme. We would also like to thank Dr. Jim Liebert for having made available to us the preprint of his study of WD0135-052.

References

Canizares, C.R., Fabbiano, G., Trinchieri, G. 1987, *Ap. J.*, **312,** 503.

Fabbiano, G. 1986, *PASP*, **98,** 525.
Greenstein, J.L. 1986, *Ap. J.* **92,** 867.
Greggio, L., Renzini, A. 1983, *Astron. Astrophys.* **118,** 217.
Iben, I.Jr., Tutukov, A.V. 1984, *Ap. J. Suppl.* **54,** 335.
Koester, D., Schulz, H.,. Weidemann, V. 1979, *Astron. Astrophys.* **76,** 262.
Liebert, J., Probst, R.G. 1987, *Ann. Rev. Astron. Ap.* **25,** 473.
Matteucci, F., Greggio, L. 1986, *Astron. Astrophys.* **154,** 279.
McCook, G.P., Sion, E.M. 1984, *A Catalogue of Spectroscopically Identified White Dwarfs,* Villanova University Press.
Nomoto, K., Iben, I.Jr. 1985, *Ap. J.*, **297,** 531.
Pier, J.R. 1983, *Ap. J. Suppl.* **53,** 791.
Probst, R.G., O'Connell, R.W. 1982, *Ap. J. Lett.* **252,** L69.
Renzini, A., Fusi Pecci, F. 1988, *Ann. Rev. Astron. Ap.* in press; *ESO Preprint* No. 565.
Robinson, E.L., Shafter, A.W. 1987, *Ap. J.* **322,** 296.
Saffer, R.A., Liebert, J.W., Olszewski, E. 1987, *Bull. A.A.S.* **19,** 1041.
Saio, H., Nomoto, K. 1985, *Astron. Astrophys.* **150,** L21.

A Search for Flare Stars With the GPO Astrograph

R. ANIOL, H.W. DUERBECK, W.C. SEITTER, Astronomisches Institut der Universität Münster, F.R. Germany
M.K. TSVETKOV, Department of Astronomy, Academy of Sciences, Sofia, Bulgaria

1. Flare Stars in Young Stellar Aggregates

The first systematic investigation of flare stars by the Mexican astronomer Guillermo Haro marks the beginning of long-term, multi-site studies of these objects in young stellar aggregates. His first series of observations with the Schmidt telescope of the Tonantzintla Observatory already showed the close relation between stars in the T Tauri stage and cool dwarf stars with enhanced UV activity (= flare stars), both types of objects being still in their early stages of evolution.

After 30 years of subsequent investigations, some of the conclusions by Haro are substantiated on the basis of extensive observational material, while the new results also gave a clearer picture of the nature of flare stars. Some of the main achievements and results to be substantiated by further studies are:

- More than 1,000 flare stars in the aggregates of Orion, the Pleiades, NGC 7000 (North America nebula), Praesepe, Coma, and others were discovered.
- The physical correspondents of flare stars in aggregates are the UV Ceti stars in the solar neighbourhood.
- By observing multiple flares in given stars, the lower limit of the number of flare stars in various aggregates could be estimated: Orion – 1,500; Pleiades – 1,000, NGC 7000 – 400, Praesepe – 300, Coma – 100 stars.
- It was found that, for a given aggregate, the spectral type of the brightest flare star and the maximum flare amplitude both correlate with the age of the aggregate.
- In stellar evolution, the T Tauri stage is followed by the flare star stage.
- There are two major types of flares, fast and slow ones. It is concluded that all flares have the same physical origin, since there are also rare flares of intermediate speed.

The close correspondence between flare stars in aggregates and in the solar vicinity, as well as some analogy between the flares in these stars and the solar flares suggest theoretical models for the underlying physical process(es). However, a general picture which includes all aspects of the problem of correlating the properties of flare stars, UV Ceti stars and older main sequence stars, has not yet been developed.

2. The GPO Astrograph

The GPO astrograph was one of the first telescopes on La Silla. At its previous location Zeekoegat in South Africa (1961–1966) and during its first years on La Silla, it was mainly used to obtain objective prism spectra of stars in the direction towards the Magellanic Clouds. One of the rare spectra of Sk – 69° 202, the star that later became SN 1987A, was taken with this instrument.

A new chapter for the GPO was opened with increasing interest in direct plates. Most of them are used for *astrometric* purposes: for asteroid observations, proper motion studies, and for the input catalogue of the HIPPARCOS astrometric satellite mission. Recent highlights of the southern sky, Halley's Comet and the Supernova 1987A, tempted more observers to "try" the GPO. We will report on one of our two *photometric* surveys, the search for flare stars with the GPO. Figure 1 displays the observational activity of the last two decades.

3. The Suitability of the GPO for a Flare Star Search

Until now, patrol observations of flare star fields were predominantly carried out with Schmidt telescopes in the northern hemisphere. The Schmidt telescopes in the southern hemisphere were to a large extent occupied by atlas

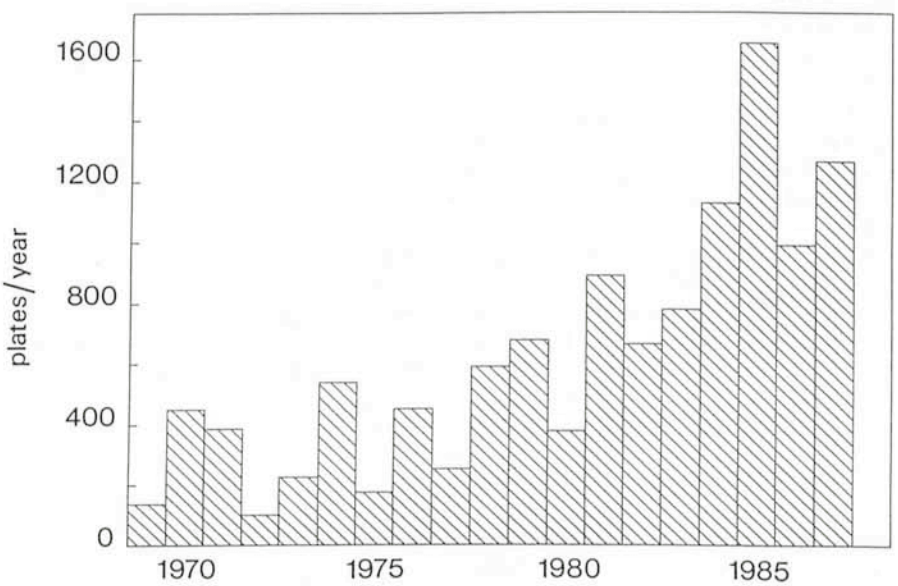

Figure 1: *Number of plates per year taken with the GPO telescope since the beginning of its operation on La Silla.*

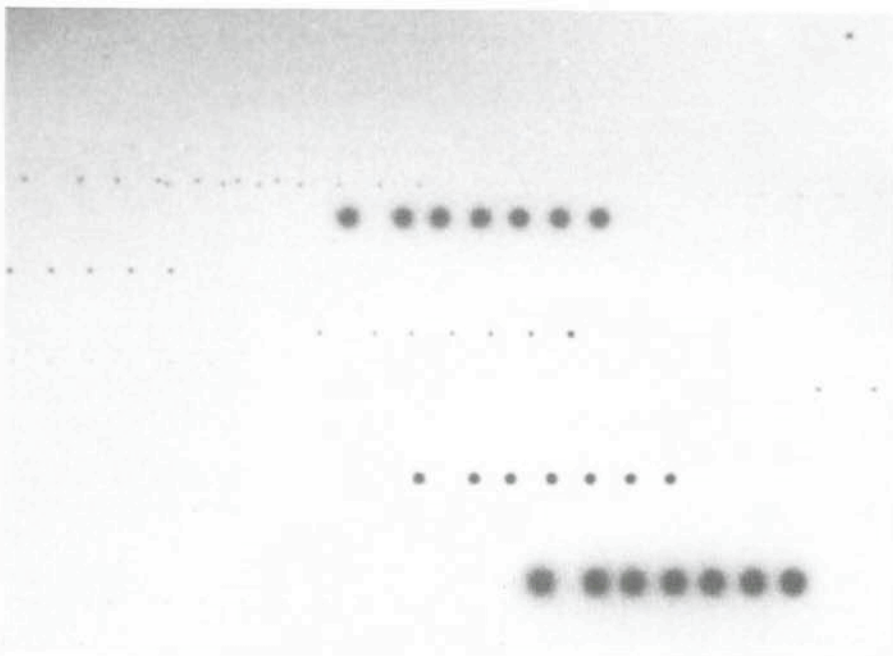

Figure 2: *Section of a multiple exposure plate of the Orion nebula region, showing the rise of a slow flare of KO Ori (emulsion IIa–O, exposure time 6×10 minutes).*

work. It thus seemed worthwhile to try the GPO telescope for a survey of southern fields.

While an astrograph has weak transmission for ultraviolet light, where most of the radiation of the flare is emitted, it has a more suitable image growth which makes small magnitude differences better measurable. In order to calibrate the *detection power* of the GPO, we chose the well studied region of the Orion nebula (M42/M43), the centre of the richest field of UV Ceti and T Tauri stars.

The visual inspection of the test plates (by M.K.T.) showed that the UV deficiency is indeed compensated by the enhanced image growth and that at least as many flare events per unit area and unit time are discovered on GPO plates as on Schmidt plates (Tsvetkov et al., Comm. Konkoly Obs. No. 86, Budapest 1986, p. 429.)

New fields of the survey are the young clusters o Vel (IC 2391), Θ Car (IC 2603), and the dark cloud regions Cha T1, Sco-Oph, ϱ Oph, and Sco-Sgr.

4. Methods of Reduction

Generally, five to seven exposures of ten minutes duration each, separated by 30″, are made per plate. An example is shown in Figure 2, which portraits one of the rare *slow* flares, here of the star KO Ori.

For the beginning of the flare star project, we intended to reduce the multiple-exposure plates fully automatically. All plates are scanned with the PDS 2020GM plus microdensitometer at the Astronomical Institute Münster. The programme package developed by one of us (R.A.) includes:

1. plate preprocessing
2. chain recognition
3. search for flare event candidates
4. history of variability.

In part one, the data are brought into the form needed for the subsequent processes. Image segmentation and restauration is performed with a programme written by H. Horstmann for a galaxy survey on ESO/SRC atlas plates. The microdensitometer coordinates are transformed into celestial coordinates, using an astrometric programme written by H.J. Tucholke. The first step is the transformation of the coordinates for a single long exposure *master plate.* This is necessary because the deep plate registers stars which may be visible on the multiple exposure plate only during a stellar brightening. The accuracy is better than 1″, when stars from the SAO catalogue are used. Next, coordinate transformations are made between the master plate and the multiple exposure plates. The coordinates are assigned to the eastern image of each *chain of exposures.*

Finally, the *machine magnitudes* of the images are calculated using a standard characteristic curve.

The data are now ready for the second part of the programme, whose purpose it is to determine the mean distances between the images in the chains and their standard errors. Chains with a smaller number of images (weak stars drowned in a variable sky background) or chains with more images than exposures (caused by the almagamation of two chains with equal coordinates in declination) are not analysed at this stage. The resulting mean distances between images are determined within 0.5″ to 1.0″.

It is now possible to look for *all* chains. The amalgamated chains can generally be separated without difficulty on account of their larger number of members. Shorter chains and even single images can be found using the coordinate list of objects found on the master plate. Before storage, the chains are marked with identifiers, which give the total number of images. Incomplete chains or single images are stored separately, because they have a higher probability of resulting from a flare star.

The third part of the programme is devoted to the search for flare events. A *standard light curve* (variation of magnitude across a representative chain) must be known in order to determine the presence of a flare by comparison with a given chain. Because of the scatter in the magnitudes of individual chains, a *mean* light curve must be used. In order to avoid systematic effects, mean light curves are obtained separately for given magnitude intervals.

A chain showing at least one significant deviation from the mean lightcurve marks a flare candidate, though, as a rule, a true flare produces several devia-

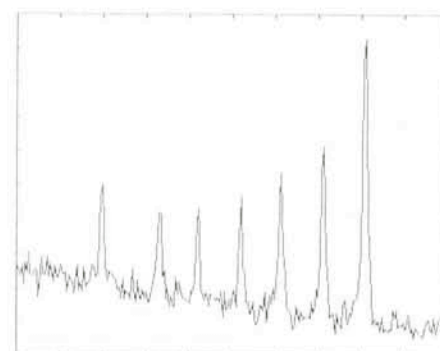

Figure 3: *Intensity tracing of the slow flare of KO Ori.*

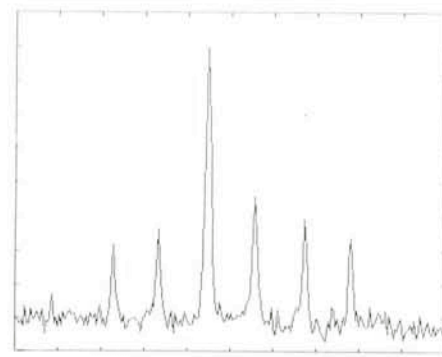

Figure 4: *Intensity tracing of a fast flare observed in a newly discovered flare star in Orion.*

tions. The method is very sensitive. By visual inspection, only flares of amplitudes larger than $0^m.6$ are found. Here it seems possible to decrease the limit to about $0^m.3$. The method also yields useful results for plates taken under non-photometric conditions; such plates, however, are rarely obtained at La Silla.

The flare candidates are stored in a "flare-file". This file contains also information about celestial coordinates, magnitudes of the images and density of the sky background. The last value is especially important for checking the reliability of a reported flare event, because a strong variable background, even when properly subtracted, can produce systematic exposure effects. Another problem appears for almagamated chains in regions of *high* star density. It occasionally happens that stars from the two chains merge into single images of higher brightness. This can occur at any position in the chain.

At last, the discovered flare events can be inspected in the form of tracings or digitized images of the chain. The images reveal only flare events with sufficiently large amplitudes, while the tracings clearly show also the fainter flares and the variations of the sky background. Two examples of flare stars are given in Figures 3 and 4.

The final part of the programme, which is under development, offers the user the possibility to combine results from *different* plates, in order to study the complete available history of all stars in the field. For flare stars, this means better confirmation, especially in cases of low amplitude flares of higher frequency, and thus higher sensitivity of the photographic flare search. Also, typical time scales for more frequent flares can be determined. Finally, other types of variables with longer periods can be detected.

Dust in Early-Type Galaxies

M. P. VÉRON-CETTY and P. VÉRON, Observatoire de Haute-Provence, France

Introduction

A brief historical review of the discovery and exploration of elliptical galaxies has been published by de Vaucouleurs (1987). We have made use of it to write this introduction.

The most widely used classification system for galaxies is that proposed by Hubble in 1926. The sequence of classification, as originally presented, consisted of a series of elliptical nebulae ranging from globular (E0) to lenticular (E7) forms, and two parallel series of unwiding spirals, normal (S) and barred (SB). The figure following the symbol E is equal to the ellipticity (a−b)/a with the decimal point omitted, a and b being respectively the major and minor axis of the galaxy.

Elliptical galaxies have been described by Hubble as highly concentrated objects with luminosity falling rapidly away from bright, semistellar nuclei to undefined boundaries; small patches of obscuring material are occasionally silhouetted against the luminous background, but otherwise these nebulae present no structural details.

No elliptical galaxies are known that are flatter than E7; galaxies which are flatter invariably show an outer region of low surface brightness which resembles a thin fundamental plane.

The transition from E7 to Sa appeared very abrupt. With accumulating data, and especially with the increasing number of good photographs taken with the 100-inch Mount Wilson reflector, numerous systems have been recognized as soon as 1936 by Hubble which are later (flatter) than E7, but which show no spiral structure. These galaxies fill the gap between E7 and Sa and are called S0 or SB0 (Sandage, 1975).

The S0 class has been described for the first time in 1961 by Sandage. S0 galaxies appear to form a transition between the E galaxies and the true spirals; the transition from E to S0 is smooth and continuous. The division between E and S0 is made on the basis of the presence or absence of an outer amorphous envelope or thin fundamental plane surrounding the nuclear regions. Some S0 galaxies exhibit a structureless envelope similar to that of the normal S0's, but a sharp, narrow absorption lane is found within the lens; the lane is in an arc concentric with the nucleus. These galaxies are called $S0_3$.

A more quantitative way to separate E from S0 has emerged from the study of the light distribution in galaxies. De Vaucouleurs (1959) has pointed out that elliptical galaxies have a single-component surface brightness distribution which follows closely the de Vaucouleurs relation:

$$\log I(r) \propto r^{1/4}$$

(r is the distance from the centre of the galaxy) while the surface brightness distribution for spirals and S0 galaxies show two main components: an inner spheroidal component which follows the de Vaucouleurs law, and an outer exponential component (disk) with:

$$I(r) = I(o) \times e^{-\alpha r}$$

This result has been confirmed since by a number of more recent works (see for instance: Freeman, 1970; Kormendy, 1977 a, b and c).

However, the classification of most galaxies has been made by visual inspection of photographic plates rather than by measurement of the brightness distribution leading to some misclassification especially when the galaxy contains dust.

Dust was clearly visible on a photograph of NGC 1316 taken in 1943 by Paraskevopoulos; but it was mistaken as plate defects by Shapley who could not believe that an elliptical galaxy could contain dust (Hodge, 1975). Probably because of the presence of this dust, NGC 1316 was called Sa pec by Sandage and Tammann (1981); however, Schweizer (1980) has shown that it is a typical Morgan D-type galaxy with an elliptical-like spheroid embedded in an extensive envelope.

In the course of a survey of bright southern galaxies, a pair of abnormal objects have been observed by de Vaucouleurs (1953) which shared most of the characteristic peculiarities of the bright radio galaxy NGC 5128 (Centaurus A), i.e. radio emissivity and dust; these galaxies are NGC 1316 (Fornax A) and NGC 1947, to which de Vaucouleurs added a northern galaxy, NGC 2537; however, at the time, radio positions were not accurately measured; the errors were of the order of 1°, and only NGC 1316 has been confirmed as a radio source; moreover, NGC 2537 is an Sc galaxy and of no interest here. NGC 1947 is indeed an early-type galaxy ($S0_3$ pec), but not a radio source (Möllenhoff, 1982).

Shobbrook (1963) has discovered a dust lane in the elliptical galaxy NGC 4696 and used it as an argument for the identification of this galaxy with

a radio source now known as PKS 1245–41; this identification has since been confirmed.

Westerlund and Smith (1966) have identified the early-type galaxy NGC 612 with the radiosource PKS 0131–36 and noted the presence of a dust lane. The identification has been confirmed by Bolton et al. (1965).

In the meantime, it was shown that powerful extragalactic radio sources were always associated with elliptical galaxies rather than with spiral or S0 galaxies (Matthews et al., 1964), and therefore two ideas emerged: that elliptical galaxies could contain dust and that dusty ellipticals are more often radio sources than galaxies without dust.

Dust is now known to be frequent in E and S0 galaxies (see for instance Hawarden et al., 1981, and Ebneter et al., 1988); moreover, a number of early-type galaxies have been detected at 100 μm by the **I**nfra-**R**ed **A**stronomical **S**atellite (IRAS) (Neugebauer et al., 1984), and this far-infrared emission is attributed to thermal emission by cold dust (Jura, 1986).

We have made a study of a complete volume limited sample of 78 early-type galaxies, looking for the presence of dust in order to check if there is any correlation between the presence of dust and that of radio or far-infrared emission.

The Observations

The revised Shapley-Ames Catalogue (Sandage and Tammann, 1981) contains 47 ellipticals and 29 S0 galaxies at declination $\delta < +20°$, with

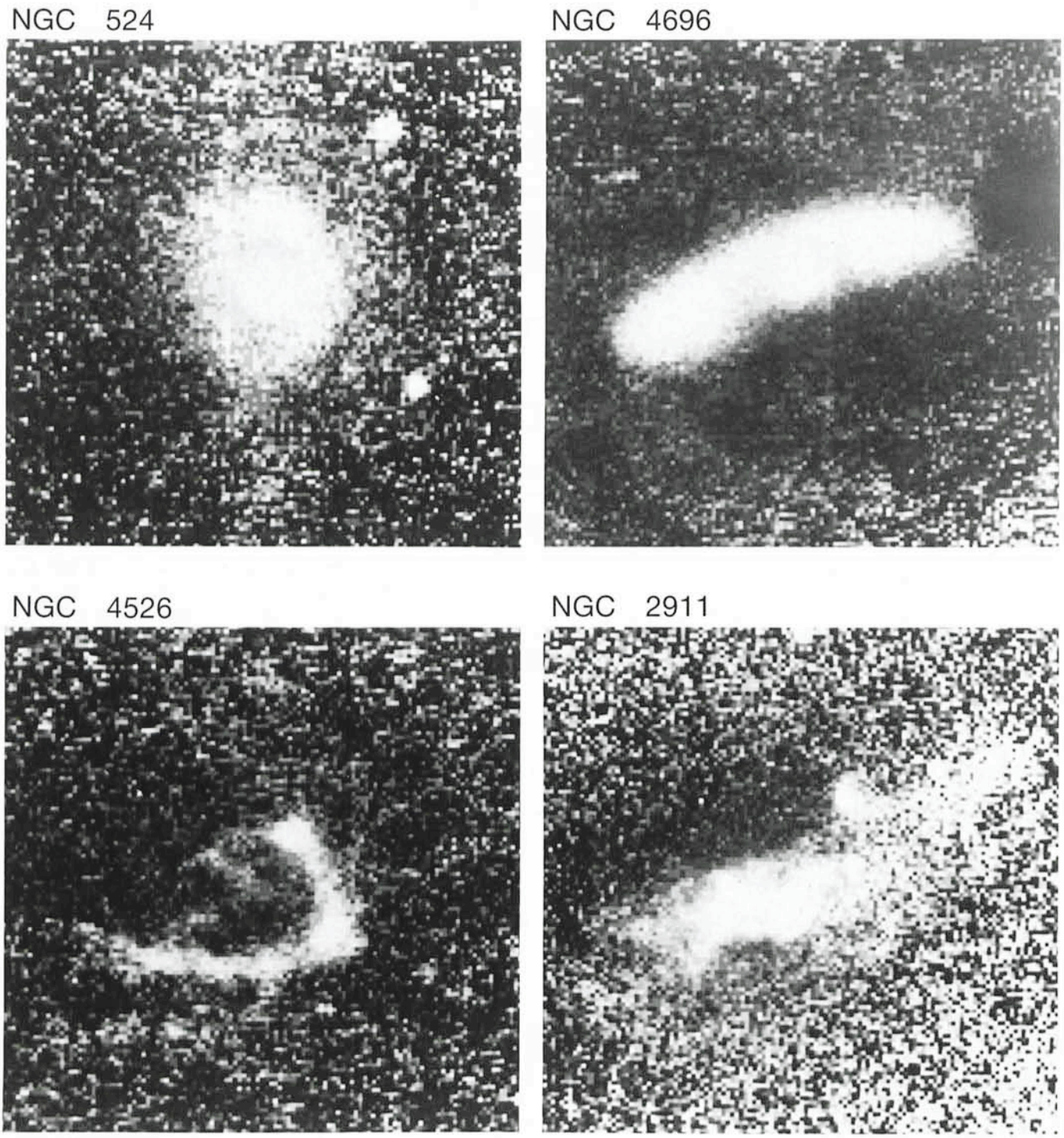

Figure 1. *This figure shows the ratio of the B to the z images for four of the galaxies with obvious dust clouds. Red, i.e. dust, shows up in white. In NGC 524, the dust appears to form an almost face-on disk; in NGC 4526, the dust is a very regular disk or torus seen almost edge-on; in NGC 4696, there is a thin filament of dust first discovered by Shobbrook in 1963; while in NGC 2911, the dust is in a very irregular cloud.*

a galactocentric radial velocity $V_o < 3{,}000$ km s^{-1} and a blue total absolute magnitude $M_B < -21$. If the RSA catalogue was complete to $m_{pg} = 12.9$, this would constitute a volume limited sample; however, according to Sandage and Tammann, at $m_{pg} = 12.9$, the completeness of the RSA catalogue is only 28%. Two other galaxies, NGC 1316 and 7213, classified as Sa by Sandage and Tammann, have been added to the sample; as we have seen above, NGC 1316 is a Morgan D-type galaxy while, according to Phillips (1979), NGC 7213 is a pole-on S0.

In the course of four observing runs at La Silla (October 1984, February and June 1985 and September 1987), we observed 69 of the galaxies with the 2.2-m telescope. For each galaxy, we have obtained two ten-minute direct images through a Johnson B and a Gunn z filter (Schneider et al., 1983) with a thin, back-illuminated RCA CCD having 512×320 30 μm pixels. The scale of these images is 0."36/pixel.

In addition, on January 24, 1988, one of the sample galaxies, NGC 2911, was observed with EFOSC (Dekker et al., 1988) at the Cassegrain focus of the 3.6-m telescope. The detector was a thin back-illuminated RCA 15×15 μm pixel CCD used in the 2×2 binned mode; the effective scale corresponds to 0."675 per 30 μm pixel. The exposure time was 6 minutes with each of the B and z filters.

In the near-infrared, fringes on the RCA CCD chip are very prominent; to remove them, we have obtained flat-fields during each observing run, by taking three sky images in a field almost void of stars, the telescope being moved by a few arcseconds after each exposure; comparison of the three exposures (with the routine FCOMPARE of IHAP) allows the removal of the stars and results in a flat-field which removes almost perfectly the fringes.

The sky level, estimated from the corners of each frame, was removed from each image and then, for each galaxy, we have divided the B by the z frame.

The presence of dust was detected by visual inspection of these images in 16 galaxies (four examples are given in Fig. 1) to which one can add NGC 1316, 5018 and 5128 for which we have no observations, but which are well known to contain dust.

Elliptical and S0 Galaxies

Of the 19 galaxies with dust, 6 are ellipticals, 12 S0 and one Sa (according to Sandage and Tammann, 1981), suggesting that dust is more frequent in S0 than in E galaxies (there are 47 E's and 29 S0's in the complete sample). However, as we have seen above, galaxies may have been misclassified and, more specifically, E galaxies with dust may have been called S0, just because for a long time it was believed that there is no dust in ellipticals. For instance, Sandage and Tammann have classified NGC 6868 as an E3/$S0_2$ and NGC 7196 as an E3/$S0_3$, suggesting that they are elliptical with dust.

A careful study of NGC 5266, classified as an $S0_3$ pec by Sandage and Tammann, has shown that it is an E4 galaxy, without trace of disk (Varnas et al., 1987). Similarly, van den Bergh (1976) has concluded that NGC 5128 is an E0 galaxy. NGC 1316 is an Sa pec according to Sandage and Tammann (1981), however, the brightness profile established beyond doubt that it is essentially an elliptical (Schweizer, 1980).

It is therefore necessary to measure the brightness profile of all the dusty galaxies to determine without ambiguity if they have a disk or not and find out the fraction of ellipticals and S0s which contain dust.

Dust and Radio Sources

Out of the 78 galaxies studied, 17 have a 5000 MHz flux density larger than 0.1 Jy. At the level of detection, 31% (6/19) of the dusty galaxies are radio sources, while 19% (11/59) of the non dusty galaxies are radio sources. There is therefore no strong evidence in our data for early-type radio galaxies to preferentially contain dust.

Dust and Infrared Emission

Jura (1986) has found that at least a third of all early-type galaxies are detected in the far-infrared by IRAS. The infrared emission is strongest at 100 μm and quite often the far-infrared luminosity is in excess of 10^8 $L_\odot$; the infrared flux most probably results from dust reprocessing of starlight (Jura, 1982).

Of the 78 galaxies in our sample, one has no IRAS coverage (NGC 3078) and 21 have been detected in the infrared (Lonsdale et al., 1985). Among the 21 galaxies detected by IRAS, 14 contain dust visible on the direct images, while of the 19 galaxies with dust, 14 have been detected by IRAS, all at 100 μm.

In our sample of 78 galaxies, 21 have been detected in the infrared. Let us assume that there is no correlation between the presence of dust as seen on direct images and the detectability at 100 μm. We have found 19 galaxies with dust; we expect five of them to be detected at 100 μm while there are 14. The probability to find 14 or more galaxies with dust in the IRAS subsample is about 10^{-6}; this is a strong indication that the assumption that dust and infrared emission are independent is not valid and that, therefore, the infrared emission of early-type galaxies is indeed due to thermal emission by cold dust.

One of the brightest galaxies at 100 μm is NGC 7213; however, in this galaxy, the presence of dust has been suspected (Phillips, 1979) but has still to be confirmed. It is a Seyfert 1 (Filippenko and Halpern, 1984) and, in this case, the infrared emission could be related to the activity of the nucleus rather than due to cold dust. Jura et al. (1987) have detected NGC 4486 at 12, 60 and 100 μm; this infrared spectrum is rather "hot", and unlikely to be due to cold dust; it could rather be associated with the optical jet discovered by Curtis in 1918. A good photograph of this jet has been published by Nieto and Lelièvre (1982).

Conclusions

The two main conclusions we have reached are that:

1. There is no clear evidence that radio galaxies more often contain dust than radio quiet galaxies.

2. Galaxies detected at 100 μm by IRAS are those which show clear evidence for dust on direct images, indicating that the infrared emission is most probably due to thermal emission by this dust. However, galaxies with an active nucleus and showing no evidence for dust may have a detectable far-infrared flux, in which cases this infrared emission would be associated with the activity of the nucleus.

References

van den Bergh, S., 1976, *Astrophys. J.* **208,** 673.

Bolton, J.G., Clarke, M.E. and Ekers, R.D., 1965, Australian *J. Phys.***18,** 627.

Curtis, H.D., 1918, *Publ. Lick Obs.* **13.**

Dekker, H., D'Odorico, S. and Arsenault, R., 1988, *Astron. Astrophys. J.* **189,** 353.

Ebneter, K., Djorgovski, S. and Davis, M., 1988, *Astron. J.* **95, *Astron.*** 422.

Filippenko, A.V. and Halpern, J.P., 1984, *Astrophys. J.* **285,** 458.

Freeman, K.C., 1970, *Astrophys. J.* **160,** 811.

Hawarden, T.G., Elson, R.A.W., Longmore, A.J., Tritton, S.B. and Corwin, H.G., 1981, *Monthly Notices Roy. Astr. Soc.* **196,** 747.

Hodge, P.W., 1975, *Sky and Telescope* **49,** 354.

Hubble, E., 1926, *Astrophys. J.* **64,** 321.

Hubble, E., 1936, *The realm of Nebulae,* Yale University Press.

Jura, M., 1982, *Astrophys. J.* **254,** 70.

Jura, M., 1986, *Astrophys. J.* **306,** 483.

Jura, M., Kim, D.W., Knapp, G.R. and Gahathakurta, P., 1987, *Astrophys. J.* **312,** L11.

Kormendy, J., 1977a, *Astrophys. J.* **214,** 359.

Kormendy, J., 1977b, *Astrophys. J.* **217,** 406.

Kormendy, J., 1977c, *Astrophys. J.* **218,** 333.
Lonsdale, C.J., Helou, G., Good, J.C. and Rice, W. 1985, "Catalogued galaxies and quasars observed in the IRAS Survey", JPL publication D. 1932.
Matthews, T.A., Morgan, W.M. and Schmidt, M., 1964, *Astrophys. J.* **140,** 35.
Möllenhoff, C., 1982, *Astron. Astrophys.* **108,** 130.
Neugebauer, G. et al., 1984, *Astrophys. J.* **278,** L1.
Nieto, J.-L. and Lelièvre, G., 1982, *Astron. Astrophys.* **109,** 95.
Phillips, M.M., 1979, *Astrophys. J.* **227,** L121.
Sandage, A., 1961, *Hubble Atlas of galaxies,* Carnegie Institution of Washington Publication 618.
Sandage, A., 1975, in *Galaxies and the Universe,* Sandage, A., Sandage, M. and Kristian, J. eds. University of Chicago Press; p. 1.
Sandage, A. and Tammann, G.A., 1981, *A revised Shapley-Ames catalog of bright galaxies,* Carnegie Institution of Washington Publication 635.
Schneider, D.P., Gunn, J.E. and Hoessel, J.G., 1983, *Astrophys. J.* **264,** 337.
Schweizer, F., 1980, *Astrophys. J.* **237,** 303.
Shobbrook, R.R., 1963, *The Observatory,* **83,** 36.
Varnas, S.R., Bertola, F., Galletta, G., Freeman, K.C. and Carter, D., 1987, *Astrophys. J.* **313,** 69.
de Vaucouleurs, G., 1953, *The Observatory,***73,** 252.
de Vaucouleurs, G., 1959, *Handbuch der Physik* **53,** 311.
de Vaucouleurs, G., 1987, IAU Symp. 127, p. 3.
Westerlund, B.E. and Smith, L.F., 1964, *Australian J. Phys.*. **17,** 340.

Long-Term Walraven Photometry of Cataclysmic Variables

S. VAN AMERONGEN and J. VAN PARADIJS,
Astronomical Institute "Anton Pannekoek", University of Amsterdam, the Netherlands

During the last seven years we have been observing cataclysmic variables (CV's) with the Walraven photometer behind the 90-cm Dutch telescope at La Silla. An advantage of this photometric system for strongly variable blue sources is that it allows simultaneous detection in five passbands, extending from the optical (5400 Å) to the ultraviolet (3200 Å). We have observed these CV's by monitoring them for several hours, and reduced the measurements differentially with respect to nearby comparison stars.

Results obtained so far include measurements of changes in the rotation periods of accreting white dwarfs in CV's, quite strong upper limits to secular changes in optical brightness of dwarf novae (DN) between outbursts, and the recognition that accretion instabilities similar to DN outbursts also occur in systems not classified as such.

Introduction

Cataclysmic variables are close binary stars consisting of a white dwarf and a low-mass ($< 1\ M_{\odot}$) near-main-sequence companion. This "secondary" star fills its so-called Roche lobe, i.e. the critical equipotential surface, outside which matter is no longer bound to the star (see Fig. 1). At the point on the line through the two stellar centres, where the Roche lobes of the secondary and the white dwarf touch each other, matter from the secondary can easily fall into the gravitational potential well of the white dwarf.

Such matter, flowing from the secondary star, has angular momentum with respect to the white dwarf, due to the orbital revolution of the binary. It will therefore settle into a more or less Keplerian orbit around the white dwarf. It is generally believed that viscous processes give rise to exchange of angular momentum, by which an initially formed ring spreads and forms a flat disk-like configuration, the accretion disk, around the white dwarf. Matter transferred from the secundary gradually spirals inward along quasi-Keplerian orbits. During this diffusion of the particles, the other half is radiated away.

This radiation from the accretion disk generally dominates the optical and UV luminosity of cataclysmic variables. The kinetic energy of the inflowing material is eventually dissipated close to the white dwarf surface, e.g. in a transition region from the accretion disk to the white dwarf surface.

Based on observational characteristics, cataclysmic variables have been divided into several groups. During our observing project, we have paid most of our attention to the following types of cataclysmic variables:

Dwarf Novae

In the dwarf-nova systems the accretion rate onto the white dwarf changes in a spasmodic way. Long time intervalls of the order of months of a low accretion rate (and therefore luminosity) are interrupted by outbursts, lasting for a few days to about two weeks, during which the accretion rate increases by a large factor (see Fig. 2).

Intermediate Polars

In these cataclysmic variables the white dwarf has a magnetic field that is strong enough to dominate the motion of the inflowing matter within a certain distance from its centre. Within this "magnetospheric radius" the matter is channeled onto regions near the magnetic poles of the white dwarf. Inside this magnetosphere an accuration disk cannot exist; what fraction of the accretion disk remains depends on the size of the magnetosphere, relative to that of the Roche lobe around the white dwarf.

Brightness Variations

Most cataclysmic variables with an accretion disk show brightness variations with the orbital period, which are

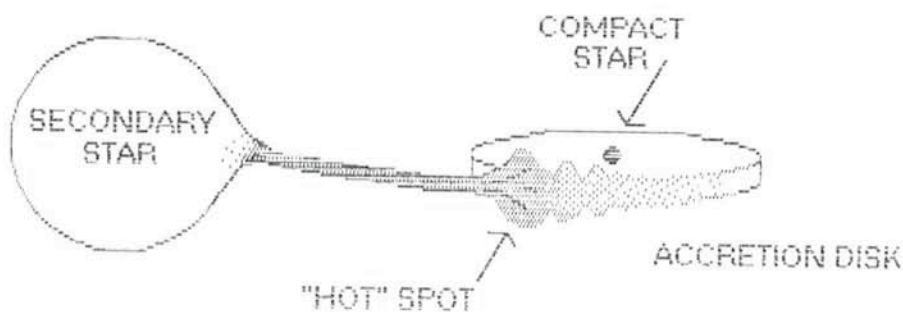

Figure 1: *A sketch of the structure of a cataclysmic binary. Matter from the secondary falls into the potential well of the white dwarf and hits the accretion disk at the bright or "hot" spot.*

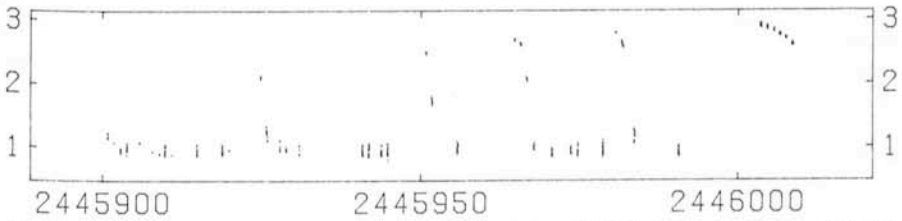

Figure 2: *An overview of the optical observations of the SU UMa-type dwarf nova VW Hyi during July–November 1984, when the source went into a normal outburst 4 times and finally went into a superoutburst. Drawn is the Walraven-B-flux in log F_v, with F_v in units of milli-Jansky's, against Heliocentric Julian Day.*

due to a so-called "bright spot" at the outer edge of the disk, where it is hit by the stream of matter flowing in from the secondary (see Fig. 1). In systems with a magnetized white dwarf the light can also be modulated with the white dwarf rotation period, due to the higher emissivity from the magnetic pole regions and their general non-alignment with the rotation axis of the star. In these systems the light can also be modulated with a third period, the beat period between the white dwarf rotation period and the binary revolution period, which is the rotation period of the white dwarf in the reference frame of the binary. Modulations with the beat period are due to processing of electromagnetic radiation from the rotating white dwarf by parts of the binary system that are not distributed axially-symmetric around the white dwarf, e.g. the secondary and the bright spot on the accretion disk's outer rim (see Fig. 3 for an example of these modulations).

Dwarf Novae

Two types of models have been proposed to explain the outbursts of dwarf novae. In the disk-instability model [1] the accretion disk can exist in two different modes, corresponding to a high and a low value of the mass accretion rate through it. In the quiescent state the accretion rate through the disk is smaller than the the mass transfer rate from the secondary, so that the density in the disk builds up steadily. Coupled to this secular increase of the density one expects an increase of its brightness (mainly in the optical and UV). When the density has reached a particular value, the disk cannot remain in this state of low accretion, but suddenly switches to a state with a high accretion rate. During this outburst the mass accretion rate onto the white dwarf is higher than the mass transfer rate from the secondary. When the density has declined sufficiently, the disk returns to its quiescent state. In the mass-transfer-instability model [2], the outbursts are explained by mass-transfer bursts from the secondary, which are directly transported through the disk to the white dwarf. During quiescence, when the accretion rate onto the white dwarf equals the mass transfer rate from the secondary, no secular changes are expected in the accretion disk's state.

One of the aims of our long-term photometric project of cataclysmic variables was an attempt to distinguish between these two types of model, by studying the possible secular brightness variations of dwarf novae in quiescence. For this purpose we have observed the system VW Hyi during 42 nights over a time interval of 4 months, during which 5 outbursts occured. These observations were coordinated with observations with EXOSAT, Voyager, IUE, and Walraven [3] (see Fig. 2). The main outcome of this study is that there is no evidence for a significant trend in the optical brightness from the system between outbursts (see Fig. 4). The same was found in the X-ray and UV observations (if any change is discernable it is a secular decrease, not an increase). This result is not easy to reconcile with simple versions of the disk-instability model.

At the end of our campaign VW Hyi went into a so-called superoutburst. VW Hyi belongs to a subgroup of dwarf novae, the SU UMa systems, that show two rather different types of outbursts (superoutbursts and "normal" outbursts). Superoutbursts are different from normal outbursts – in their rate of occurrence (less often), their duration (longer), and their maximum luminosity (higher). Apart from this, it is found that during superoutburst, the optical brightness is strongly modulated; these so-called superhumps recur with a period that is slightly longer than the orbital period; also this superhump period is not exactly constant, but increases through the superoutburst. The superhumps have always been a big problem, which resisted theoreticians' attempts to model them. However, recently Whitehurst has proposed that the superhump phenomenon might be the result of a mass-transfer burst from the secondary, leading to a slowly precessing, more or less eccentric disk, as the result of tidal distortion by the secondary of the orbits of particles in the outer disk regions [4]. His model successfully accounts for many of the strange properties of the superhumps.

Our Walraven observations of the superoutburst of VW Hyi, which were done in five channels simultaneously, have led to the discovery of another strange property of superhumps: the whole superhump-modulation light curve arrives later when seen at longer wavelengths. The total shift from 3200 Å to 5400 Å is + 0.06 in phase of the superhump period [5]. We cannot offer an explanation for this finding.

Intermediate Polars

In intermediate polars the influence of the white-dwarf magnetic field does not

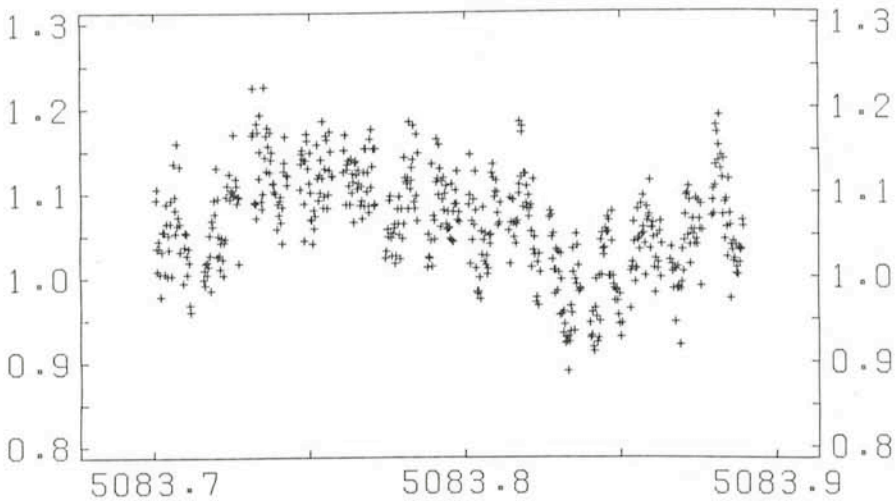

Figure 3: *Modulations of the Walraven-B-band brightness of the intermediate polar V1223 Sgr on 1982 April 24. A long-term modulation with the binary revolution period of 3.4 hours (0.14 day) and a modulation with the beat period between the white rotation period and the orbital period, of 13.2 minutes (0.0092 day), can be seen. The flux is given in flux units of a local comparison star; time is given in HJD-2440000).*

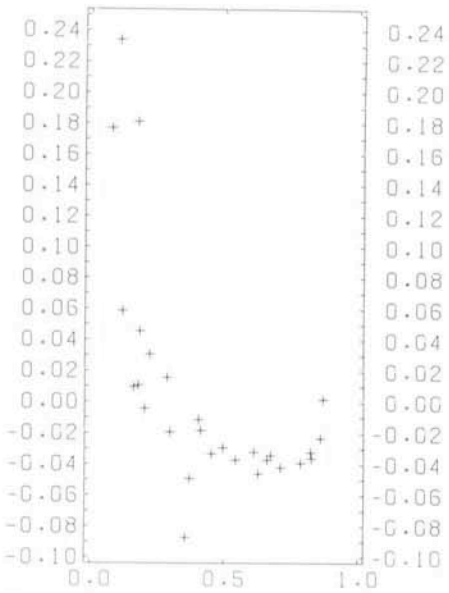

Figure 4: *VW Hyi. The residual flux in the Walraven-B band, averaged over one orbital cycle, relative to the overall average orbital light curve, is given against the relative phase in time between two successive normal outbursts. Apart from the decline of the flux after an outburst, no rising or falling trend is seen in the brightness of VW Hyi during the quiescent state of the dwarf nova.*

time scale of the binary; therefore these changes in the mass transfer rate should occur very often in the lifetime of the binary [6]. As there is no reason why this should only happen in intermediate polars, it is likely to occur in all cataclysmic variables.

A possible explanation for long-term variations in the mass transfer rate from the secondary, might be the occurrence of thermonuclear flashes on the surface of the white dwarf (classical nova outbursts), in which about 10^{-5} $M_\odot$ is lost. These classical novae possibly lead to an increasing separation of the two stars and a temporary disconnection of the secondary from its Roche lobe, so that the mass transfer process stops (or at least becomes much smaller) [7]. In the following stage of "hybernation" of the cataclysmic variable, the two stars will gradually come closer to one another as the result of loss of orbital angular momentum, due to emission of gravitational radiation and to magnetic braking, and mass transfer will restart when the secondary again touches its Roche lobe.

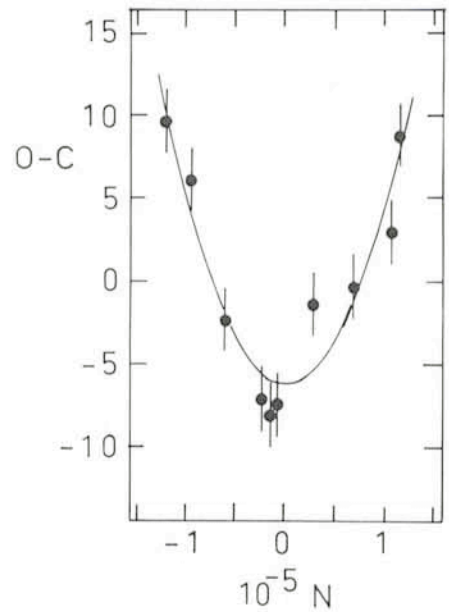

Figure 5: *The deviations (O–C, in units of 0.0001 day) of the optical beat pulse arrival times in the intermediate polar V1223 Sgr from a linear fit against their cycle-number (N). The parabolic curve drawn gives an estimate of the rate of increase of the white dwarf rotation period (spin-down). The spin period is 0.0092 day.*

extend to the secondary. Consequently, matter spiralling inward in the outer accretion disk region becomes connected to the magnetic field (and will corotate with the white dwarf) only within the magnetosphere of the white dwarf. When it is connected, it either looses angular momentum to the white dwarf or gains angular momentum from it. This accretion torque accelerates or decelerates the white dwarf's rotation, until the white dwarf has reached an equilibrium period at which the net torque vanishes (this equilibrium period depends on the magnetic field strength and the mass accretion rate).

From our long-term observations of intermediate polars we found that the white dwarf in V1223 Sgr spins down, while in H2252-035 it spins up (see Fig. 5); Pakull & Beuermann also found a down-spinning white dwarf in H2215-086. Previous to our observations, only spin-ups of accreting magnetized white dwarfs had been found. From models which link the accretion torque to the rate of change of the spin period of the white dwarf, we found that the white dwarfs do not spin close to their equilibrium spin rate. One way in which these white dwarfs could be unable to reach their equilibrium spin period, is by large changes in the mass accretion rate. We estimate that such equal changes in the mass transfer rate take place on time scales less than 10^{5-6} years, which is very short compared with the evolution

Do All Cataclysmic Variables Burst?

During recent observations of the intermediate polar TV Col we encountered a surprising feature, only seen once before in this system. Within one week this source showed two outbursts, that looked remarkably similar [8]. Both bursts lasted less than about half a day, and reached an amplitude of 2 magnitudes; they last therefore much shorter and are less luminous than dwarf nova outbursts. We have in 1984 also detected a similar short burst in V1223 Sgr, with the same characteristics as the bursts in TV Col (see Fig. 6). In addition to the photometry, the observers (H. Schwarz of ESO and M. Heemskerk of Uv Amsterdam) collected spectra of the second outburst. From the spectral line information obtained, it became clear that this outburst developed in a different way than normal dwarf nova outbursts do.

It is attractive to relate the differences in the outburst characteristics of the intermediate polars and dwarf novae, with the difference in their accretion disk structure. It looks as if the absence of an inner disk in the intermediate polars precludes the full development of the burst as a real dwarf-nova outburst.

It appears valuable to follow the cataclysmic (physically) variable

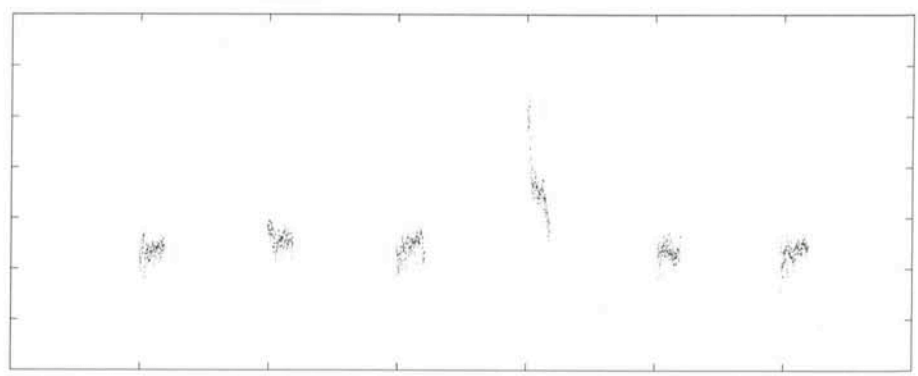

Figure 6: *Spectral continuum flux, close, to the Hydrogen-alpha emission line, of the intermediate polar V1223 Sgr during six successive nights of observations with the Boller & Chivens spectrograph behind the 1.5-m ESO telescope. Flux is given in linear arbitrary units against time in units of days. The decline of a burst is visible in the 4th night of observations (on 1984 Aug 31). During the declination of the flux, the more or less sinusoidal orbital modulation of the light is visible.*

binaries, to see how they behave on a long time scale. The spasmodic emission of radiation due to the unstable mass transfer/accretion process, makes it necessary to open the observing window a bit more in order to detect crucial phenomena at the right moment. From the long-term behaviour of these systems we have probably been able to derive information on their evolutionary scenario.

References

[1] Osaki, Y., 1974. *Publ. Astron. Soc. Japan*, **26,** 429.

[2] Bath, G.T., 1975. *Mon. Not. R. Astr. Soc.*, **171,** 311.

[3] Pringle, J.E., Bateson, F.M., Hassall, B.J.M., Heise, J., Holberg, J.B., Polidan, R.S., van Amerongen, S.F., van der Woerd, H., van Paradijs, J., and Verbunt, F., 1987. *Mon. Not. R. Astr. Soc.*, **225,** 73.

van Amerongen, S., Damen, E., Groot, M., Kraakman, H., and van Paradijs, J., 1987. *Mon. Not. R. Astr. Soc.*, **225,** 93.

Verbunt, F., Hassall, B.J.M., Marang, F., Pringle, J.E., and Warner, B., 1987. *Mon. Not. R. Astr. Soc.*, **225,** 113.

Polidan, R.S., and Holberg, J.B., 1987. *Mon. Not. R. Astr. Soc.*, **225,** 131.

van der Woerd, H., and Heise, J., 1987. *Mon. Not. R. Astr. Soc.*, **225,** 141.

[4] Whitehurst, R., 1987. In preparation (preprint).

Honey, W.B., Charles, P.A., Whitehurst, R., Barrett, P.E., and Smale, A.P., 1988. *Mon. Not. R. Astr. Soc.*, **231,** 1.

[5] van Amerongen, S., Bovenschen, H., and van Paradijs, J., 1987. *Mon. Not. R. Astr. Soc.*, **229,** 245.

[6] van Amerongen, S., Augusteijn, T., and van Paradijs, J., 1987. *Mon. Not. R. Astr. Soc.*, **228,** 377.

[7] Shara, M.M., Livio, M., Moffat, A.F.J., and Orio, M., 1986. *Astrophys. J.*, **311,** 163.

[8] Schwarz, H.E., and Heemskerk, M.H.M., 1987. I.A.U. Circular No. 4508.

Schwarz, H.E., van Amerongen, S.F., Heemskerk, H.M., and van Paradijs, J., 1988. *Astr. Astrophys.*, submitted.

IRAS Molecular Clouds in the Hot Local Interstellar Medium

P. ANDREANI[1,2], R. FERLET[1], R. LALLEMENT[1,3] and A. VIDAL-MADJAR[1]

[1] *Institut d'Astrophysique, CNRS, Paris, France*

[2] *ESA Fellow on leave from Dipartimento di Fisica, Università di Roma, La Sapienza, Roma, Italy*

[3] *Service d'Aéronomie, CNRS, Verrières le Buisson, France*

1. Introduction

The picture of the nearby ($d \leq 100$ pc) interstellar medium, as resulting from the observations in the wavelength range from X-ray to radio, consists of a very hot, low-density gas, forming a hot bubble, filled with many cloudlets of ionized and neutral material and located near to an interstellar condensation (see the "Local Interstellar Medium", NASA CP-2345, 1984; and Cox and Reynolds, 1987).

Only recently the existence of a colder counterpart in the nearby gas was argued by Magnani, Blitz and Mundi (1985), who reported the detection of a large number of "local" molecular clouds at high galactic latitude and inferred from statistical arguments an average distance of about 100 pc.

A comparison with the IRAS maps showed that all the high latitude molecular clouds can be identified with the cores of the new discovered infrared (60 and 10 μm) features: "the IRAS cirrus" (Weiland et al., 1986).

Nearby molecular clouds are then associated to the cold interstellar material with temperatures ranging from 14 to 40 K.

In order to understand the physical properties of the local medium and their effect on other observations, it is interesting to tackle the problem of the coexistence of a cold and neutral gas with a hot medium and the mixing between these two gaseous phases.

The distance, the morphology and other properties of the clouds, belonging to the local interstellar medium, can be determined by mapping the interstellar absorption lines toward stars at different distances and projected along the line of sight to these clouds.

The feasibility of this procedure has already been demonstrated by Hobbs et al. (1986) who estimate the distance of the cloud Lynds 1457/8 at about 65 pc.

We selected several high latitude clouds detected by IRAS and/or at CO wavelength (2.6 mm) by Magnani, Blitz and Mundi (1985) and gathered echelle spectra of a few stars with the ESO CAT telescope at La Silla, Chile.

2. The Observations

From the IRAS HCON1 survey (see IRAS Explanatory Supplement, 1984), we selected those clouds at 100 μm, which were already detected at the CO band (Magnani et al., 1985) and located at high galactic latitude ($|b| \geq 25°$).

The MIDAS software package (ESO Operating Manual No. 1, 1984) has been used to analyse the IRAS maps. The whole procedure of IRAS images analysis will be published elsewhere (Andreani et al., 1988).

Table 1 lists the known properties of the clouds from infrared and CO measurements. The position, photometry, spectral type and distance are taken from the Bright Star Catalogue for the brightest programme stars, and from the HD Catalogue for the others. Stars were chosen to be bright, hot, and of early spectral type.

High-dispersion CaII K and NaI D spectra were gathered during 1986–1987 with the Coudé Echelle Spectrometer fed by the 1.4-m CAT telescope and equipped with either a

TABLE 1. *Infrared and CO Properties of the Clouds*

	Cloud	Coordinates				IRAS					CO
#	Name	α (h)	δ (°)	l (°)	b (°)	12 μ	25 μ	60 μ (MJy/sr)	100 μ	T_d (K)	T_a (K)
20	L1642	4 33	−14 20	210.9	−36.5	–	–	.3 ± .2	11.2 ± 2.8	20	6.8
126	ϱ-Oph	16 16.3	−19 48	355.5	−21.1	–	–	10 ± 3	12 ± 3	29	9.2
113	–	15 17.1	−29 25	337.8	−23.04	–	–	13 ± 4	12 ± 4	32	6.1

Reticon or a CCD detector at the ESO Observatory at La Silla, Chile. The resolving power was 60,000 for the CCD spectra and 100,000 for the Reticon ones. The wavelength calibration is provided by a thorium lamp and its internal accuracy is of ± 3 m Å. Details of the observational and reduction procedure can be found in Ferlet and Dennefeld (1984). In order to get rid of the atmospheric water absorption lines, NaI spectra were compared with template spectra of hot stars taken during the same nights of observation (Vidal-Madjar et al., 1986).

3. The Results

Wherever the D lines are clearly free from saturation, the column densities are derived by applying the usual relation for the linear part of the curve of growth, independent of the unknown velocity spread parameter b. On the other hand, saturation allows only to infer lower limits on the N(NaI).

The presence of the clouds is clearly revealed (see Fig. 1) by the sharp and deep absorption features seen in front of the stars HR 1423, HD 30332, HR 5655, HD 135951, HR 5984, HR 5985, HR 6027 and HR 6118. Small structures detected in front of the stars HR 1438 and HR 6153 could be due either to the fainter boundry of the cloud or to a totally independent, low density nearby medium.

Cloud no. 20

Cloud no. 20 is a suitable candidate because of its small optical extinction and its isolated position towards the galactic anticentre. Its dust properties have been investigated by means of CO and IRAS data (Weiland et al., 1986) and photoelectric and photographic surface brightness observations (Laureijs et al., 1987). The results of our analysis agree with the previous determinations.

From our observations we can infer a distance range between 70 and 220 pc and a mass range of 0.5 and 3.5 $M_\odot$.

Cloud no. 126

The CO cloud no. 126 belongs to the ϱ Ophiucus region, its infrared data at 12 and 25 μm are strongly affected by the zodiacal emission of the ecliptic plane, however, values at 60 and 100 μm are well corrected for this and the incertainties are mainly due to systematic errors related to the calibration problems (IRAS Explanatory Supplement).

Its distance should be of about 100 pc. The estimation to its mass gives 0.15 $M_\odot$.

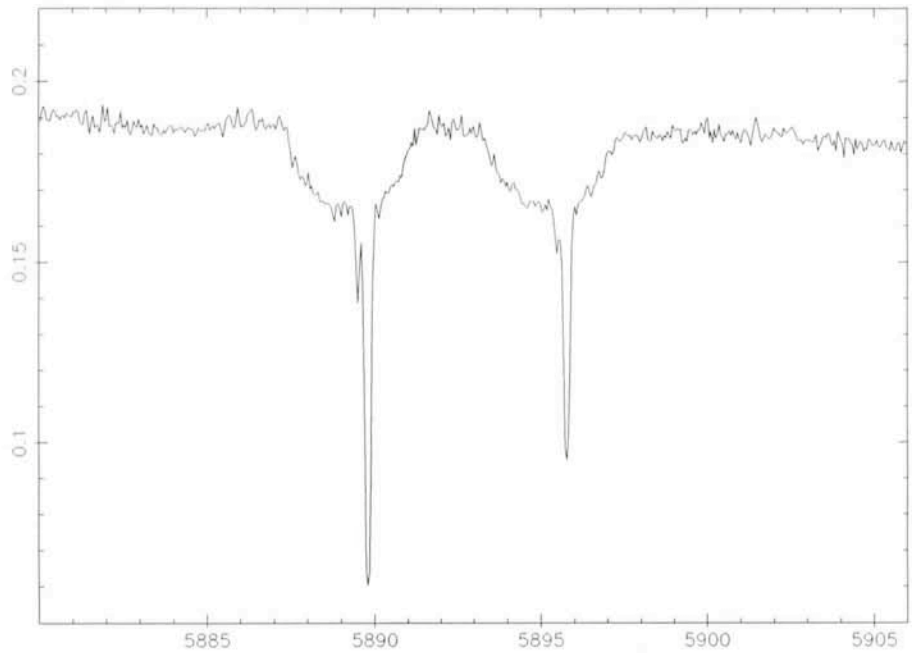

Figure 1: *A one-hour exposure in May 1987 towards HD 135951 at the CAT telescope with the CES and CCD detector. The strong NaI interstellar doublet seen in absorption shows that cloud no. 113 must be less than 90 pc from the sun.*

Cloud no. 113

Only an upper limit to the distance can be deduced since stars located in front of the cloud are not included in our survey. The cloud lies at a distance less than 90 pc and the lower limit to its mass is of .007 $M_\odot$.

4. Conclusions

If the neutral gas in which the strong Na lines arise belong to the IR-CO clouds, then these latter lie relatively close to the Sun and an upper limit to their distance can be inferred from the distance of the selected stars.

Therefore, some molecular clouds very likely lie within the hot, low-density interstellar gas. The new picture of the local interstellar medium resulting from these data must take into account the coexistance of hot and cold gas. New observations are required in order to sketch the properties of the local space and, because of that, several other molecular clouds are under investigation with this procedure.

References

P. Andreani, R. Ferlet, A. Vidal-Madjar, in preparation.

D.P. Cox and R.J. Reynolds, *Ann. Rev. Astron. Astroph.*, **25,** 303 (1987).

R. Ferlet, M. Dennefeld, *Astron. Astroph.*, **138,** 303 (1984).

L.M. Hobbs, L. Blitz and L. Magnani, *Ap. J.*, **L109,** (1986).

I.A.U. Colloquium 81, NASA CP-2345 (1984), "The Local Interstellar Medium", eds. Y. Kondo, F.C. Bruhweiler and B. Savage.

IRAS Explanatory Supplement, 1984, edited by C.A. Beichman, G. Neugebauer, H.J. Habing, P.E. Clegg and T.J. Chester.

R.J. Laureijs, K. Mattila and G. Schnur, *Astron. Astroph.*, **184,** 269 (1987).

L. Magnani, L. Blitz and L. Mundi, *Ap. J.*, **295,** 402 (1985).

A. Vidal-Madjar, R. Ferlet, C. Gry, R. Lallement, *Astron. Astroph.*, **155,** 407 (1986).

J.L. Weiland, L. Blitz, E. Dwek, M.G. Hauser, L. Magnani, L.J. Rickard, *Ap. J.*, **306,** L101 (1986).

LETTER TO THE EDITOR

Fontenelle (*The Messenger*, No. 50, p. 40, December 1987)

I was pleased to read about Fontenelle, but surprised to learn that this author was unknown to you until recently . . . It appears that his celebrity first of all is due to the fact that he lived a hundred years and that, as Perpetual Secretary of Académie des Sciences, he occupied a privileged position in France. On the occasion of the 300th anniversary of the first edition of "Entretiens", the Rouen University organized a 5-day colloquium in October 1987. What concerns more recent editions, there was one by Marabout Université, Editions Gérard et Cie, Bruxelles, in 1973. Fontenelle is also mentioned in the article by J. Lévy (l'Astronomie, December 1986, 549).

S. DÉBARBAT (Observatoire de Paris)

Rapid Spectral Variations of Old Novae

M. FRIEDJUNG, Institut d'Astrophysique, Paris, France
A. BIANCHINI, Osservatorio Astronomico, Padova, Italy
F. SABBADIN, Osservatorio Astrofisica, Asiago, Italy

Novae are a subclass of cataclysmic variables. The latter all appear to be binary with a white dwarf component and a companion usually near the main sequence. This companion seems to fill its Roche lobe and lose mass to the white dwarf via the inner Lagrangian point. Unless the magnetic field of the white dwarf is very strong, the transferred mass is expected to spiral slowly to the white dwarf in an accretion disk, whose presence explains many observations. Different kinds of cataclysmic variable exist, such as different sorts of dwarf novae with outbursts generally having an amplitude of a few magnitudes at intervals of the order of weeks. The orbital periods determined up to April 1987 (Ritter 1987) lie between 2.00 days (the nova GK Per) and 0.052 days (the dwarf nova AF Cam), with a "period gap" between 0.118 and 0.086 days (only one known period inside the gap).

Classical novae brighten very rapidly by a factor in the majority of cases of more than 10,000 in the optical, then fading to what is normaly the pre-outburst brightness. This brightening is associated with the ejection of material at velocities of the order of 10^3 km s^{-1}. After optical maximum, novae go through a number of stages in their development; the speed of this development is referred to by the expression "speed class", and can be quantitatively measured for instance by t_3 the time to fade 3 magnitudes. An approximate anticorrelation exists between t_3 and the absolute brightness at optical maximum; however, novae in outburst show important differences, which appear hard to describe by only one parameter.

More or less all who study the causes of the outbursts of classical novae agree that outbursts are due to thermonuclear runaways in the material accreted by the white dwarf, though the situation is less clear for recurrent novae, i.e. for novae for which more than one outburst has been observed. A great success of the theory was the prediction that fast nova outbursts (that is with a rapid development and a small t_3 required overabundances in the CNO elements, confirmed by analyses of observations. However, many "details" are far from clear, including in particular the effects of departures from spherical symmetry.

The relation of the characteristics of novae in outburst to those before outburst is not really known. This is especially the case because the processes after the initial explosion are badly understood. It appears necessary, however, to invoke the presence of a very strong wind, which should play a major role in these processes (Friedjung 1987a, 1987b).

The fourth edition of the catalogue of cataclysmic binary orbits by Ritter (1987) lists 13 classical novae for which periods have been measured. However, all of those were not well observed during their outbursts: t_3 is even not known for 2 of them. No clear relation between t_3 and the period emerges for the others, which is not surprising in view of the fact that outburst properties can be expected to depend on a number of different characteristics of the binary such as period, white dwarf mass (which when near the Chandrasekhar limit should radically change element abundances according to theory), inclination of the orbit to the line of sight, etc. Therefore, far more orbital data are needed, particularly for novae well observed during outburst.

It was for such reasons that we started our programme to observe the spectra of old novae. Rapid spectral variations should be produced by orbital motion, but if the white dwarf is strongly magnetic, its rotation could cause other variations (DQ Herculus star), while flickering can also be present.

In our first observing run in May 1984 with the ESO 1.5-m telescope and the IDS, we obtained striking first results for the old nova CP Pub (which had a very small t_3 in outburst). Rapid variations were seen, suggesting a very short period. In a first examination (Bianchini et al. 1985a, 1985b) we studied the radial velocity variations of the Hα, Hβ and HeII 4686 Å emission lines. Periodicity was investigated using the method of power spectra, and several possible periods were detected (see Fig. 1). The reason for the detection of so many periods was that observations were only made during a few hours (generally of the order of 0.1 day or less) on 4 successive nights for Hβ and HeII 4686 Å at 59 Å/mm (and one night for these lines plus Hα at 114 Å/mm). Therefore, there was a lot of aliasing between the true period and the period of rotation of the earth. We sought the periods which gave the least scatter about the radial velocity curves for Hβ and HeII 4686 Å. We also used physical and geometrical arguments suggested by various effects such as an apparent Hβ eclipse in one observation. We concluded that a period of 0.06115 days was the most probable, but others such as 0.05765 or 0.06977 days could not be excluded. If really orbital, this is the first classical nova period determined below the period gap, and contradicts a suggestion made some years ago that such a period is impossible for a nova.

However, the radial velocities were obtained by eye estimates of the profile peaks, and in view of the noise, doubt can be cast on this procedure. Indeed, the first author of this article was quite disgusted when he saw profiles on a screen! We therefore decided to reduce our first observations differently. We found the mean wavelength of lines averaging the emission over the profile (Bianchini et al. 1985c). Power spectrum analysis however gave results which were less clear than previously! There was an indication of a possible secondary period at 0.04 days, as well as a main period defined by Hβ of 0.0605 or 0.0571 days, though HeII 4686 Å gave a better fit for a period below the minimum for cataclysmic variables.

If we had been alone this would not have been too encouraging. But thank God for colleagues! Our discovery of a very short period for CP Pup was confirmed soon after by two independent studies. Warner (1985) studied CP Pup

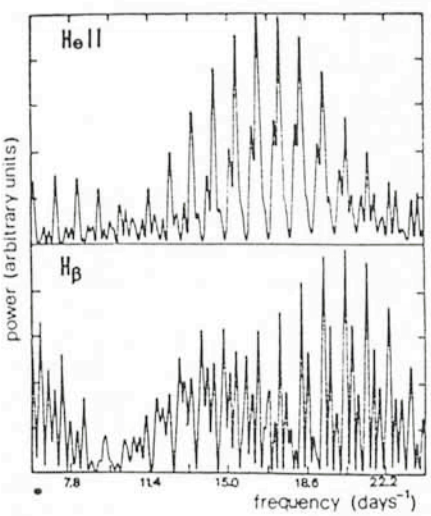

Figure 1: *Power spectra of HII λ 4686 and Hβ radial velocities in CP Pup.*

photometrically and found a period of 0.06196 days or its alias 0.06614 days. Duerbeck et al. (1987) analysed radial velocities from spectra, and obtained a period of 0.0614215 days. The lesson, especially if one wished to go further, was that more observations were required, if possible with more powerful instrumentation. The line flux variations also needed more study.

We again obtained time in March 1988 on the ESO 1.5-m telescope with a CCD. Reductions are not yet complete; up to now we have concentrated on the analysis of observations of the very old nova V 841 Oph (1848) for which we did not detect variations in 1984. The study of this nova is especially interesting, as theory and observation have both been used to support models in which very old novae go into "hibernation". The idea is that mass transfer decreases or stops, so the accretion disk disappears or becomes very faint. At present these ideas have run into theoretical problems, and the situation is not clear . . .

Our 1988 results for V 841 Oph are for 14 epochs. HeII 4686 Å emission is stronger than that of Hβ, the latter being apparently in broad absorption. Line flux variations seem to be large. The best preliminary period is 0.385 days but 0.63 days or perhaps even a period near 2 days are possible. The semi-amplitude of the velocity variation is about 130 km s^{-1} for Hβ, but only about 80 km s^{-1} for HeII 4686 Å. Reductions are proceeding, but in view of the probably rather long period, more observations, if possible in two runs a few weeks apart, are desirable.

The recurrent nova T Pyx also observed in the last 1988 run may be mentioned. No variations were immediately apparent.

The main conclusion that can be drawn is that far more observations are required, if one wishes to relate the properties of novae in outburst to those of their orbits. This is necessary if theoretical speculations are not to become too wild!

References

Bianchini, A., Friedjung, M., Sabbadin, F. 1985a, IBVS No. 2650.

Bianchini, A., Friedjung, M., Sabbadin, F. 1985b, in "Multifrequency Behaviour of Galactic Accreting Sources". Ed. F. Giovanelli, p. 82.

Bianchini, A., Friedjung, M., Sabbadin, F. 1985c, in "Recent Results on Cataclysmic Variables", ESA-SP 236, p. 77.

Duerbeck, H.W., Seitter, W.C., Duemmler, R., 1987, *Mon. Not. R. Astron. Soc.* **229,** 653.

Friedjung, M., 1987a, *Astron. Astrophys.* **179,** 164.

Friedjung, M., 1987b, *Astron. Astrophys.* **180,** 155.

Ritter, H., 1987, preprint.

Warner, B., 1985, *Mon. Not. R. Astron. Soc.* **217,** 1 p.

NEWS ON ESO INSTRUMENTATION

Status of the ESO Infrared Array Camera – IRAC

IRAC is currently being tested in Garching in preparation for its installation and first test on the 2.2-m telescope at the end of June 1988. Assuming there are no unpleasant surprises, it is intended in July/August 1988 to issue a formal announcement of its availability for visiting astronomers in Period 43, i.e. as of April 1989. In the meantime, it is hoped that this article will serve as a useful introduction to this new instrument and its observational capabilities.

IRAC Characteristics

With its presently installed Hg:Cd:Te array detector, this camera provides for direct imaging over the wavelength range 1 to 4.3 μm. In addition to the standard near infrared broad-band filters, it is also equipped with circular variable filters (CVF) for imaging spectral features and the nearby continuum at R ≃ 50. There is also a choice of four magnifications which are selectable online. Table 1 summarizes the most important parameters required for planning observational programmes. The detector performance figures quoted were derived from the first test measurements of a new array received only a few weeks ago. Some caution is therefore necessary. In principle, however, it should be possible to reach sky background limited magnitudes of 20–21 mag. in the J, H and K bands with this array. In practice, of course, this will depend on whether or not the required stability and accuracy of flat-fielding (~ 1 in 10^4) can be achieved.

Optical Design

Figure 1 shows the optical arrangement. The input doublet acts as the cryostat window and forms a small (2.5 mm) image of the telescope pupil at the position of the filter wheel which carries both the broad-band and CVF filters. Behind this is located a second wheel carrying the various objectives which re-image the field on the array at a variety of magnifications. For each magnification there are, in fact, two objectives which are coated and adjusted separately for the 1–2.5 μm and 2.5–5 μm ranges. In addition to positioning the various objectives, the lens

TABLE 1: *IRAC Characteristics*

Array Detector:	Hg:Cd:Te/CCD 64 × 64 pixels, 48 μm pitch Wavelength cut-off ≃ 4.3 μm Overall efficiency ≃ 70 % Read noise ≃ 200 e Dark current ≃ few 10^3 e/s (52 K) Well capacity 2.10^6 e
Optics:	Magnifications (remotely selectable) 0.3, 0.5, 0.8, 1.6″/pixel (2.2 m) Maximum field ∅ = 1.6′ (2.2 m)
Filters:	J(1.25 μm), H(1.65 μm), K(2.2 μm), L′(3.8 μm) CVF(R ≃ 50) 1.45–2.65 μm, 2.5–4.5 μm
Magnitude Limits: (3 σ, 1 hr)	20–21 mag./pixel in J, H, K bands (highly provisional)

wheel can also be used to micro-scan images across the array, e.g. for the purpose of removing dead pixels.

Adapter

IRAC is designed to be mounted on the F/35 infrared adapters at the 2.2-m and 3.6-m telescopes and will therefore have the same TV acquisition and guiding facilities as the infrared photometers.

Software

As with most of the major ESO instruments, IRAC will be controlled via menus, form-filling and typed commands at the HP instrument terminal in the control room. Images will be displayed on a RAMTEK monitor and a graphics terminal will be provided for status and IHAP displays. The actual user interface and terminology will appear very familiar to those who have used IRSPEC. It would be premature here to describe the various observing and display modes currently foreseen, however, as these may still be revised following our actual experience at the telescope.

A. MOORWOOD, ESO

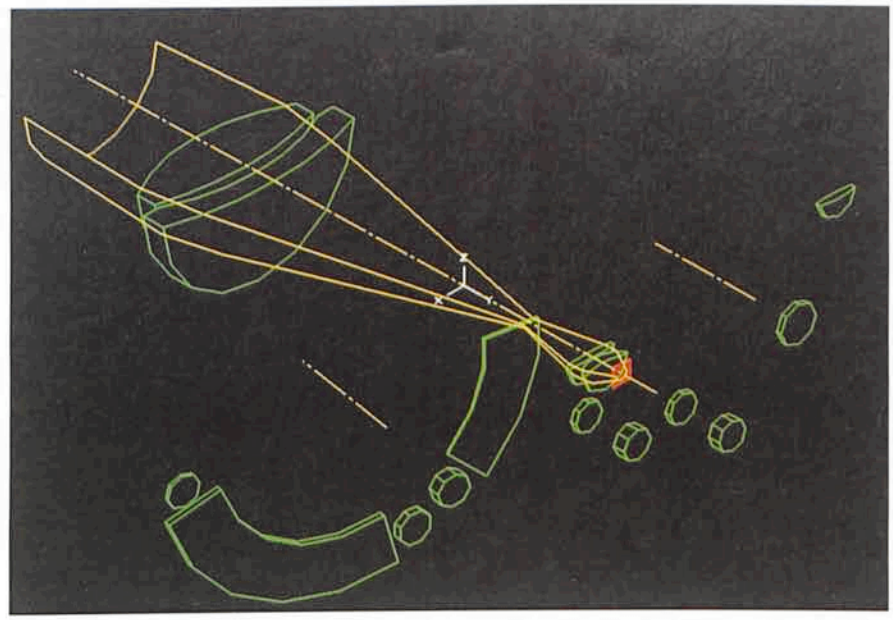

Figure 1: *IRAC optical layout. The filter wheel is located at an image of the pupil formed by the input doublet and carries both broad-band and CVF filters. Immediately behind is a lens wheel containing several objectives which provide a range of image scales at the array detector.*

Optical Instrumentation for the NTT: EMMI and EFOSC2

With the New Technology Telescope a little more than six months from "first light", work is going on intensively at ESO on the instrumentation to be used at the two Nasmyth foci of the telescope.

A detailed, final description of the instruments will be made available after they have been tested in the laboratory and at the telescope. These specifications will be distributed as usual with the relevant Call for Observing Proposals. We give here a short preview of the main characteristics to prepare the community to their use.

Before introducing the instruments, it is important to note that an essential interface between telescope and instruments are the two adapter/rotators (one for each Nasmyth focus) designed and built under the supervision of the NTT Group. They are complex devices which include two TV guide probes, the system to analyse the quality of the optical image for the adjustment of the active supports of the main mirror and the calibration system. The adapters rotate to compensate the field rotation given by the Alt-Az configuration of the telescope.

Two optical instruments are currently being assembled for the NTT:

EMMI (ESO Multi-Mode Instrument) and EFOSC2, a revised version of the EFOSC operating at the 3.6 m. EMMI will ultimately be the NTT optical workhorse, conceived to be semipermanently mounted at the telescope to reduce the maintenance needs and stabilize its performance at an optimal level. It is a two-chanel instrument (UV-blue and Visual-Red) with 6 main observing modes: imaging in the UV-B and V-R channels, grism spectroscopy in V-R, grating, medium resolution spectroscopy in UV-B and V-R and high resolution echelle spectroscopy in V-R. The capability to do multi-object spectroscopy has also been foreseen and will be implemented in a second step. The observers will be able to switch remotely between these observing modes, thus having the greatest flexibility in tackling their scientific objectives. Flexible scheduling to adapt the observing programme to the prevailing sky conditions (transparence, but above all seeing) could also be easily implemented and thoroughly tested. The optical design and the expected capability of EMMI are described in a published article (1986, *SPIE* Vol. **627,** 339) to which we refer those who are interested in more details. The instrument will be assembled in Garching in the course of this year: we will report on its progress and on the most interesting features which characterize it.

EFOSC2 will be, if you like, an intruder at the NTT. In November 1987 we saw the possibility to satisfy two different needs with a single effort. On the one hand, there had been pressure from the community to get an EFOSC-type instrument at the 2.2 m to improve the capability at that telescope for faint object spectroscopy and imaging of non-stellar objects over a large field. On the other hand, we saw the convenience to have in the first months of operations of the NTT a simple, easily removable instrument which could be used both for the necessary tests and for scientific programmes. Add to this that the project had to be completed in one year and that the recipe for EFOSC2 was almost fully defined. The specifications for the optical layout were laid down by the Optical Instrumentation Group. It was decided that the instrument had to be optimized for use at the 2.2-m telescope, its ultimate assignment. Secondly, the overall mechanical structure and the remotely controlled slit, filter and grism wheels had to remain unchanged to minimize the redesigning of mechanics and control electronics.

Still the project could not have been realized without the involvement of the TRS staff in La Silla. They took the responsibility of the redesign and the construction of the mechanics and of the

integration of the electronics and optics. The assembly of the instrument is now scheduled for November of this year. The La Silla staff will also adapt the EFOSC1 software to the NTT computer environment. This remarkable effort made possible the introduction of the project in the ESO planning without major disruptions of the projects already on their way in Garching.

Let us now briefly look at the capabilities of EFOSC2. There are two major improvements with respect to EFOSC1: the optically corrected field is about 30 × 30 mm at the detector and the UV transmission of the optics is expected to be significantly better (about 70 % at 3600 Å vs 35 % for EFOSC1). At the CCD, one arcsecond corresponds to 113 μm at the NTT and to 52 μm at the 2.2 m.

Note that because of the optimization for the 2.2 m, EFOSC2 tends to oversample the stellar images (or the slit) at the NTT in average seeing conditions. The actual performance will depend on the detector which will eventually be used. At present we consider three possibilities: a high density RCA (1,024 × 640 pixels, 15 × 15 μm in size), a mosaic of four Thomson CCDs (1,160 × 80 pixels, 23 × 23 μm) and a Thomson THX 31156 (1,024 × 1,024 pixels, 19 × 19 μm). The table summarizes the pixel matching and the available fields for the three detectors. Of these, the RCA CCD is the only one with well tested properties as it is used currently at EFOSC1. The other two are still in the development phase and their performance "in the field" will be known by the beginning of 1989 only.

Pixel Matchings and Fields of View of EFOSC2

	Detector	Pixel size (arcsec)	Field of view (min of arc)
At the NTT			
	HR RCA (2 × 2 binned)	0.26	2.2 × 1.4
	Mosaic 2 × 2	0.20	3.9 × 2.7
	THX 31156	0.17	2.9 × 2.9
At the 2.2 m			
	HR RCA	0.29	4.9 × 3.1
	Mosaic 2 × 2	0.44	8.4 × 5.7
	TH 31156	0.36	6.2 × 6.2

Finally, a few words on the schedule of these projects. It is foreseen to mount EFOSC2 at the NTT in the spring of 1989 and in July of the same year it should become available to visitors for a fraction of the time.

Applicants for observing time in period 43 with EFOSC1 at the 3.6 m will be asked to indicate whether they would consider acceptable to carry out their scientific programme or part of it with EFOSC2. This will leave open to the OPC the possibility to divert a fraction of the programmes to that instrument, thus relieving the present oversubscription rate of the 3.6-m telescope. EMMI and IRSPEC (the latter to be adapted to the other Nasmyth focus of the NTT) are expected to be offered in period 44. When EMMI will be operational, EFOSC2 will be moved to the 2.2 m, where it should be available from period 45. *S. D'ODORICO, ESO*

A Note on Equivalent Widths at the CES

It has come to my attention through my own observation and through discussions with other users of the CES, that there are substantial differences between the equivalent widths measured with the short camera plus CCD and those measured with the long camera plus Reticon. These differences are in the sense that the CCD widths are larger than for the Reticon. These differences appear to be wavelength dependent being larger in the blue and can be as large as 20–30 % around 3880 Å.

Although this is at first sight disturbing, it appears that programmes which compare equivalent widths in the same spectral region have no worries since both detectors have linear output. This is probably due to scattered light in the long camera, but this is not yet proved.

I am interested in further investigating this effect especially with a comparison of data taken with the long camera and both detectors, and in the blue and red regions of the spectrum. Thus I would like to request that CES users send me any information that will help track down the origin of this problem affecting our data. *P. CRANE, ESO*

MIDAS Memo

ESO Image Processing Group

1. Application Developments

A new package for reduction of data from the ESO Infrared Spectrograph, IRSPEC, has been developed in collaboration with M. Tapia. The package is described in more detail in a contribution of this issue of The Messenger. The new software, available as a CONTEXT inside MIDAS, includes a tutorial procedure that can be used as an on-line manual for first time users and also as a test for certifying new installations. This software and the corresponding manual will be released with the 88NOV version of MIDAS!

The package CLOUD, used for the analysis and modelling of interstellar absorption lines, has been substantially upgraded by M. Pierre.

A new project to organize and define the calibration information inside MIDAS has been started in collaboration with L. Johansson.

With the completion of the reduction software for IRSPEC, the first priority project in the area of applications is now the support of EFOSC in its different modes.

2. MIDAS Workshop

The MIDAS Workshop on April 28, 1988, was attended by approximately 70 people, 50 of whom came from other institutes. The morning was reserved for presentations of the general status of MIDAS and new applications such as the IRSPEC package. J. Nichols-Bohlin from the IUE project at NASA, Goddard Space Flight Center, presented the implementation of the IUESIPS package in a MIDAS environment which is now used for the production calibrations.

The standard Image Display Interfaces were described briefly with a more detailed discussion of the first IDI implementation for X-window systems made in Trieste Observatory.

The afternoon was devoted to the portable MIDAS. The new portable set of Standard and Table interfaces was reviewd. These new interfaces represent an enhanced version of the old ST and TBL routines which will still be supported for VAX/VMS systems.

The version 3.0 of AGL, used for plotting in the portable MIDAS, was presented by L. Fini from ASTRONET. Further, the increased capabilities of the plotting package available in the portable MIDAS was demonstrated with a new plotting tutorial. Finally, an extensive set of tests and benchmarks on work-stations from 12 vendors was discussed.

MIDAS courses were discussed again and a decision made to try and arrange these once the portable MIDAS has been released.

3. New Release Dates for MIDAS

With the growing number of institutes now receiving MIDAS (more than 80 sites), our workload is increasing with each release and the summer release is causing problems due to the vacation period. It has therefore been decided to change the MIDAS release dates to May 1st and November 1st. Thus, the next release will be made November 1st, 1988, and be named 88NOV. A first version of the portable MIDAS will be offered at this release. The present VAX/VMS version of MIDAS with minor updates will also be made available to sites which e.g. at that time have not updated their IDI routines to the final standard used in the portable MIDAS.

4. Portable MIDAS

The basic tests of the portable version of MIDAS have been completed successfully by implementing and benchmarking the system on more than 18 different computer models from 12 vendors. These vendors include : HP, Apollo-Domain, SUN, Bull, Tektronix, Masscomp, Alliant, IBM, DEC, Prime, PCS and Eltec. The very high degree of portability was demonstrated by the easy installation of MIDAS on all these systems representing 13 different operating systems (VAX/VMS and 12 UNIX-like systems from pure BSD to SYS V), 5 RISC CPU's and 3 CISC processors. For a typical system, the full installation, testing and benchmarking were performed in less that two working days.

These tests have fully proven the design and portability concept of MIDAS. The main task is now to migrate and test the application programmes with the portable MIDAS. At this stage, the table and plotting applications have been redesigned and implemented in the portable version of MIDAS. This part includes about 40 commands now running in the VMS and UNIX environments. It is expected that a major part of the applications will be available before the 88NOV release.

5. MIDAS Hot-Line Service

The following MIDAS Support services can be used in case of problems to obtain fast help:

- EARN: MIDAS@DGAESO51
- SPAN: ESOMC1::MIDAS
- Tlx.: 52828222 eso d, attn.: MIDAS HOT-LINE
- Tel.: +49-89-32006-456

Also, users are invited to send us any suggestions or comments. Although a telephone service is provided it should be used in urgent cases only. We prefer that requests are submitted in written form through either electronic networks or telex. This makes it easier for us to process the requests properly.

IRSPEC Spectra Reduced within MIDAS

D. PONZ, M. TAPIA, ESO*

1. Introduction

The ESO 32-channel infrared (1–5 μm) grating spectrometer, IRSPEC, was put into operation and made available for Visiting Astronomers in October 1986. In this contribution we describe the reduction scheme implemented in MIDAS to process IRSPEC data taken in any of the two – discrete or continuous – instrumental modes. The Instrument itself has already been described in detail in another contribution to the *Messenger* (ref. 1).

The main purpose of this package is to provide the tools for converting the raw data counts into spectral flux, calibrated in wavelengths. The design of the reduction method is very flexible, in the sense that the user can process the data in different ways, using the basic tools provided by MIDAS, according to his/her own preferences. One important point in the design is to allow for the propagation of errors when an arithmetic operation is performed between two spectra and, of course, the ability to display and plot the error bars. This may be important as the present range of spectral resolutions available in IRSPEC is such that the intrinsic noise level of a measurement may not be well represented by the average pixel to pixel variations in the final spectra. Plotting the final error bars will, for example, tell the observer whether the main source of noise was introduced by bad cancellation of telluric absorption features or detector noise.

All the intermediate data are stored in tabular format. The calibrated flux can then be converted into a one-dimensional image, so that it is possible to use the spectral analysis facilities already available in the system to compute line intensities, equivalent widths, central wavelengths, etc.

2. The Reduction Steps

Spectra obtained with IRSPEC are read from magnetic tapes written in FITS format. Therefore, if a visiting astronomer anticipates reducing these data using MIDAS, he/she should request the computing centre at La Silla to write his/her magnetic tapes in FITS format. Otherwise, the IHAP tapes can be copied into FITS format before reduc-

* Alexander von Humboldt Foundation Fellow, on leave from Instituto de Astronomía, UNAM, Ensenada, México

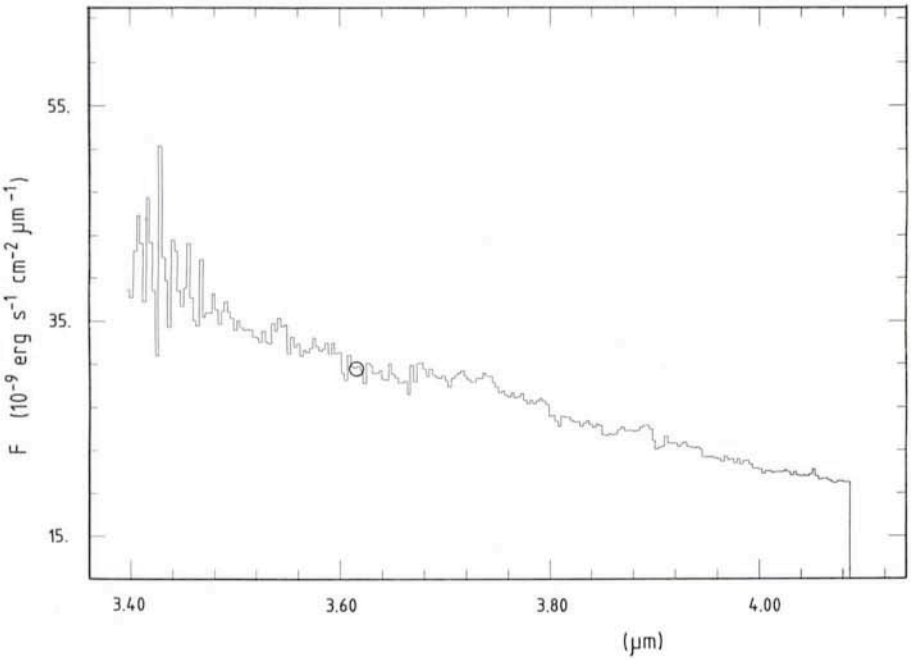

Figure 1: *Reduced spectrum of the standard star HR 5459, calibrated using the standard star HR 6746. The circle corresponds to the flux of HR 5459, determined photometrically in the L band.*

tion (see refs. 2 and 3 for details about the data format).

The basic steps of the basic IRSPEC reduction are:

(1) To perform wavelength calibration. The wavelength calibration is made by converting pixel positions into wavelengths, using a polynomial fit to laboratory measurements of a spectral calibration lamp and the theoretical dispersion formula. This calibration is done in a fully automatic procedure. As explained in ref. 2, the observer does not need to worry about making independent wavelength calibration, as the laboratory calibration formula provides accuracy to a fraction of a pixel. The grating position and stability of the instrument may be checked before each observing night in the way described in ref. 2. As a matter of safety, the observer may also record calibration spectra of any of the spectral line lamps available.

(2) To detect and correct "spikes" present in the scans. During this interactive step it is possible to reject individual pixels in a given scan or to eliminate one or several scans completely. New average counts with corresponding errors are then calculated using the selected information.

(3) To merge all spectra taken with the same wavelength parameters in a table. This table will be used as a working space where all the reduction operations will be carried out. Therefore, it is essential to make the observations of programme objects and standard stars – and optional calibration lamp exposures – in sets with *precisely the same wavelength parameters.* Otherwise, each individual spectrum, calibrated in wavelengths, will have to be rebinned into an image file, losing the possibility of error information and decreasing the flexibility of the reduction scheme.

(4) To compute the ratios between object counts and standard star counts. The detailed mathematical computations between spectra are decided by the user, depending entirely on the programme and methodology set by the observer. Basically, the result will be a series of spectra of programme objects divided by standard stars, cancelling in this way both the instrument response and atmospheric transmission characteristics.

(5) Flux calibration. This is done by fitting the coefficients A and B in the function $F_\lambda = A\lambda^B$ to the broad-band photometric data of a selected standard star. The coefficients are then used to convert the count ratios, computed in the step above, into flux. Tables with the fluxes of the observed standard stars have to be provided. Because of the flexibility of the reduction scheme, it is possible to select the standard stars from the ESO list of JHKLM standards, with the user's choice of zero-magnitude fluxes, or to include tables with standard stars defined in the system of your choice.

(6) To convert the final reduced spectra into one-dimensional images, so that any of the standard spectral analysis commands may be used.

At any of the previous stages, it is possible to generate plots or to use any of the available table commands to interact with the intermediate results. The present implementation includes a tutorial procedure to illustrate all the reduction steps described above.

3. Comments on the Accuracy of the Reduction

The actual accuracy achieved in the wavelength calibration step depends on how well calibrated the grating position was at the time of the observations. Naturally, this can be checked before each observing night. The estimated rms error for the measured lines in four independent calibration lamp exposures in the J and H bands was 0.0002 μm, which is about two tenths of a pixel.

The flux calibration is, at present, accurate to at best 5%. This depends strongly on the choice of the standard star and, naturally, on the sky transparency stability. As an illustration, Figure 1 shows the spectra of the standard star HR 5459 calibrated using standard star HR 6746, this time in the 3.5 to 4.05 μm region. The symbol ◯ marks the L band flux of HR 5459 determined photometrically.

As another example, the J band IRSPEC spectrum reduced with the MIDAS IRSPEC reduction package of the supernova 1987A in the Large Magellanic Cloud is shown in Figure 2. These data were obtained by T. Le Bertre the night of 29/30 May 1987. Figure 2a displays the counts with associated error bars. Figure 2b is the calibrated flux, the symbol ◯ marks the independent J-band photometric flux corresponding to that night.

Acknowledgement

We are indebted to A. Moorwood and A. Moneti for their contributions during the design of the reduction method. We

ESO Book Soon Available in Spanish and French

A Spanish edition of the ESO book "Exploring the Southern Sky" (see the *Messenger* **49,** 43) is now being prepared. It will soon become available in major bookstores in Spain and other Spanish-speaking countries, also in South America. Information about this edition may also be obtained from the publisher: Equipo Sirius (Tribuna de Astronomía), Desengaño 19–10°, E-28004 Madrid, Spain (telephone: [91] 521 60 08).

A French version will become available from Les Editions de Physique later this year.

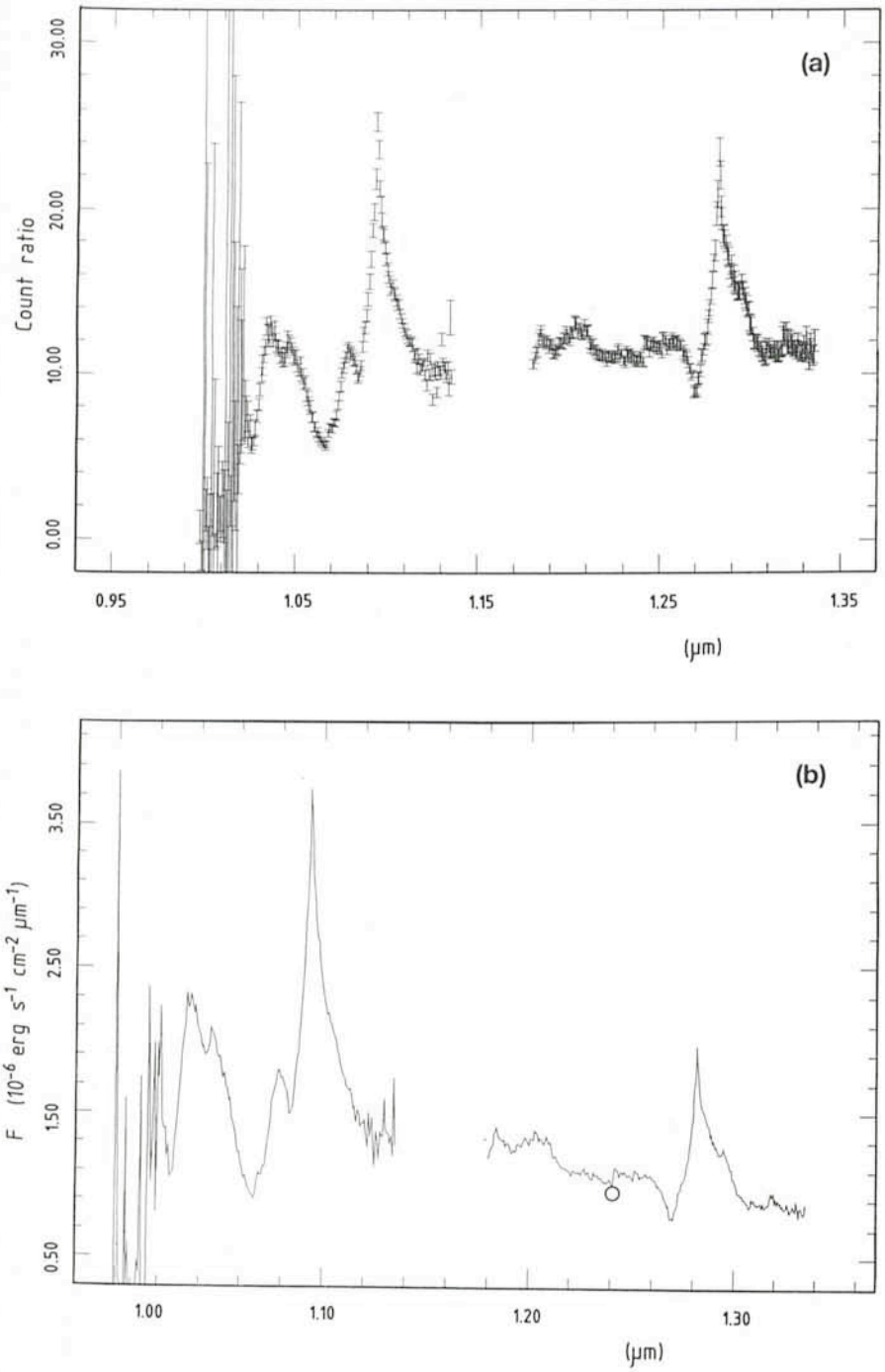

Figure 2: *Spectrum of SN 1987A in the J band observed during the night 29/30 May 1987, reduced with the IRSPEC package in MIDAS. (a) Observed counts with associated errors. (b) Calibrated flux, the circle marks the J band photometric flux, determined independently during the same night.*

are also indebted to T. Le Bertre for providing the SN 1987A data used for testing purposes.

References

1. A. Moorwood, P. Biereichel, G. Finger, J.-L. Lizon, M. Meyer, W. Nees and J. Paureau: 1986, *The Messenger*, No. 44, p. 19.
2. A. Moorwood: 1986, *IRSPEC Operating Manual.*
3. P. Biereichel: 1986, *IRSPEC Software Operating Manual.*

ESO at the IAU General Assembly

The XXth IAU General Assembly will take place in Baltimore, from August 2–11, 1988. Following the previous Assemblies, in Greece (1982) and in India (1985), it is expected that at least 2,000, perhaps even 3,000 astronomers will convene this year to discuss almost any aspect of modern astronomy. The General Assembly therefore also provides an excellent forum for presentation of the organizations connected with this science.

Among other exhibitors, mostly from North America, ESO will mount a small display in a booth at the Assembly. The 16-m Very Large Telescope will be shown by a new model and various aspects of the science and technology at ESO will be illustrated by drawings and photos. Brochures with details about ESO will also be availble for hand-out.

See you at the ESO booth in Baltimore!

ESO Grid Processing Machine

After much testing and several modifications, the prototype of the automatic ESO Grid Processing Machine (see also *The Messenger* **46,** 7, December 1986) is now ready. Its superiority over the Tray Rocker has been confirmed, both in terms of development efficiency and uniformity. It will therefore replace the Tray Rockers at ESO for the processing of large photographic plates. Practical tests will be made later this year at the ESO Schmidt telescope, together with the new Kodak T-max plates. When properly sensitized, these plates appear to reach fainter limiting magnitudes than the IIIa-J emulsion. Thus, it is thought that the combination of the new emulsion with the more efficient development technique may lead to higher detective quantum efficiency. The results of these tests will be announced in a later issue of the *Messenger*. Interested observatories can obtain further information about the Grid Processing Machine from the ESO Information Service (address on last page).

ESO, the European Southern Observatory, was created in 1962 to . . . establish and operate an astronomical observatory in the southern hemisphere, equipped with powerful instruments, with the aim of furthering and organizing collaboration in astronomy . . . It is supported by eight countries: Belgium, Denmark, France, the Federal Republic of Germany, Italy, the Netherlands, Sweden and Switzerland. It operates the La Silla observatory in the Atacama desert, 600 km north of Santiago de Chile, at 2,400 m altitude, where thirteen optical telescopes with diameters up to 3.6 m and a 15-m submillimetre radio telescope (SEST) are now in operation. A 3.5-m New Technology Telescope (NTT) will become operational in late 1988 and a giant telescope (VLT = Very Large Telescope), consisting of four 8-m telescopes (equivalent aperture = 16 m) is under construction. Eight hundred scientists make proposals each year for the use of the telescopes at La Silla. The ESO Headquarters are located in Garching, near Munich, FRG. It is the scientific-technical and administrative centre of ESO, where technical development programmes are carried out to provide the La Silla observatory with the most advanced instruments. There are also extensive facilities which enable the scientists to analyze their data. In Europe ESO employs about 150 international Staff members, Fellows and Associates; at La Silla about 40 and, in addition, 150 local Staff members.

The ESO MESSENGER is published four times a year: normally in March, June, September and December. ESO also publishes Conference Proceedings, Preprints, Technical Notes and other material connected to its activities. Press Releases inform the media about particular events. For further information, contact the ESO Information Service at the following address:

EUROPEAN
SOUTHERN OBSERVATORY
Karl-Schwarzschild-Str. 2
D-8046 Garching bei München
Fed. Rep. of Germany
Tel. (089) 32006-0
Telex 5-28282-0 eo d
Telefax: (089) 3202362
Bitnet address: IPS@DGAESO51

The ESO Messenger:
Editor: Richard M. West
Technical editor: Kurt Kjär

Printed by Universitäts-Druckerei
Dr. C. Wolf & Sohn
Heidemannstraße 166
8000 München 45
Fed. Rep. of Germany

ISSN 0722-6691

The ESO Milky Way Panorama

Several organizations, planetaria, etc. have expressed interest in acquiring the unique Milky Way panorama which was described in the last issue of the *Messenger* (**51,** 20). It has therefore been decided to offer the panorama for sale in a limited edition.

A preliminary estimate has shown that the net cost of one panorama is around 5,000 DM. This includes especially sturdy packing to avoid the risk of damage in transit. The transport costs from ESO Garching are not included in the mentioned price and would depend on the desired transport mode and the distance.

Each panorama consists of 8 panels with high-quality photographic prints (see the full-scale photo on page 21 in *Messenger* **51**), mounted on aluminium boards. For each panel, black edge protectors will be delivered. The combined dimension is about 1.5 m (height) × 8 m (width).

Interested parties are herewith requested to contact the ESO Information Service (address on this page) before September 15, 1988. Immediately after that date, and depending on the number of copies to be made, a definitive price will be established and prospective customers will be able to place firm orders. It is expected that delivery would follow within 6 weeks after receipt of orders.

Kindly note that the panorama will remain copyright ESO and that in order to ensure the best possible quality, no reproductions outside ESO control will be allowed.

Libro de la ESO en venta en español

Se está preparando una versión en español del libro de la ESO "Explorando el Cielo Austral" (ver el *Mensajero* n° 43). Pronto se podrá obtener en las librerías más importantes de España y otros países de habla española, y en Sudamérica.

Informes sobre esta edición pueden obtenerse también en la editorial: Equipo Sirius (Tribuna Astronomía), Desengaño 19–10°, E-28004 Madrid (fono: 91–521 6008).

Contents